Dissertation

submitted to the

Combined Faculties of the Natural Sciences and Mathematics

of the Ruperto-Carola-University of Heidelberg, Germany

for the degree of

Doctor of Natural Sciences

Put forward by

Sanjaya Paudel

born in: Kamalamai, Nepal

Oral examination: 1st Jun, 2011

Early-type dwarf galaxies:
Insight from stellar population studies

Referees:	Dr.T. Lisker	Examiners:	Prof. Dr. E. K. Grebel
	Prof. Dr. C. Dullemond		Prof. Dr. J. Schaffner-Bielich

Abstract

We have studied the stellar population properties of a sample of early-type dwarf galaxies (dEs) in Virgo cluster. We derived the simple stellar population (SSP) parameters age and metallicity using the method of Lick indices.

We found that not all dEs exhibit the same stellar population properties. The dEs with disc features are relatively younger and more metal enhanced than dEs without disc. We also found the nuclei of dEs have smaller ages and higher metal content than the respective galactic main bodies. Comparing the SSP parameters at the same local density, where the Ultra Compact Dwarf galaxies (UCDs) are located, we do not find any difference in the stellar population properties of dEs nuclei and UCDs.

We confirmed that the metallicity correlate with the galaxies luminosity in all classes of early-type galaxies i.e. Es, dEs and dSphs and dEs luminosity-metallicity relation has the steepest slope among all classes. We discovered a clear break in this relation in the dEs region. The bright and metal rich dEs seem to follow a faint end extension of Es and the metal poor and old dEs either hold a genuine class of early-type dwarf galaxies or just a bright end extension of dSph.

Zusammenfassung

Wir untersuchten die Eigenschaften der stellare Populationen eines Samples von Zwerggalaxien des frühes Typs (elliptische Zwerggalaxien) im Virgo Galaxienhaufen. Mit Hilfe der Lick-Index-Methode wurden die Alters- und Metallizitäts-Parameter äquivalent zu einer einfachen stellaren Population (SSP) abgeleitet.

Wir fanden, dass nicht alle dEs die selben stellaren Eigenschaften aufweisen. dEs mit einer Scheibenkomponente sind relativ jünger und metallreicher als dEs ohne Scheibe. Weiterhin fanden wir, dass der Kern der dEs ein geringeres Alter und eine höher Metallizität als die jeweilige galaktische Hauptkomponente aufweist. Beim Vergleich der SSP-Parameter, die sich bei der selben lokalen Dichte wie die Ultra-kompakten Zwerggalaxien (UCDs) befinden, konnten wir keine Unterschiede zwischen den Eigenschaften der stellaren Populationen der dE-Kerne und den UCDs feststellen.

Wir konnten bestätigten, dass die Metallizität mit der Leuchtkraft der Galaxien in allen Klassen von Galaxien des frühes Typs, z.B Es, dEs und dSphs, korreliert. Die Leuchtkraft-Metallizitäts-Relation der dEs zeigt den steilsten Anstieg innerhalb aller Klassen. Wir entdeckten einen eindeutigen Bruch in der Leuchtkraft-Metallizitäts-Relation im Gebiet der dEs. Die hellen und metallreichen dEs scheinen der leuchtschwachen Verlängerung der Es zu folgen und die metallarmen und alten dEs bilden entweder eine eigenständige Klasse von Galaxien frühen Typs oder sie sind nur die leuchtkräftige Verlängerung der dSph.

Declaration

This thesis contains no material that has been accepted for the award of any other degree or diploma.

Dedicated to my parents

Contents

List of Figures

List of Tables

1 Introduction

Abstract

This thesis is a study of stellar population characteristics of early-type dwarf galaxies (dEs) in the Virgo cluster using a spectroscopic data set. This introductory chapter gives a brief introductory overview of dEs and highlights the possible formation and evolutionary scenarios for dEs, emphasizing their importance in understand large-scale cosmology. Next, the goals of this study are given and an outline of the thesis.

Contents

Figures

1.1 Motivation

Galaxies are vast collections of star, dust and possibly dark matter. They are found in several different environments like in the dense cluster to isolated field, and in a variety of shapes and colors. In general, there are two different classes of galaxies according to color and morphology. Blue and star forming galaxies, which contain a large amount of neutral Hydrogen fueling ongoing star formation activity, are called late-type galaxies. The features like spiral disks, bars and star formation knots are frequent in these galaxies. The others are red in color with smooth light distribution called early-type or Elliptical galaxies (Es). In addition, the red and smooth galaxies with prominent disc feature are called lenticular galaxies (S0).

Figure 1.1: Example of different types of galaxies. The galaxies are placed according to classification of Hubble called Hubble's tuning-fork diagram. It starts with elliptical in left and S0 are in the centre as intermediate class. In the right part of the sequence, it branches into two different subsequences of bar and spiral shaped late type galaxies.

Observations have suggested that the existence of a relation between the galaxy morphology and the density of the host environment (e.g. Dressler, 1980). Early-types (Es and S0) are preferentially found in dense environments such as the clusters and groups, while late-type galaxies are more numerous in the low-density environments such as fields. The dense core regions of the cluster are richer in early-type galaxies, interestingly almost all cluster's Bright Central Galaxies (BCG) are early-types. Late-type galaxies are predominantly distributed in the outskirts of the cluster. Such a morphology-density relation suggests that the environment must play an important role in the galaxy evolution. The proposed idea is that gas rich star-forming galaxies get transformed into the red ellipticals as they fall into a cluster environment.

The almost all light of galaxies in the optical band, which makes the galaxies visible, comes from stars. Therefore the visible properties of the galaxies such as color and optical spectrum are dependent on the properties of its stellar constituent. Star inside the galaxies are also evolved with time, they are born in the inter stellar cloud and died with ejecting a lot of metal which enriched the Inter Stellar Matters (ISM) and the next generation of stars with higher meal content are formed. Therefore the study of metal content in the galaxies is directly related to the star formation and metal enrichment history of the galaxies, and by consequently the evolution of the galaxies. And study of optical light of a galaxy is the study of its stellar constituent.

Galaxy clusters provide an excellent opportunity to study the evolution of galaxies, because they host not only a large number of galaxies but also a variety of types at different evolutionary stages. The dominant red galaxies in particular are thought to be the most evolved galaxies. This

thesis tries to get an evolutionary picture of these early-type galaxies in a cluster environment through the study of stellar population characteristics using the optical spectroscopic data sets.

1.2 Dwarf elliptical galaxies

Historically low mass dwarf galaxies have been overlooked due to their low surface brightness and were not discovered until early 40's. However, present days observation show that they dominate the population of the universe by number. The current large-scale structure formation theory (i.e. ΛCDM) also predicts that the over abundance of these low mass system even in our local vicinity. It is believed that our own Milky Way is built with the gradual agglomeration of many smaller dwarf galaxies (Ferguson & Binggeli, 1994). Thus in recent years increasing attention has been paid to the study of these systems in order to understand their crucial role in galaxy formation and evolution. It is becoming a widely investigated topic in extragalactic research, and are the cornerstone of the most popular and accepted theories of galaxy formation (e.g. Blumenthal et al., 1984).

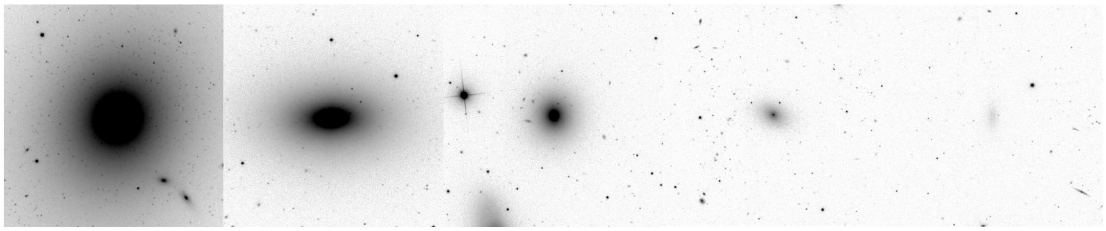

Figure 1.2: Elliptical galaxies with varying luminosity: VCC 1316 (M87), VCC1231, VCC1146, VCC0750, and VCC0011 (from left to right) chosen such that they form a sequence in brightness.

A galaxy is classified as an early-type dwarf (dE) if its blue magnitude is fainter than $M_B = -18$ and it has a smooth appearance (Ferguson & Binggeli, 1994). However, they span a magnitude from $M_B \approx -18$ to -8, with a sequence of increasing mean surface brightness with increasing luminosity. Note that, there is a separation among the early-type dwarf galaxies comprising dwarf-ellipticals (dEs) and dwarf Spheroidals (dSphs). In Grebel (2001), dSphs are defined as the objects with low luminosity ($M_V \gtrsim -17$ mag) and the typical surface brightness of $\mu_V \lesssim 21$ mag arcsec^{-2}. However, most of the authors treat them (dEs and dSphs) as the same types of galaxies (see Lieder et al. in preparation).

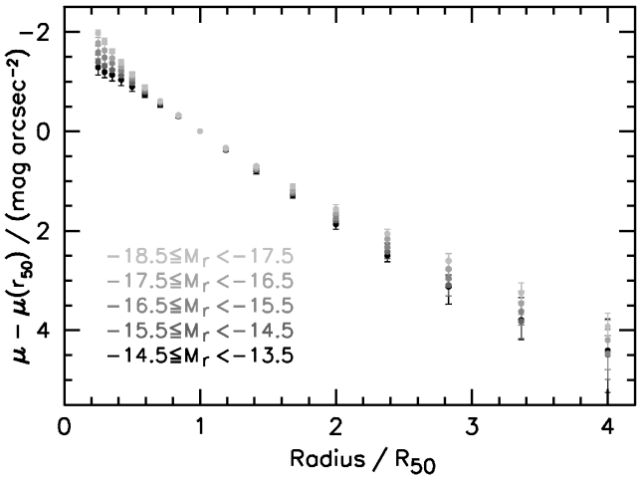

Figure 1.3: Relative radial surface brightness profiles of Virgo dEs in SDSS-r: Lisker (2009).

dEs are slightly more flattened than normal Es (Binggeli & Popescu, 1995; Ryden & Terndrup, 1994). Their light profiles are better described by an exponential fit than a de Vaucouleurs. Whether the fundamental plane[1] of dEs similar to that of bright counterpart, normal ellipticals (Es), is a matter of debate and provide a platform to discuss whether the dEs are the faint end extension of Es or not. Some claim that dEs do follow a low-mass extension of 'fundamental plane' defined by Es (Nieto et al., 1990). The relation between the size and luminosity is consistent to show that dEs and Es are same class of object. In contrast to this, other studies show that dEs do not follow the giant-ellipticals scaling relations (Bender et al., 1992), however both set of studies have a large scatter in the dE region. The measurement of mass to light ratio in dEs shows that dEs are more massive than Es for a given luminosity, in other word mass to light ratios of dEs are higher than those of Es and this discrepancy is interpreted as dominant present of dark matter in these low mass system.

Dynamical studies show that dE population is a mixture of rotating and non-rotating system. Study of Bender et al. (1991) found only a negligible fraction of dEs are rotating, though they had observed very few dEs. However, recent observations have discovered that a notable fraction of dEs shows a significant rotational support (De Rijcke et al., 2001, 2003; Pedraz et al., 2002; van Zee et al., 2004; Toloba et al., 2009). In addition, study of van Zee et al. (2004) discovered a relation between rotation amplitude and galaxy luminosity in dEs, which is called Tully-Fisher relation of galaxies.

1.2.1 Color and spectroscopic properties of dEs

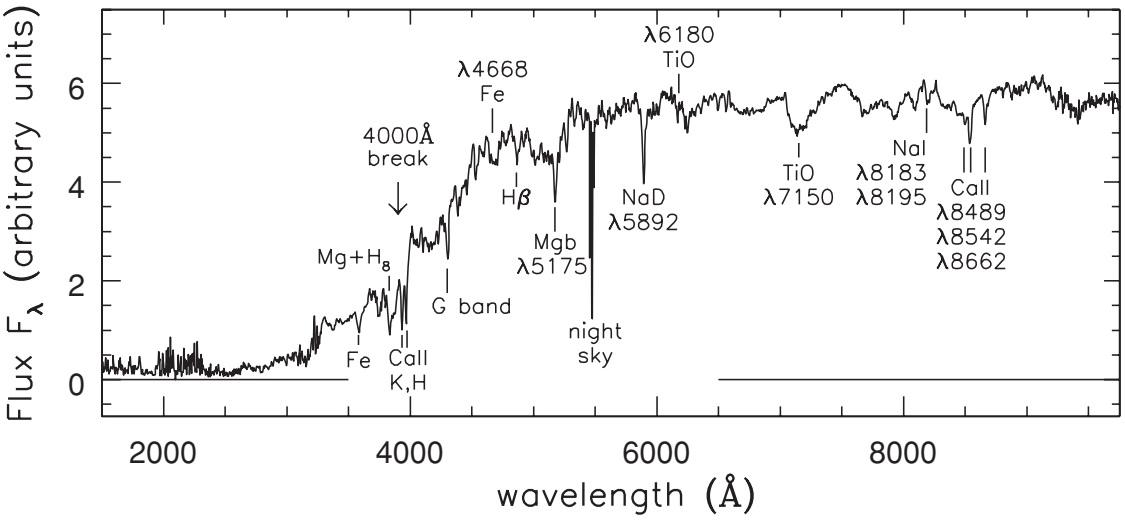

Figure 1.4: Example spectrum of an early-type galaxy: adopted from book Galaxies in the Universe (L.S. Sparke & J.S. Gallagher, III.).

By definition the early-type dwarfs are mostly gas deficient and devoid of any sign of current or recent star formation activity - although it has been noticed in some cases, that a weak star formation activity presents in the centre of dEs[2] - which means that their spectral energy distribution is dominated by red stars. Unlike late type galaxies the integrated spectra of dEs are heavily dominated by the deep absorption lines (see Figure 1.4). The spectrum shows a break

[1]The fundamental plane of early type galaxies is a relation between the three observable parameters of galaxies, i.e. effective radius (r_e), surface brightness (I) and central velocity dispersion (σ), and the relation can be written in the form of $r_e \propto \sigma_0^A I_e^B$ with A $\approx$ 1.4 and B = −0.9.

[2]Those types of dEs are classified as blue centered dEs, see Section 4.2.

at 4000 Å that corresponds to a jump by a factor of ~2 in the flux of early-type galaxies, since lines of metals absorb much of the light at shorter wavelengths.

Early-type galaxies are red in color. The universal relation between the color and luminosity, however, reveals that fainter/less luminous early-type galaxies are bluer than their brighter counterparts. This is called Color-Magnitude Relation (CMR). Es show only a small scatter in this relation while dEs deviate form the standard linear CMR defined by giant ellipticals. An extensive study on this relation (Janz & Lisker, 2009) using a large sample of early-type galaxies in Virgo cluster from the Sloan Digital Sky Survey (SDSS), reveals that CMR is not linear and has relatively large scattering in the dwarf regime. However, they show that both giant and dwarf early-type galaxies follow a continuous CMR that is best described by an S shape. The physical origin of CMR is still a mater of debate but the suggestion is that it is caused either by a variation of metallicity along the sequence (Arimoto & Yoshii, 1987; Kodama & Arimoto, 1997) or by a combination of age and metallicity variations.

1.3 Cosmological importance of dEs and formation scenario

Galaxies are the major constituents of the universe. Large-scale structures such as galaxy cluster, group and filament are the collection vast number of galaxies. Our knowledge of how the universe is formed and then subsequently evolved with time is also dependent on our understanding of galaxy formation and evolution. Starting with the primordial density fluctuation in the universe, which is the seed of galaxy formation, the galaxies hold important information about the content of the universe.

There are two competing models of galaxy formation in the universe. The early idea was the galaxies formed with collapse of single gas clouds called “protogalaxies” and fragmented into the stars later (so called monolithic collapse, Eggen et al., 1962). The gas mass is converted to stellar mass with huge burst of star formation activity in the early universe. Therefore they host a large amount of old stars and almost no leftover gases for present day star formation activity. The early-type galaxies are the prime example of monolithic collapse of galaxy formation as they host mostly old-stellar populations. Therefore, this simple model can successfully explain the origin of old-stellar population characteristic in Es but failed to explain the detail dynamical and luminosity dependent properties such as dimensional angular momentum and tidal features presence in Es.

A different but popular idea is hierarchical growth of the cosmological structure beginning from the primordial density fluctuations. This model assumes that galaxies are not formed through a single collapse but rather built up by the agglomeration of smaller ones through collisions and mergers (Searle & Zinn, 1978). According to very successful Cold Dark Matter (CDM) vision of structure formation in the universe, the dwarf-size dark matter haloes are the first to form then galaxies build their potential well by merging these haloes, and baryonic matter follows these potential with converting gas mass to the stellar mass (e.g. White & Rees, 1978; White & Frenk, 1991). These small galaxies, with a similar mass to the dwarf halos we see today, may be the primordial galaxies and carry the information from early universe to today. Therefore the study of dwarf galaxies can reveal the secrets of these first galaxies.

However, the recent study have shown that the star formation activity in lower mass galaxies is ended later than in giant galaxies. In other words, massive galaxies assemble their stellar mass earlier and more quickly (Cowie et al., 1996; Gavazzi & Scodeggio, 1996) then dwarf. Growing evidences also suggest that the dEs are formed at relatively late epochs with influence

of environment (e.g. Moore et al., 1998). The fact that, they are predominately found in cluster environment as we observed in pronounced morphology-density relation (e.g., Dressler, 1980; Binggeli et al., 1987). These evidences suggest that the dEs are either formed in high-density environments such as cluster and group or got their present shapes through the transformation of late type galaxies that fell into a cluster, i.e. morphologically transformed. However, the actual formation mechanisms are still a matter of debate, especially the way of influence of environment in the galaxies is not clear. A number of processes are suggested, i.e.

1. Ram pressure stripping.
2. Gas loss due to gravitational harassment.
3. Gas removal by galactic winds due to supernovae.

1.3.1 Gas stripping

Stripping of gases from the galaxies in the dense cluster environment was first proposed by Gunn & Gott (1972). A let type gas rich galaxy can loss its considerable fraction of gas through this process as it move through the hot intra-cluster medium. Which is commonly known as Ram-Pressure Stripping (RPS). The another gas removal process in the cluster environment is starvation (Larson et al., 1980), which removes the extended gaseous halo surrounding the galaxy and interrupts the continuous in-fall of gas into the galaxy. Both RPS and *starvation* are typical processes in a cluster environment and are not restricted to the central region (Tonnesen et al., 2007).

RPS on a disc galaxy can truncate its gas disc down to the stripping radius without affecting the stellar and dark matter components. Ram pressure is expected to be more efficient at gas removing from low mass galaxies than massive galaxies. The Virgo spiral NGC 4388 shows a strong evidence of ram-pressure stripping in the recent history (Cayatte et al., 1990), and it is presented as an example of an on going transformation of spiral to a dE in a cluster environment. As late-type to early-type transformations are expected in cluster environment through RPS, direct evolution from Irregular galaxies (Irrs) to dEs may face some problems: metallicity of Irrs is lower than dEs (Grebel et al., 2003) and the surface brightness will also be much lower than dEs after the cessation of star formation (Lisker, 2009). Secondly, since it is unlikely that ram-pressure stripping promotes the formation of globular clusters, dEs are expected to have a similar specific frequency of globulars (S_N) to Irrs. The removal of gas can result a quenching of star formation, which leads to conserve the number of globulars clusters.

1.3.2 Galaxy harassment

Tidal interactions are common in dense environment such as galaxy group and cluster. These interactions can leave a profound impact on the affected galaxies. In clusters, encounters between galaxies happen at high velocity and can affect the galaxy two different ways. One is tidal shocking; it occurs on a short time scales during the high-speed encounters between two galaxies. The other, which operates over long time scales, is the tidal heating, where galaxy can feel a strong tidal force associated with the deep potential well of the cluster. Harassment is a combined effect of both encounters (Smith et al., 2010), and can transform a low surface-brightness disc galaxy into a dE or dSph. Moore et al. (1996) have showed that during harassment the repeated high velocity encounters combined with the tidal field of the cluster can cause the galaxies to become anemic. The simulations of Mastropietro et al. (2005) have shown that only those galaxies that

end up on the orbits within the central cluster region experience such a strong transformation. Those with more eccentric and/or outer orbits retain more of their original disc structure, as well as a larger ratio of rotational to dispersion velocities, i.e. v/σ. In addition to this, Smith et al. (2010) found the effects of harassment are highly dependent on the orbit of the galaxy within the cluster, such that newly accreted dwarf galaxies typically suffer only mild harassment. A study of galaxy-galaxy interactions was performed by Aguerri & González-García (2009), who confirmed that these processes are efficient mechanisms to transform late-type disc galaxies into dEs, and whose simulated remnants are at least able to populate part of the fundamental plane locus of dEs.

1.3.3 Cosmological origin with internal feed-back

With the discovery of large numbers of dwarf galaxies in the nearby universe, the picture of large structure building by the accretion of smaller structures has become the standard model for the growth of cosmological structure in the universe (Jerjen, 2010). The dEs are predicted in the ΛCDM universe are often considered building blocks of more massive galaxies in models of hierarchical structure formation. In a ΛCDM Universe, the initial small density fluctuations grow due to gravitational instability and eventually form virialized objects called "dark matter halos". Halos grow as a result of mergers, assembling mass in a hierarchical fashion, with less massive halos merging to form more massive ones. Cosmological simulations of galaxy cluster do predict a large number of dark matter sub-haloes that appropriately hosts the dEs (e.g. Moore et al., 1999), and there is no "missing satellites problem" for the clusters. However, this scenario produces fairly metal poor dEs. Energy feedback from supernova explosions and stellar winds, have been proposed as a major factor in truncating the star formation activity in the dwarf galaxies. As a result, a dE is composed of old and metal-poor stars.

1.4 The Virgo cluster

The Virgo Cluster lies in the centre of Local Supercluster. It extends over $\sim$10° on the sky having the largest collection of early-type galaxies in the nearby universe. It lies at a distance of $\sim$17 Mpc with a mean velocity of $\sim$1200 kms^{-1} (Binggeli et al., 1987). It is an Abell richness Class I cluster containing more than 2000[3] optically catalogued galaxies (Virgo Cluster Catalogue (VCC), Binggeli et al. 1985). The Virgo cluster Virial mass is $\approx 2.5 \times 10^{14}$ M$_\odot$ (Girardi et al., 1998) as expected for a cluster as rich as this. It contains vast quantities of X-ray emission extending over most of the optically visible cluster (Böhringer et al., 1994), and reveal that a large part of the mass of the cluster is centered on the galaxy M87, with smaller concentrations around M86 and M49.

The earliest systematic studies of the cluster were done by Shapley and Hubble. Subsequent studies by Zwicky (1957) and Holmberg (1958) had furnished both a better understanding of its spatial structure and a more complete census of cluster members. The study of de Vaucouleurs (1961) confirm its vast richness and large dynamical mass, and identified it as the centre of the Local Supercluster. Surveys of the Virgo Cluster by Bruno Binggeli, Allan Sandage and Gustav Tammann (Binggeli et al., 1984, 1985; Sandage et al., 1985; Binggeli et al., 1987) built a extensive catalog of galaxies in Virgo cluster. This catalog of galaxies contain 2096 and thought to be completed in the luminosity greater than B_T = 18 and also provide the most reliable morphological classification of galaxies in the Virgo cluster.

[3] but only $\sim$1500 are spectroscopically confirmed non-background galaxies.

From previous observations of galaxy clusters, we know that environment can have a significant effect on the properties of galaxies and their evolution. In particular the star formation rate, gas content and morphology are strongly dependent on the density of the surrounding environment (Balogh et al., 2000; Moss & Whittle, 2000). As we summarized above, there are many mechanisms that can drive the galaxy evolution in dense environment. The relative importance of those different physical processes on the observable galaxy properties is still a matter of debate. This thesis provides an opportunity to discuss the probable dominant mechanisms that influence galaxy formation and evolution of galaxies in a cluster environment. The Virgo cluster is probably the most widely studied cluster of galaxies. This gives us an advantage when interpreting our results and comparing with precisely constrained cluster parameters such as local projected densities, cluster centric distances etc.

1.5 Thesis outline

The aim of this thesis is to put new and more robust constraints on our understanding of dEs formation process, by studying the physical properties of stellar population in present-day galaxies. We try to search for a link between the observed stellar population properties and the evolutionary history of dEs and their possible consequences. We study in detail the stellar population properties of a sample (see Chapter 3) early-type dwarf galaxy in Virgo cluster. Several data sets from the literatures have been used during the analysis of our results. Which makes this study focuses not only on the dEs, but also on overall range of early-type galaxies.

In Chapter 2, we provide a short description of methodology, which is used to study the stellar population from the integrated light of galaxies. Furthermore, we briefly describe some basic elements of stellar population synthesis models and parameters. We then review the stellar population characteristics of early-type systems over the complete range of magnitude i.e. Es to dSph. In Chapter 3, we describe the basic properties of our original sample of the galaxies, their observation and reduction. The first results from the analysis of central stellar population parameters of dEs are presented in Chapter 4. In this study, we use an additional sample of dEs from the study of Michielsen et al. (2008), which makes this is the largest sample of dEs for similar types of studies to date. With the help of galaxy morphology and observed galactic parameters we analyze the estimated stellar population parameters of dEs. Ultimately, we seek the main driver(s) of dEs evolution and try to answer the questions: How are these connected with their environment? Are dEs a single family differing only in substructure?

Next, to probe nature of the central nuclei of dEs, we investigate a spatially resolved stellar population characteristics of the original sample dEs in Chapter 5. An important aspect of this work is that, contrary to most previous studies of stellar populations in dEs, we compare of the stellar populations between the central nuclei and the surrounding galactic main bodies of dEs. This is made possible using a special technique to subtract the galactic light from the nucleus spectrum and estimate the stellar population parameters from the pure nuclear spectrum. Moreover, with the advantage of spatially resolved spectra, we also try to examine the presence of gradients in stellar population parameters for the 13 brightest dEs of our sample, which permit us to measure the absorption line strengths with sufficient signal-to-noise ratio up to 1.2 kpc (15 arc-sec) radial distance from the center.

We then focus to study the stellar population properties of a sample of Ultra-Compact Dwarf galaxies (UCDs) in the Virgo cluster. The aim is to provide a quantitative estimate of age, metallicity and α/Fe-abundance ratio of UCDs, and compare with the estimated stellar population parameters of dE nuclei. Which helps to put constrains in the formation scenario of UCDs.

The results and discussions are presented in Chapter 6, which provide an opportunity to test whether the UCDs are stripped nuclei of dEs or not.

Finally, we discuss the overall stellar population properties of dEs by comparing a large set of different class of early-type galaxies. We expand this study of the luminosity range $M_b = -23$ to $M_b = -9$, which includes the normal ellipticals (Es) to dwarf Spheroidals (dSphs), and try to answer the question of whether the diffuse early-type galaxies constitute a genuine class of galaxies or are merely a low luminosity extension of Es.

2

Integrated light stellar population studies in galaxies

Abstract

In this chapter, we provide a short description of the methodology that is used to study the integrated light stellar population. We then introduce the evolutionary population synthesis models as a principal tool to interpret the spectro-photometric properties of galaxies. The meanings of stellar population parameters such as age, metallicity and [α/Fe]-abundant ratio are explained. We briefly describe the different stellar population models that have been used to derive the stellar population parameters. Finally, We review the stellar population characteristics of all classes of early-type galaxies (i.e. Es to dSph) of entire magnitude range.

Contents

Figures

2.1 Introduction

Stellar populations within galaxies are a fossil record of their star formation and chemical evolution. A comparative analysis of the stellar population properties with the global galactic properties helps to differentiate between competing scenarios of galaxy formation and evolution. In the following sections, we will describe the basic methods that have been used to study the stellar population properties of galaxies using the optical integrated light spectra of galaxies.

2.1.1 Stellar population parameters

Age, metallicity and α-element abundance ratio are used to describe the stellar population characteristic of a galaxy. Young age indicates a recent star formation activity. The metallicity, [Z/H][1], indicates the overall content of all elements (Z) heavier than Helium (He) relative to Hydrogen (H) and is defined as

$$[\mathrm{Z/H}] = \log(\mathrm{Z/H}) - \log(\mathrm{Z/H})_{\odot} \tag{2.1}$$

where $\log(\mathrm{Z/H})_{\odot}$ is the solar ratio equal to 0.02. The abundances of specific element provide a direct evidence of specific the nucleosynthetic process that occurred during the formation and evolution of the star in the course of galaxy evolution. The modern picture of galactic chemical evolution involves different paths of stellar evolution from main-sequence stars all the way to supernovae, and different types of elements are formed through the different stellar evolutionary processes. Such as, Magnesium (like the other $\alpha-$elements[2] C, O) is formed in the explosion of type-II supernovae, which occur rapidly a few Myr after a burst of star formation. Most of the Fe-peak elements are formed later by type-Ia supernovae which lag behind type-II SN by at least 1 Gyr (Nomoto et al., 1984; Woosley & Weaver, 1995). Therefore α-element abundant ratios (i.e., [α/Fe]) are commonly used as a tracer of the star formation time-scale, since it decreases with increasing the duration of star formation activity. Thomas et al. (2005) find the following linear relationship between [α/Fe] and star formation timescale t,

$$[\alpha/\mathrm{Fe}] \approx \frac{1}{5} - \frac{1}{6}\log \mathrm{t} \tag{2.2}$$

Usually stellar population models provide the total metallicity, [Z/H], not [Fe/H]. However, [Z/H] can be converted to [Fe/H] on the Zinn & West (1984) scale with the following (model-dependent) scaling [Fe/H] = [Z/H] − 0.94 [α/H] (Tantalo et al., 1998; Trager et al., 2000a; Thomas et al., 2003).

2.1.2 Stellar population synthesis

It is not possible to perform the resolve stellar population study in a galaxy at the Virgo distance therefore the studies of their stellar populations are restricted to observation of integrated light. A well-known method of interpreting the integrated stellar light of the galaxies is the stellar population synthesis technique. The integrated light of a stellar population is simply superposition of the different stellar populations of various ages and metallicities. The pioneering work of

[1] Note that, for the easy use, some time metallicity can be expressed as simply Z instead of [Z/H].

[2] Elements are formed in supernova type II explosion mainly nuclei with even number of proton. Because, they are formed in the nuclear reaction chains, where successive nuclei in this chain are obtained by adding an α-particle.

Tinsley (1972) lead to the development of the evolutionary synthesis models of stellar populations in galaxies used today. The star formation rate (SFR) and the Initial Mass Function (IMF) are used as the model input parameters with which the stellar population models are synthesized and some time chemical enrichment rate are also used as another free parameter. The goal of population synthesis modeling is to describe the time-dependent evolution of integrated light spectra of galaxies (Bruzual & Charlot, 2003).

In this study, we use so-called single-age and single-metallicity models (i.e. Simple Stellar Populations SSPs). These models assume that all stars are formed at the same time with a mass distribution given by the chosen IMF and with an identical chemical composition. Such SSP models can be created following way: A library of individual stellar spectra is used to assign spectra to stars in various stages of the isochrones [3]. The spectral energy distribution of SSP is then obtained by summing the spectra of individual stars along the isochrone according to a chosen stellar *IMF*.

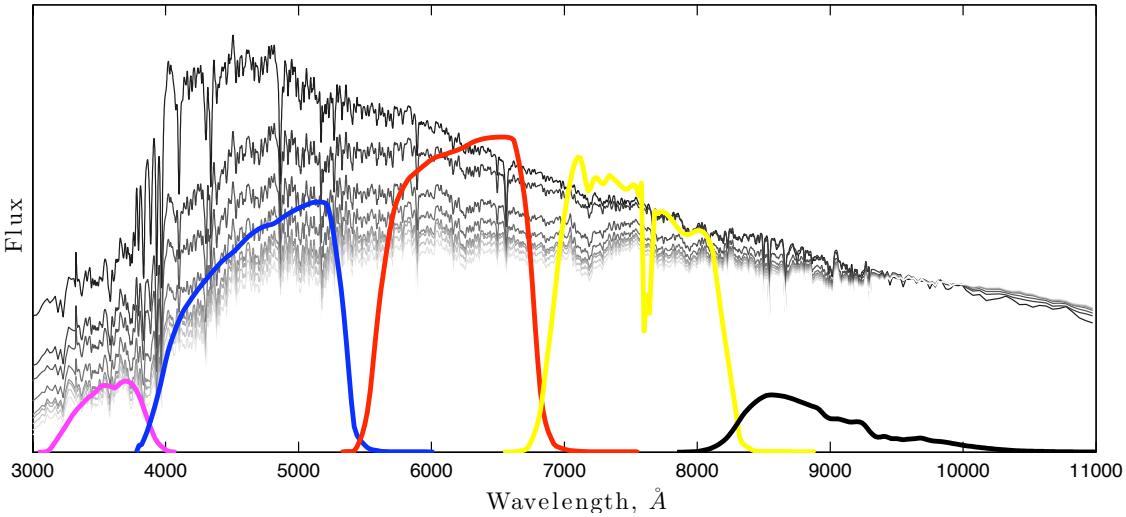

Figure 2.1: Evolution of optical spectra (i.e., wavelength range: 3000Å to 1100Å) of a Simple Stellar Population of solar metallicity obtained from the Bruzual & Charlot (2003) population synthesis code. The blue light dominates the spectra at the young ages (indicated as such younger are darker). The superimposed color lines represent the SDSS filter band-pass: u-magenta, g-blue, r-red, i-yellow, z- black.

Figure 2.1 illustrates the spectral evolution of an SSP of solar metallicity from 1 to 15 Gyr computed using the SSP synthesis code of (Bruzual & Charlot, 2003). When the populations are young, the spectra are dominated by the light from short-lived, massive stars at the blue part of the spectrum. As the time goes by the most massive stars leave the main sequence and evolve into the red giant branch, causing the light decrease in blue and increase in red part of the spectrum.

The interpretation of observed galaxy spectra in terms of physical parameters often relies on the comparison between their broadband colors and the predictions from population synthesis models. The main problem in this respect is the similar effect that age and metallicity have on the integrated light of a stellar population (Worthey et al., 1994a). The ages and metallicities derived from integrated galaxy color are therefore highly degenerate. This problem is further

[3] Isochrone is a time dependent evolutionary tracks of stars with same initial composition and various initial masses.

complicated in galaxies with a significant dust content, which produces a reddening of the optical spectrum similar to that caused by increase of age or metallicity.

A well-established method to solve this degeneracy is to use spectral diagnostics that involve several spectral absorption features, which have different sensitivity towards the age and metallicity. The most successful combinations of absorption features are those involving a Hydrogen Balmer line as a diagnostic of age and 'metallic' features sensitive to the different elements such as Fe or Mg (González, 1993). Moreover, these spectral absorption features are defined over narrower wavelength ranges than colors so they are believed to be almost insensitive to the reddening of the continuum due to dust absorption.

2.2 Simple stellar population models

There are several stellar population models which are used to compute the absorption line strengths for stellar populations of different ages and metallicities (Worthey et al., 1994a; Weiss et al., 1995; Buzzoni, 1995; Vazdekis et al., 1996; Bressan et al., 1996; Maraston, 1998; Tantalo et al., 1998). The models adopted in this work are those of Bruzual & Charlot 2003, hereafter BC03[4], Vazdekis et al. 2010, hereafter AV/MILES[5] and Thomas et al. 2003, hereafter TMB03. The first two models are based upon the fixed solar α-abundant ratio and they provide the optical model spectra to compare with observed galaxy spectra. The later model, TMB03, has variable α-abundant ratio from which one can estimate [α/Fe] directly with comparing the model predicted and observed absorption line strengths.

2.2.1 Model BC03

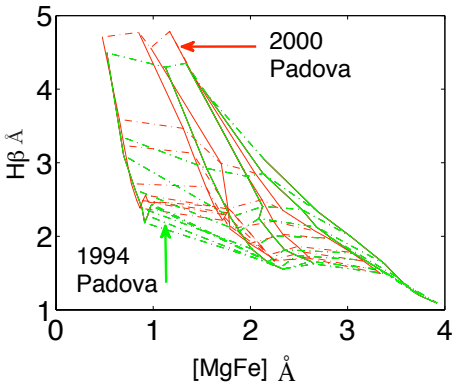

Figure 2.2: Comparison of different BC03 model grids that obtained by selecting the different evolutionary tracks i.e. Padova 2000 and Padova 1994.

The model BC03, also called the Galaxev model, provides the population synthesis codes with a variety of options for selecting evolutionary tracks: Padova 94, Padova 2000 (Girardi et al., 2000) and Geneva Schaller et al. (1992). In this work, we adopted Padova 94 because Padova 2000 overestimates the ages with systematic of positive offset in Hβ indices Koleva et al. (2008): see Figure 2.2. They cover metallicities between −2.8 and +0.5 dex. The advantage of this code is one can compute spectra of desirable age in SSP or with some arbitrary SFR history. These models are built using the STELIB library (Le Borgne et al., 2003). Which covers the

[4] http://www.cida.ve/~bruzual/bc2003
[5] http://www.iac.es/galeria/vazdekis

wavelength range 3200−9500 Å with the resolution ~3 Å FWHM. STELIB contains 249 spectra of star, among them only 187 stars have measured metallicity.

2.2.2 Model AV/MILES

AV/Miles models are an updated version of the models of Vazdekis & Arimoto (1999); Vazdekis et al. (2003) using the a new stellar spectral library MILES[6] (Sánchez-Blázquez et al., 2006; Cenarro et al., 2007). They use the Padova 2000 isochrones. Salpeter initial mass function is used to combine the library spectra. They cover ages between 0.1 and 17.8 Gyr and metallicities between −1.7 and +0.2 dex. The MILES library (Sánchez-Blázquez et al., 2006) used for these models has a 2.3 Å spectral resolution (FWHM), cover the wavelength range from 3525 to 7500 Å with a dispersion of 0.9 Å pix^{-1}. This library is believed to be better flux calibrated than any other (Koleva et al., 2009).

2.2.3 Model TBM03

The TMB03 models take into account the effects on the absorption line strengths from ratio change in element abundance. Hence, they provide the absorption line strengths for simple stellar populations not only as a function of age and metallicity, but also as a function of the $[\alpha/Fe]$ ratio. The models are derived using the evolutionary population synthesis code of Maraston (1998). A response function of Tripicco & Bell (1995) is used to compute the elemental ratio changes. Because of the inclusion of element ratio effects, the models allow for a clear distinction between total metallicity [Z/H] and the α to iron-peak elements ratio $[\alpha/Fe]$ (Thomas et al., 2005). The latter can be best derived from the classical absorption indices Mgb and Fe5270 and/or Fe5335 (Maraston et al. 2003, TMB03). This model covers the range of ages 1 to 15 Gyr, metallicities $-2.25 \leq [Z/H] \leq 0.67$ dex, and the abundance ratios $-0.3 \leq [\alpha/Fe] \leq 0.5$ dex.

2.3 Stellar population analysis

There are two different methods of stellar population analysis using the integrated spectra of early-type galaxies: full spectrum fitting and analysis of absorption line strength. The first, full spectrum fitting, matches observed and model spectra pixel by pixel: for example ULYSS[7] code (Koleva et al., 2009). Although this method has a benefit of using all available information form the spectra, it only provides a better estimate of stellar the population parameters when the observed spectra are moderately high-resolution. On the other hand, optical spectra of early-type galaxies present a number of absorption features whose strength depend on stellar population properties such as star-formation activity and metal content. Furthermore, these features can be easily measured from the low-resolution integrated light spectra of galaxies. Therefore it is also possible to perform the stellar population analysis using the low-resolution spectra. An advantage to using low-resolution spectra from galaxies is one can achieve reasonable signal-to-noise ratios (SNR) without using long exposure times for the faint objects such as dwarf galaxies.

[6] http://www.iac.es/proyecto/miles/
[7] http://ulyss.univ-lyon1.fr

2.3.1 Lick/IDS System

Table 2.1: Lick/IDS system index definitions

Name	Index Bandpass	Blue Bandpass	Red Bandpass	Units
CN_1	4142.125 - 4177.125	4080.125 - 4117.625	4244.125 - 4284.125	mag
CN_2	4142.125 - 4177.125	4083.875 - 4096.375	4244.125 - 4284.125	mag
Ca4227	4222.250 - 4234.750	4211.000 - 4219.750	4241.000 - 4251.000	Å
G4300	4281.375 - 4316.375	4266.375 - 4282.625	4318.875 - 4335.125	Å
Fe4383	4369.125 - 4420.375	4359.125 - 4370.375	4442.875 - 4455.375	Å
Ca4455	4452.125 - 4474.625	4445.875 - 4454.625	4477.125 - 4492.125	Å
Fe4531	4514.250 - 4559.250	4504.250 - 4514.250	4560.500 - 4579.250	Å
C24668	4634.000 - 4720.250	4611.500 - 4630.250	4742.750 - 4756.500	Å
Hβ	4847.875 - 4876.625	4827.875 - 4847.875	4876.625 - 4891.625	Å
Fe5015	4977.750 - 5054.000	4946.500 - 4977.750	5054.000 - 5065.250	Å
Mg_1	5069.125 - 5134.125	4895.125 - 4957.625	5301.125 - 5366.125	mag
Mg_2	5154.125 - 5196.625	4895.125 - 4957.625	5301.125 - 5366.125	mag
Mgb	5160.125 - 5192.625	5142.625 - 5161.375	5191.375 - 5206.375	Å
Fe5270	5245.650 - 5285.650	5233.150 - 5248.150	5285.650 - 5318.150	Å
Fe5335	5312.125 - 5352.125	5304.625 - 5315.875	5353.375 - 5363.375	Å
Fe5406	5387.500 - 5415.000	5376.250 - 5387.500	5415.000 - 5425.000	Å
Fe5709	5696.625 - 5720.375	5672.875 - 5696.625	5722.875 - 5736.625	Å
Fe5782	5776.625 - 5796.625	5765.375 - 5775.375	5797.875 - 5811.625	Å
NaD	5876.875 - 5909.375	5860.625 - 5875.625	5922.125 - 5948.125	Å
TiO_1	5936.625 - 5994.125	5816.625 - 5849.125	6038.625 - 6103.625	mag
TiO_2	6189.625 - 6272.125	6066.625 - 6141.625	6372.625 - 6415.125	mag
Hδ_A	4083.500 - 4122.250	4041.600 - 4079.750	4128.500 - 4161.000	Å
Hγ_A	4319.750 - 4363.500	4283.500 - 4319.750	4367.250 - 4419.750	Å
Hδ_F	4091.000 - 4112.250	4057.250 - 4088.500	4114.750 - 4137.250	Å
Hγ_F	4331.250 - 4352.250	4283.500 - 4319.750	4354.750 - 4384.750	Å
<Fe>	$\frac{Fe5270+Fe5335}{2}$			Å
$[MgFe]$	$\sqrt{Mgb \times <Fe>}$			Å

In order to provide a more sensitive tool for the analysis of galactic spectra, Burstein et al. (1984) and Faber & Lin (1983) introduced a set of absorption line indices in the optical, known as the Lick system, which has become the most widely used set of absorption indices (Renzini, 2006). The Lick system is based on a stellar library in the spectral range ~4000 Å - 6400 Å with ~9 Å resolution, and was built by S. Faber and collaborators using the Image Dissecting Scanner (IDS) at the Lick Observatory. Using this library, they defined the Lick/IDS absorption-line index fitting function. Earlier they proposed eleven well defined indices. Later, Worthey et al. (1994b) expended it up to 21. Still there was only one good age indicator Hβ, so the higher order Balmer lines Hδ & Hγ are also included in Worthey & Ottaviani (1997) and the system now contains 25 features over the wavelength range from 4000 to 6400 Å.

In the Lick system, an index is defined by a central 'feature band-pass', bracketed by two 'pseudo-continuum band-passes' (Worthey et al., 1994b; Worthey & Ottaviani, 1997) (see Figure 2.3). Atomic indices are conventionally expressed in Å of equivalent width, while molecular indices in magnitudes. The average pseudo-continuum flux label is defined as

$$F_p = \left(\frac{1}{\lambda_2 - \lambda_1}\right) \int_{\lambda_1}^{\lambda_2} F_\lambda d\lambda, \tag{2.3}$$

where $\lambda_1 \& \lambda_2$ are the wavelength limits of the pseudo-continua sideband. If $F_{C\lambda}$ represents the straight line connecting the midpoints of the blue and red pseudo-continuum levels, the equivalent width is then

$$EW = \int_{\lambda_1}^{\lambda_2} \left(1 - \frac{F_{I\lambda}}{F_{C\lambda}}\right) d\lambda, \tag{2.4}$$

where F_{I_λ} is the observed flux per unit wavelength and $\lambda_1 \& \lambda_2$ are the wavelength limits of the feature passband. Similarly an index measured in magnitude is defined as:

$$Mag = -2.5\log\left[\left(\frac{1}{\lambda_2 - \lambda_1}\right)\int_{\lambda_1}^{\lambda_2} \frac{F_{I\lambda}}{F_{C\lambda}} d\lambda\right] \tag{2.5}$$

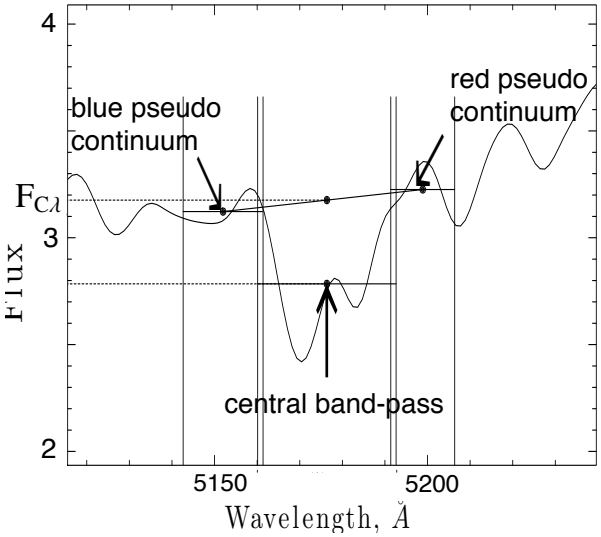

Figure 2.3: Central feature and two pseudo continuum band-passes on red and blue sides of Mg*b* index.

In the Table 2.1, we summarize the wavelength definition for all 25 Lick/IDS indices from Worthey et al. (1994b); Worthey & Ottaviani (1997). The units of the indices are shown in column 5. González (1993) suggests using a combination of indices in order to define a good mean metallicity indicator. First, the two indices Fe5270 and Fe5335 are substituted by their mean to give index <Fe> (Equation 2.6), then the [MgFe] index is defined as the geometric mean of Mg*b* and <Fe> (Equation 2.7).

$$< Fe >= \frac{Fe5270 + Fe5335}{2} \tag{2.6}$$

$$[MgFe] = \sqrt{Mgb \times <Fe>} \tag{2.7}$$

2.4 Stellar populations in early-type galaxies

Baade discovered two distinct populations of stars; Population I and Population II, in the M31 and in nearby galaxies, first introduced the concept of the stellar populations. Baade's results were based on the morphologies of the color-magnitude diagrams of the two types of stars. Faber (1973) discovered that Es integrated spectra are dominated by the light of metal rich and old stars. Later, Freedman (1995) confirmed Faber (1973) result and showed that integrated spectra of early-type galaxies and the color-magnitude diagram are dominated by G and K stars.

Early study of stellar population in early-type galaxies, using the method of Lick indices, was done by González (1993) and Trager et al. (2000a). Trager et al. (2000a) used a sample of 50 Es in both the low-density field and high-density clusters including reanalysis of González (1993) sample. They found a significant range in SSP-ages varies from 1 to 10 Gyr. The Es in field and Es with low dispersion velocity σ have relatively large age range. However, they noticed that Es are older in average and have larger non-solar abundant ratios, with [α/Fe] strongly enhanced in the most massive ones. Using a much larger sample of 200 Es, which covers a wide range in σ (hence luminosity and mass), Caldwell et al. (2003) obtain similar results. An important result they found that low σ galaxies show a larger scatter in the age than those with high σ, i.e. low-mass Es have had more prolonged star formation histories (Cecil & Rose, 2007). Furthermore, Kuntschner (2000) found all Es in the Fornax cluster have similar old stellar population properties, but that metallicity increases with σ. A recent study by Sánchez-Blázquez et al. (2006) also confirms that Es in low-density environments have greater range in age than that of their cluster counterparts. For these galaxies, an age-metallicity relation is found when metallicity is derived form Fe but not it is derived from Mg.

van Zee et al. (2004) also notice the differences in stellar population and stellar distribution between dwarf and giant elliptical galaxies. Stellar population studies show that dwarf galaxies exhibit on average younger ages as compared to their giant counterparts, and also a lower metal content according to the correlation of metallicity and luminosity (Michielsen et al., 2008). Various other studies using long slit spectra of dEs in different clusters (e.g., Poggianti et al. 2001; Rakos et al. 2001; Caldwell et al. 2003; Geha et al. 2003; van Zee et al. 2004) also provide a wide range of ages for passive dwarfs. In particular, field dEs are relatively younger than their cluster counterpart (Michielsen et al., 2008). Geha et al. (2003) present spatially resolved internal kinematics and stellar chemical abundances for a sample of dEs in the Virgo Cluster. They find that 4 out of 17 dEs are rotationally supported, while the remaining dEs have no detectable major axis rotation. However, they did not find any significant difference in the stellar population properties between the rotating and non-rotating dEs. From narrow band photometry, Rakos & Schombert (2004) inferred an age bimodality: they have found that nucleated dEs are several Gyr older than non-nucleated dEs and ages of nucleated dEs are comparable to globular clusters. Stellar population gradients were studied in the bright dEs by Chilingarian (2009) and Koleva et al. (2009), who found a range of metallicity gradients between steeply radial decreasing and constant metallicity, but no positive gradients. The stellar population age remains constant or shows a slight increase with radius. Apart from this, it is also noted that dwarf elliptical galaxies of the Virgo cluster are consistent with solar [α/Fe]-abundance ratios (Gorgas et al., 1997) indicating the slow chemical evolution in these low-mass systems. Other studies (Geha et al. 2003; van Zee et al. 2004) confirmed this result.

Star Formation (SF) and chemical evolution histories of Local Group dSphs can be studied with ground-based and Hubble Space Telescope (HST) multi-color photometry using the color magnitude-diagram and by using large aperture telescopes to obtain intermediate-resolution spectra of individual stars (Cecil & Rose, 2007). With metallicity from spectra, one can then fit isochrones to broadband photometry in order to pin down the SF history. Detailed studies of dEs and the fainter dSphs in the Local Group, based on these techniques, reveal that most dE/dSphs have a fairly extended star formation history (e.g., Mateo 1998; Grebel & Gallagher 2004), with the last star formation activity ranging from a few Gyrs ago to the time of re-ionization. However, they appear to host fairly metal poor stellar populations with small [α/Fe] ratios. As expected, mean metallicity increases with luminosity in dSphs. Grebel et al. (2003), among others, have noted that the metallicity-luminosity relation in dSphs offsets to higher metallicity at a given luminosity compared with dIrrs.

3

The sample: observation, data reduction and analysis

Abstract

In this chapter, we describe some basic properties of a sample of dEs in the Virgo cluster. The observational characteristics and important steps of spectroscopic data reduction are explained. In addition to this, we explain the adopted method to calibrate observed spectra into the standard Lick/IDS system. Finally, we comment on a comparison between the observed parameters and previously published literature values as the quality control of data sets.

Contents

Figures

3.1 Introduction

As our aim is to understand how the early-type dwarf galaxies (dEs) formed and evolved in a cluster environment, we define a sample of dEs in the Virgo cluster. In this chapter, we introduce the basic properties of this sample. We explain our selection criteria and statistics. In addition, we describe the basic reduction steps that are used in order to extract useful scientific information from the raw CCD observations. Our main aim is to study various absorption line strengths in the optical wavelength range in order to extract information about the integrated stellar populations of early-type dwarf galaxies (dEs) in the Virgo cluster.

3.2 Sample selection

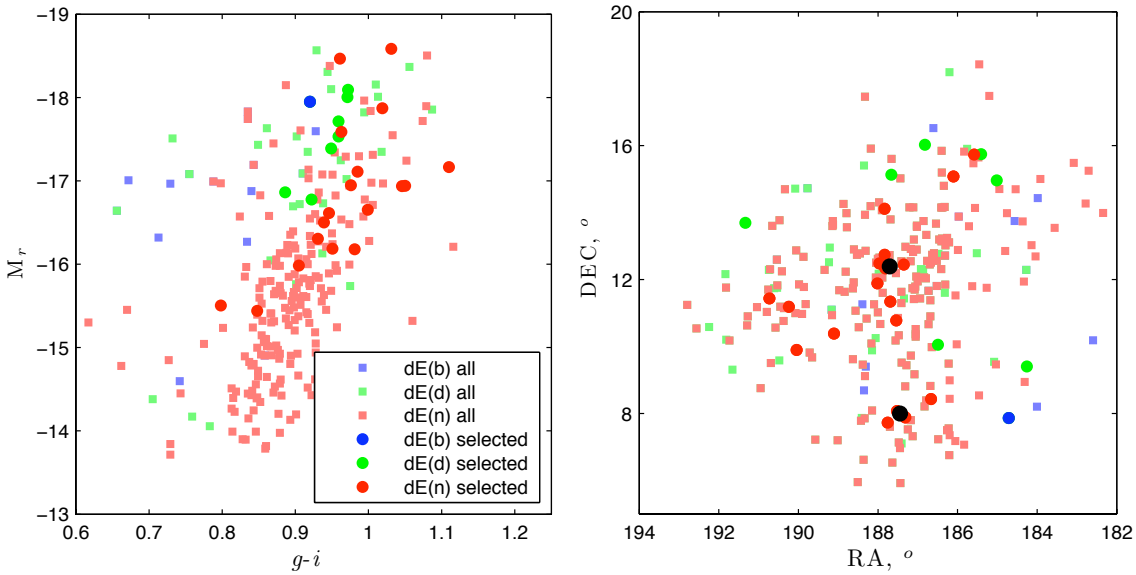

Figure 3.1: Right: the color-magnitude relation of Virgo cluster dEs with discs (green), without discs (red) and with blue centre (blue) as identified by L07. Solid circles represent the dEs of our target sample.
Left: The distribution of Virgo dEs in the sky. The symbols and colors are similar to left, except for the black solid circles that represent the galaxies M87 and M49.

From confirmed cluster members in the Virgo cluster catalogue (VCC, Binggeli et al., 1985; Binggeli & Cameron, 1993), we selected 26 nucleated dEs of differing morphologies, according to Lisker et al. (2006, 2007, hereafter L06 and L07, respectively). Our target list comprises 8 dEs with discs (here after dE(di)s) and 18 dEs without discs (hereafter dE(N)s) located different parts of the cluster (Section 4.2 for the morphological classification in dEs).

One major goal of our observations is to analyze the stellar population properties of the nucleus of dEs. Therefore, our target selection is guided both by the estimated ratio of nuclear light to the underlying galaxy light and by the Signal-to-Noise-Ratio (SNR) of nucleus and host galaxy (see Chapter 5). This sample is therefore mainly biased towards galaxies with relatively bright nuclei, both in absolute terms and relative to the galaxy's central region. We will take this into account during the discussion of respective result.

Furthermore, as shown in Lisker et al. (2007), the dE(di)s are, on average, somewhat bluer

Table 3.1: The original sample: basic properties.

Name	RA	Dec	Type	M_r	Density[a]	R_{eff}	RV	Remark
No.	h:m:s	°:':"		mag	sq^{-2}	"	Kms^{-1}	
0216	12:17:01.10	09:24:27.13	d,n	−16.78	9.4	13.3	1281 ±26	
0308	12:18:50.90	07:51:43.38	b,d,n	−17.95	3.6	18.7	1596 ±39	also in M08
0389	12:20:03.29	14:57:41.70	d,n	−18.00	15.6	17.2	1364 ±09	
0490	12:21:38.77	15:44:42.39	d,n	−18.09	31.6	27.6	1267 ±12	
0545	12:22:19.64	15:44:01.20	n	−16.61	52.6	13.3	1207 ±12	
0725	12:24:24.23	15:04:29.17	n	−16.19	26.2	25.2	1854 ±110*	
0856	12:25:57.93	10:03:13.54	d,n	−17.71	18.2	15.9	1025 ±10	also in M08
0929	12:26:40.50	08:26:08.60	n	−18.58	26.1	20.5	910 ±10	
0990	12:27:16.94	16:01:27.92	d,n	−17.39	14.8	9.9	1727±34	also in M08
1167	12:29:14.69	07:52:39.22	n	−16.95	45.1	27.3	1980±240*	
1185	12:29:23.51	12:27:02.90	n	−16.65	64.1	19.3	500 ±50	
1254	12:30:05.01	08:04:24.18	n	−17.17	68.9	14.9	1278 ±18	
1261	12:30:10.32	10:46:46.51	n	−18.47	21.0	22.5	1871 ±16	also in M08
1304	12:30:39.90	15:07:46.68	d,n	−16.86	15.1	16.2	−109±78*	
1308	12:30:45.94	11:20:35.52	n	−16.50	30.2	11.4	1721 ±45	
1333	12:31:01.07	07:43:23.04	n	−15.44	24.5	18.5	1251 ±28	
1348	12:31:15.73	12:19:54.38	n	−16.94	52.4	13.1	1968 ±25	
1353	12:31:19.45	12:44:16.77	n	−15.51	36.6	8.8	−384 ±82*	
1355	12:31:20.21	14:06:54.93	n	−17.59	29.9	29.6	1332 ±63	
1389	12:31:52.01	12:28:54.53	n	−15.98	42.9	12.8	858 ±25	
1407	12:32:02.73	11:53:24.46	n	−16.95	35.7	11.8	1019 ±03	
1661	12:36:24.79	10:23:05.25	n	−16.18	13.0	18.9	1457 ±34	
1826	12:40:11.26	09:53:45.99	n	−16.30	13.3	7.8	2033±38	
1861	12:40:58.57	11:11:04.34	n	−17.78	23.0	18.4	629 ±20	also in M08
1945	12:42:54.09	11:26:18.09	n	−17.11	26.6	21.5	1619±104*	
2019	12:45:20.44	13:41:34.50	d,n	−17.53	7.8	18.1	1895 ±44	

[a] Local projected galaxy number density.
* Those galaxies whose radial velocity are not listed in NED.

colors than the dE(N)s. This is reflected in our sample where Figure 3.1 shows that the dE(di)s tend towards the bluer side of the color-magnitude relation in *g-i*. Whether this effect is due to age or metallicity, and whether it is caused by the presence of a disc itself or by environmental density, will be addressed during the discussion of specific result and analysis (see Chapter 4).

This is a representative sample of bright-nucleated early-type dwarf galaxies in the Virgo cluster with different sub-structural types. Table 3.1 lists the sample galaxies and some of their basic properties. In column 1 we give the galaxy name according to the VCC. Column 2 and 3 give the galaxy position in RA and DEC (J2000.0), respectively. For column 4 we take the morphological classification given by L07 (with b = blue-centre; d = discy; n = nucleated). Column 5 gives the galaxy absolute magnitude in the SDSS *r*-band taking m−M = 31.09 (Mei et al., 2007), corrected for Galactic extinction (L07). Column 6 and 7 represent the local projected density (number per sq.deg., calculated from a circular projected area enclosing the 10th neighbor) and the effective radius in arcsec measured by L07, respectively. In column 8 we give the radial velocity in km/s provided by NED[1]; for those galaxies whose radial velocity is not listed in NED we measured their radial velocity from our data set, albeit with larger errors due to the low spectral resolution. In the last column we provide comments and indicate galaxies in common

[1] http://nedwww.ipac.caltech.edu/

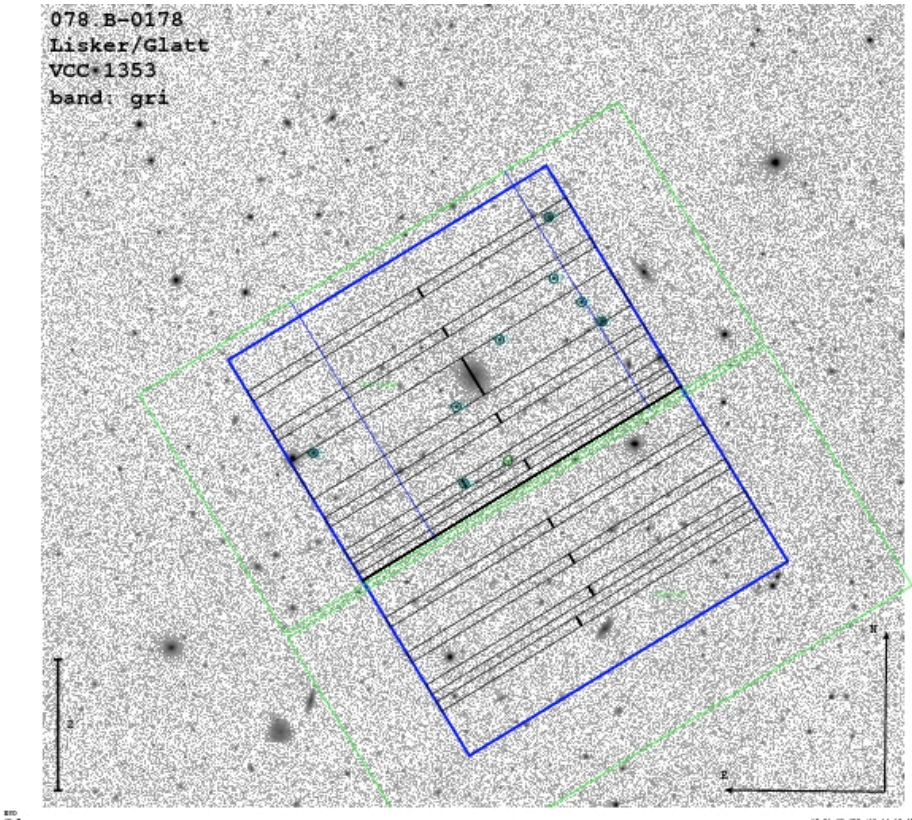

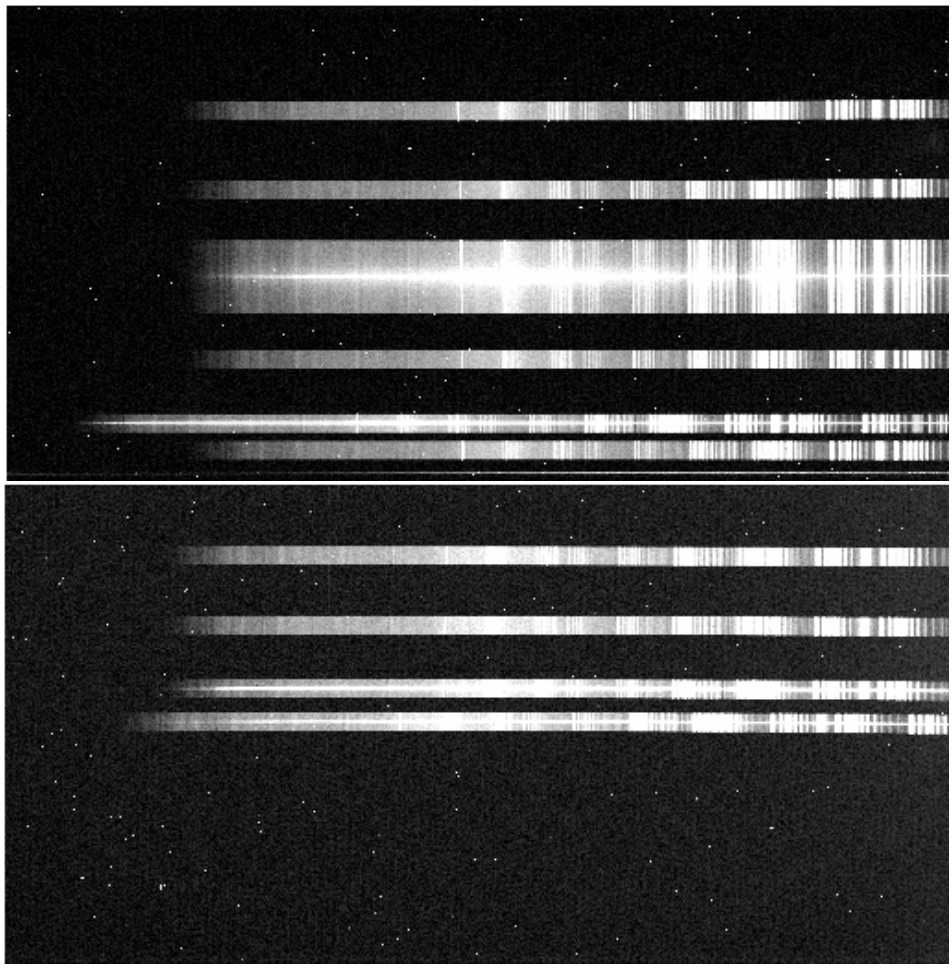

Figure 3.2: Slit mask acquisition and corresponding raw CCD frame: VCC1353.

with the study of Michielsen et al. (2008): hereafter M08, see Section 4.3.

3.2.1 Observational characteristics

VCC	Chip	Night	Exp.	SNR
No.	No.	yr-m-day	sec.	pix^{-1}
0216	1	2007-03-19	2 ×660	46
0308	1	2007-03-22	6 ×590	49
0389	1	2007-03-22	2 ×510	48
0490	1	2007-03-18	3 ×420	36
0545	1	2007-03-17	3 ×680	43
0725	1	2007-03-18	6 ×670	31
0856	2	2007-03-19	1 ×780	58
0929	1	2007-03-19	1 ×640	63
0990	1	2007-03-22	3 ×660	61
1167	1	2007-03-18	3 ×720	45
1185	1	2007-03-20	2 ×705	42
1254	2	2007-03-18	2 ×600	56
1261	2	2007-03-20	1 ×840	71
1304	1	2007-03-17	6 ×570	43
1308	1	2007-03-20	4 ×540	41
1333	1	2007-03-17	4 ×570	38
1348	2	2007-03-19	2 ×450	43
1353	1	2007-03-19	6 ×760	40
1355	1	2007-03-21	5 ×670	34
1389	1	2007-03-20	6 ×670	40
1407	2	2007-03-22	5 ×680	46
1661	1	2007-03-17	6 ×600	36
1826	1	2007-03-20	3 ×600	47
1861	1	2007-03-21	2 ×660	47
1945	1	2007-03-19	5 ×705	43
2019	1	2007-03-21	4 ×540	41

Table 3.2: Observation Log.

The observations were carried out over six half nights (three night in total) from March 16 to 22, 2007, with the ESO VLT UT1/FORS2 (Appenzeller et al., 1998) in multi object spectroscopy (MXU) mode. An example of slit mask acquisition in MXU set up and corresponding raw unprocessed CCD frames are shown in Figure 3.2. The detector in FORS2 comprises two 2k × 4k MIT CCDs with a pixel size of 15 × 15 μm^2. The standard resolution collimator and the 2-pixel binned read-out yield a image scale of 0.25 pixel^{-1}. The spectrograph slit width was chosen to be 1" and covered 40" in length, using the GRIS300V Grism providing a dispersion of 3.36 Åpixel^{-1}. This setup yields a spectral resolution, as measured from the FWHM of the arc lines, of ∼11 Å at ∼5000 Å, which is slightly below the instrumental resolution of Lick/IDS system (∼8.4 Å at 5000 Å) see Worthey & Ottaviani 1997. The dates and other observational information are provided in Table 3.2. In this table, the last two columns give the number of exposures, the exposure time, and the resulting SNR per pixel of the combined spectra measured at 5000 Å rest frame wavelength after co-adding them. Spectrophotometric standard stars were observed each night. The typical value of the seeing FWHM during the galaxy exposures was

1”.3 as measured by Gaussian fitting of the field stars.

3.3 Basic data reduction

The first step in the raw reduction was performed with the VLT FORS2 Pipeline *Gasgano*[2] implemented on *Esorex* data reduction package. An example snap shot of *Gasgano* GUI is given in Figure 3.3. This software performs the following basic tasks: bias subtraction, aperture identification, flat fielding, cosmic-ray removal and wavelength calibration (using as argon I lamp).

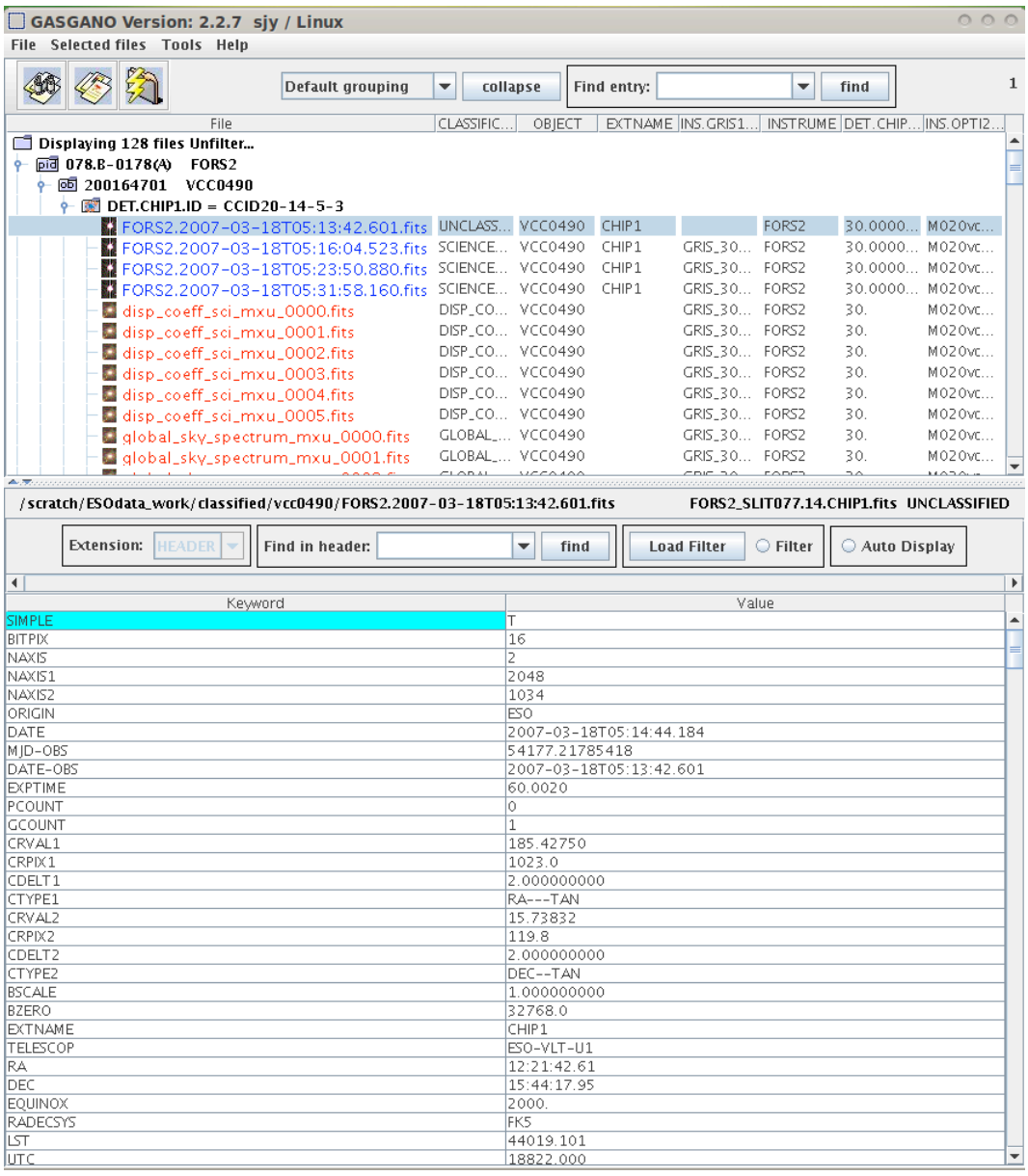

Figure 3.3: VLT/FORS2-pipeline *gasgano* window.

[2] http://www.eso.org/sci/data-processing/software/pipelines/giraffe/giraf-pipe-recipes.html

3.3.1 Sky subtraction

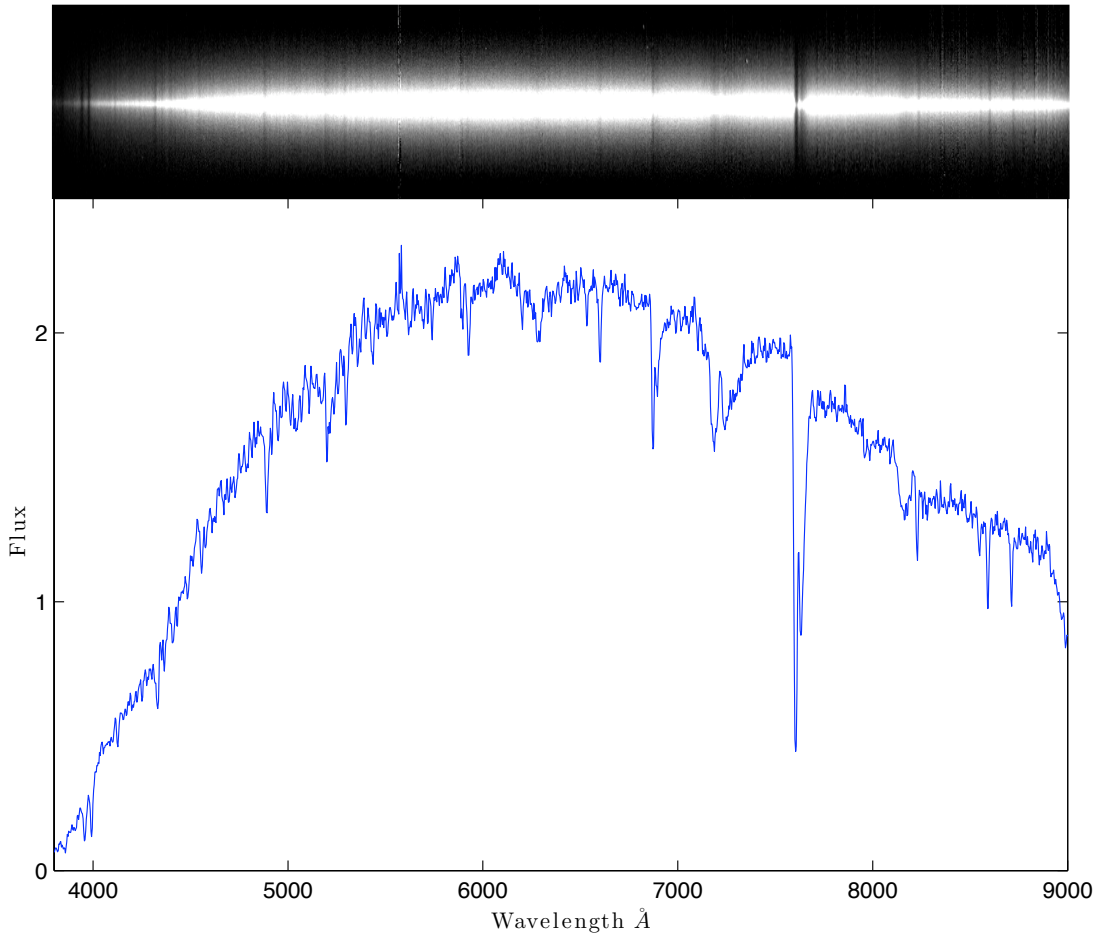

Figure 3.4: Top: An example of fully reduced galaxy frame where the wavelength runs along horizontal direction. Bottom: A one-dimensional spectrum, which is extracted form the wavelength calibrated and sky-background line subtracted frame with the spatial binning of central four pixel along the vertical axis.

Our spectra are not full long slit spectra (i.e covering the full length of the object with a sufficient additional region of sky). Rather we have used 40" arcsec slit length with MXU mode. In Figure 3.2, we can see the longest slit that almost covers the galaxy only. FORS2 Pipeline does not provide a good result for sky background subtraction for these kinds of spectra of specially extended object that cover the whole slit length (see pipeline manual) and leave significant residuals of sky signature. Therefore the night sky line removal has been done with IRAF[3] using the *background* task implemented in the *oned* package. Inherently, residuals and uncertainties from sky subtraction could mislead the line strength measurements so we have considered how this step is implemented thoroughly. The sky backgrounds are selected from the free slit, which do not have any object at the time of observation, see Figure 3.2. There are many slits of shorter length of 10", which are particularly intended to observe field star and some are left free for sky-background sampling. All the exposures have at least one free slit for the sky background. Often case there is more then one, but we find that the resulting sky-background subtracted galaxy spectrum is almost completely insensitive to how the sky region is chosen i.e. used one

[3]Image Reduction & Analysis Facility Software distributed by National Optical Astronomy Observatories, which are operated by the Association of Universities for Research in Astronomy, Inc., under co-operative agreement with the National Science Foundation. http://iraf.noao.edu/

or two sampling region for sky background. We have therefore chosen the sky regions from full length of free slit (i.e. free slit are always 10 arcsec = 40 pixel) typically 38 pixels wide and leaving one pixel either side of slit, on each side of the galaxy if possible. The final sky background subtracted frame is shown in Figure 3.4 as an example.

We observe the standard photometric stars in longslit (MOS_center) mode so we do not get any residual from the FORS2 pipeline during the sky background subtraction. This is because, in case of point like sources where plenty of sky is directly observed within the single slit, the default sky subtraction method (parameter *skylocal*) performs very well.

3.3.2 Poission error estimation

There are four sources of systematic errors that can affect the measurements of Lick indices: (1) data reduction issues resulting in additive errors, such as problems with the diffuse light or sky subtraction; (2) difference in the spectral resolution between given observations and the Model; (3) uncertainties in the determination of the radial velocities; (4) instrumental responses that could tilt the continuum of the line.

We use a parallel treatment of data and error frames and provide an associated error file for each individual data spectrum. The error spectra are produced as described by Cardiel et al. (1998) using independent processing of errors frames in the reduction of spectroscopic data sets. First, we create error frame of each science frame using the equation

$$\sigma^2 = \frac{1}{\mathrm{g}}\mathrm{N_c[j]} + \sigma^2_{\mathrm{RN}}\mathrm{[j]} \tag{3.1}$$

where σ^2 is the variance in pixel [j], g is the gain of the A/D converter = 1.43 (in e^-/ADU), $N_c[j]$ is the number of counts in pixel [j] (after processing from the Pipeline, the error produced from bias subtraction, flat-fielding, and implementation of the dispersion solution is not included), and σ_{RN} is the read-out noise = 2.9 (in ADU). In this sense, we have an error spectrum for each fully processed science spectrum that contains the propagation of initial random errors (due to photon statistics and read-out noise) that are carried throughout the arithmetic manipulations in reduction procedure.

3.3.3 Flux calibration

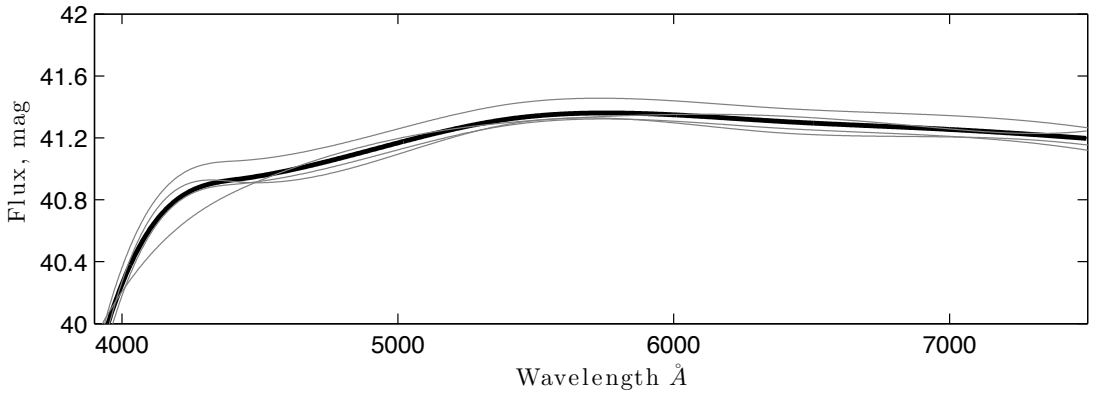

Figure 3.5: Sensitivity function derived from standard stars.The thick black line represents the average of all sensitivity functions derived from different stars.

It is also necessary to remove the overall instrument response function (IRF) from galaxy spectra prior to line strength measurement. Spectra are affected by the response of spectrographic optics, the response of the CCD, the response of grating, the atmosphere conditions and airmass. These effects can be removed by observing flux standard stars (Oke, 1990; Hamuy et al., 1994). For this purpose, we observed 5 standard stars (LTT4816, LTT6248, LTT1215, LTT2415, and Feige56). IRF is then computed from the ratios of the observed standard star spectrum and the tabulated calibrated spectrum of the respective star while considering the effect of atmospheric extinction.

To correct these effects of atmospheric extinction, we use the IRAF task *setairmass* to define the effective airmass for each spectrum. Then we apply the extinction correction (task *calibrate*) using the appropriate atmospheric extinction table (provided by ESO user support: Sabine Moehler). The galactic spectra were subsequently flux calibrated using the IRF, which allow us to transform the observed counts into relative spectral fluxes as a function of wavelength. The sensitivity functions as derived from the different stars varied by typically ∼1%, reaching ∼3% towards the edges of the wavelength range. Therefore combined them into a single function and can be reasonably confident that the resulting internal relative flux calibration is good to ∼1 % (see Figure 3.5).

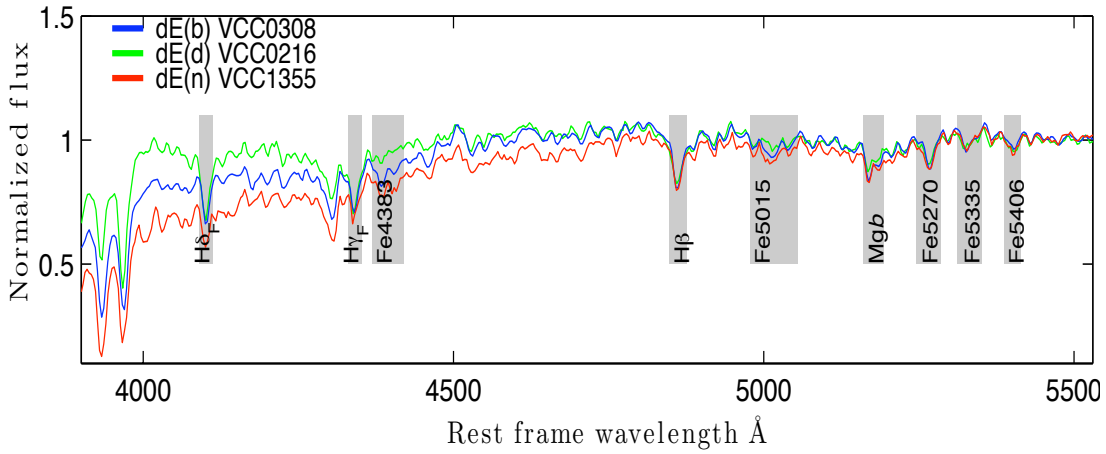

Figure 3.6: Flux calibrated spectrum of three dEs of different morphology, shifted to its rest frame wavelength. The measured LICK/IDS feature are shown in shaded region.

We then co-added the individual spectra from each exposures of given galaxy to produce a spectrum of higher Signal to Noise Ratio (SNR). Three typical flux calibrated and combined galaxy spectra are shown in Figure 3.6.

3.3.4 Spectral resolution

When measuring line strength one needs accurate knowledge of the spectral resolution. Therefore, in order to determine the resolution of our spectra, we use a arc lamp frame (see Figure 3.7). Assuming that all un-blended emission lines have a Gaussian profile and the FWHM in Å was determined for a range of lines. Generally the measured FWHMs are constant with wavelength. The resolution of spectra is sometime also quoted in kms^{-1} at particular wavelength, such as the instrumental velocity dispersion σ (Equation 3.7). Equation 3.2 to 3.5 provide the mathematical background.

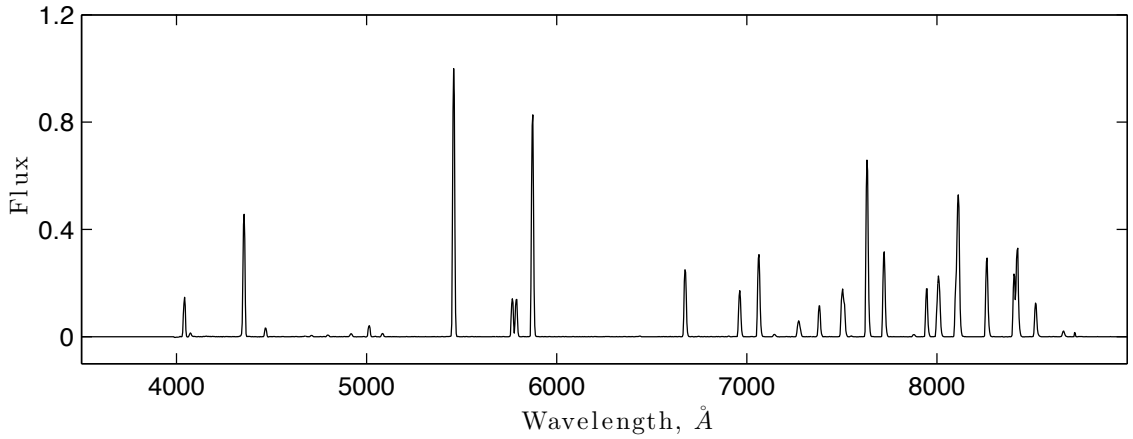

Figure 3.7: An example of a spatially summed lamp frame with emission lines.

$$f(x) = \frac{1}{\sqrt{2\pi}\,\sigma} e^{-\frac{x^2}{2\sigma^2}} \tag{3.2}$$

The full width at half maximum for a Gaussian is found by finding the half-maximum points x_1

$$f(x_1) = \frac{1}{2} f(0) \tag{3.3}$$

which implies that

$$e^{-\frac{x_1^2}{2\sigma^2}} = \frac{1}{2} \tag{3.4}$$

Solving for x_1 yields:

$$x_1 = \sigma\sqrt{2ln2} \tag{3.5}$$

The full width at half maximum is then given by

$$\mathrm{FWHM} = 2 \times x_1 = 2\sigma\sqrt{2ln2} \tag{3.6}$$

$$\frac{\mathrm{FWHM}}{\sigma} = \simeq 2.35 \tag{3.7}$$

The actual calculation of the instrumental resolution in σ [kms^{-1}] can be performed by

$$v = \frac{\mathrm{FWHM}}{\lambda} \times c\ [\mathrm{kms}^{-1}] \tag{3.8}$$

$$\sigma = \frac{v}{2.35}\ [\mathrm{kms}^{-1}] \tag{3.9}$$

where c is the speed of light and λ is the wavelength where the FWHM is measured.

To compare different data sets and models, all of them must be in equal instrumental resolution. Therefore to transform the resolution of one to another we use a Gaussian convolution to calculate a transformation function

$$\sigma^2_{\mathrm{trans}} = \sigma^2_{\mathrm{a}} - \sigma^2_{\mathrm{b}} \tag{3.10}$$

where σ_a is the instrumental resolution of low resolution resolution spectra then that of σ_b.

One should also apply a velocity dispersion correction if intrinsic broadening of the spectral lines exceeds the Lick resolution. All the objects in our sample have relatively low velocity dispersions, $\sigma_{gal} \leq 50\ km\ s^{-1}$, significantly below our spectral resolution $\sigma_{instr} \approx 280\ km\ s^{-1}$, therefore these corrections is not necessary.

3.4 Line strength measurement

In this section we describe details of the measurement of line strength in the optical wavelength range 4000 to 6000 Å and the main steps needed to calculate the line-strength specifically Lick/IDS index system (Burstein et al., 1984; Worthey et al., 1994a; Worthey & Ottaviani, 1997) using 1d spectra. This will allow us compare the results with different SSP models in order to predict the luminosity-weighted ages and metallicities.

We have considered two different programs to measure the indices in our spectra. These are INDEXF[4] and two tasks inside IRAF, *sbands & dopcor*. Using the definition of Lick index INDEXF calculates a pseudocontinuum (a local continuum level) for each spectral feature defined by the means within two pseudocontinuum bands-passes on either side of the central spectral feature (Worthey et al., 1994a; Worthey & Ottaviani, 1997). This program also estimates the uncertainties resulting from the propagation of random errors and the radial velocity errors by performing Monte-Carlo simulations. In IRAF, *dopcor* is used to put the spectra in their rest frames and then *sbands* is used to measure indices using the passbands defined in Worthey et al. (1994a); Worthey & Ottaviani (1997). However, we use only the indices measured from INDEXF during the stellar population analysis.

3.4.1 Index calibration

In this section, we introduce consistency tests between our measured indices and the different SSP model predictions of BC03 and AV/MILES. For this purpose, we compute the model indices at the resolution of our data (~11 Å). We then create index-index plots that contain those indices sensitive to the same chemical species as used in the SSP models (Kuntschner, 2000). These plots provide an idea of how accurately the models reflect the data and consequently help us interpret the results with respect to a chosen model. Moreover, it is important to check whether or not significant differences exist in the relative spectrophotometric calibrations of the data and the stellar libraries used by the models.

In Figure 3.8, different Mg indices are plotted against each other. The folded grids represent BC03 (black) and AV/MILES (red) models at 11 Å resolution, and the black dots are the indices measured from our sample dEs. The plots show a good overall agreement between the measured index values and the model predictions, with a small systematic deviation for galaxies with smaller Mg indices. Likewise, Figure 3.9 shows the relation between <Fe>, Fe5015 and Fe5406. In this plot, the scatter of the data points around the model grid locus is larger, however, this is explained by our measurement errors being larger here. Overall, the models do trace the mean trends in the data. In Figure 3.10 we present the Balmer indices Hβ, Hδ_F and Hγ_F. Here we find fairly good agreement for the AV/MILES model, while small deviation can be seen between the BC03 model predictions and the data in the Hδ_F and Hγ_F indices.

[4] http://www.ucm.es/info/Astrof/software/indexf/indexf.html

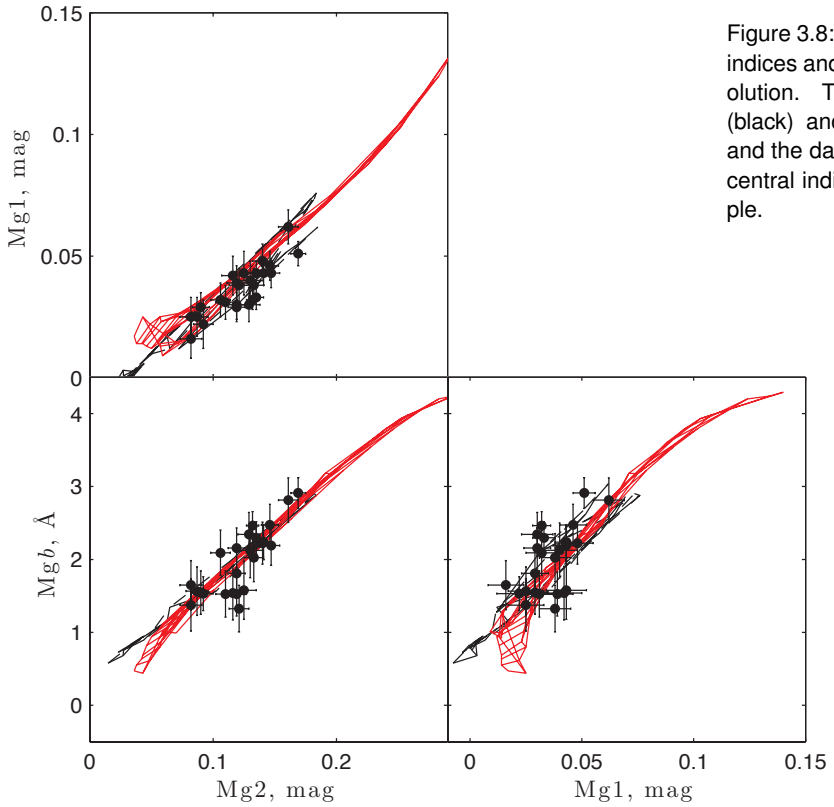

Figure 3.8: Consistency test using Mg indices and BC03 models at 11 Å resolution. The folded grids are BC03 (black) and AV/MILES (red) models and the data points correspond to the central indices measured in our sample.

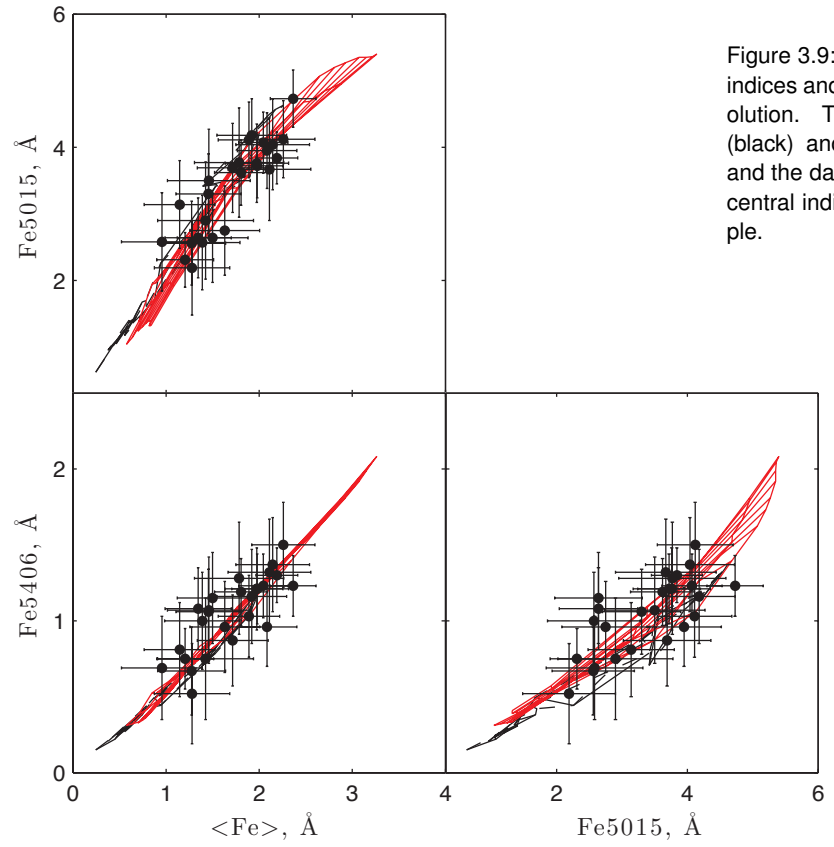

Figure 3.9: Consistency test using Fe indices and BC03 models at 11 Å resolution. The folded grids are BC03 (black) and AV/MILES (red) models and the data points correspond to the central indices measured in our sample.

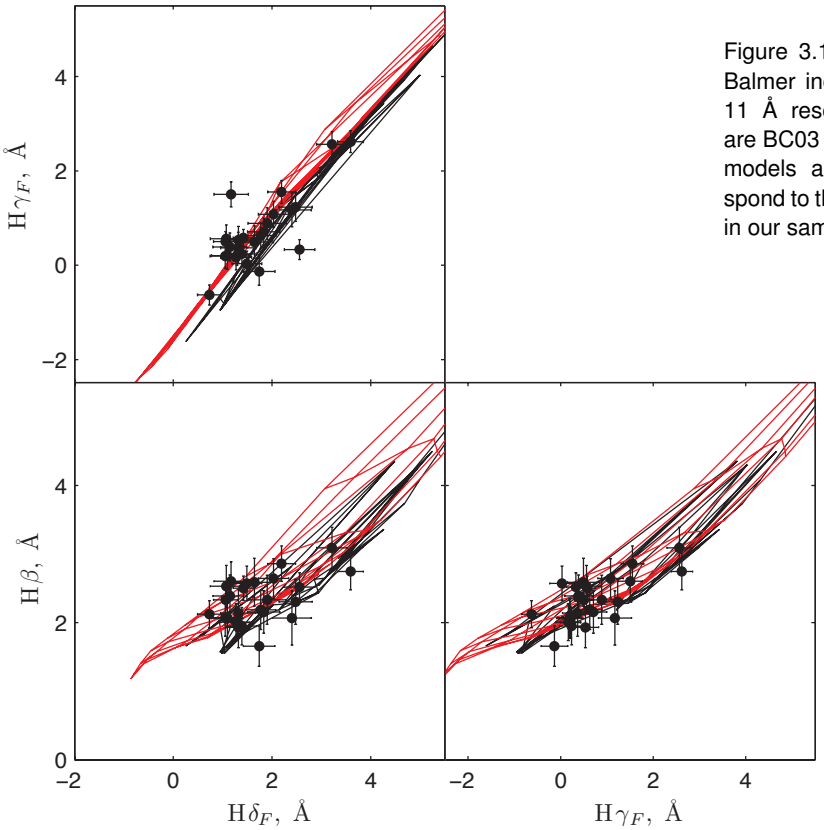

Figure 3.10: Consistency test using Balmer indices and BC03 models at 11 Å resolution. The folded grids are BC03 (black) and AV/MILES (red) models and the data points correspond to the central indices measured in our sample.

3.5 Correction to the Lick system

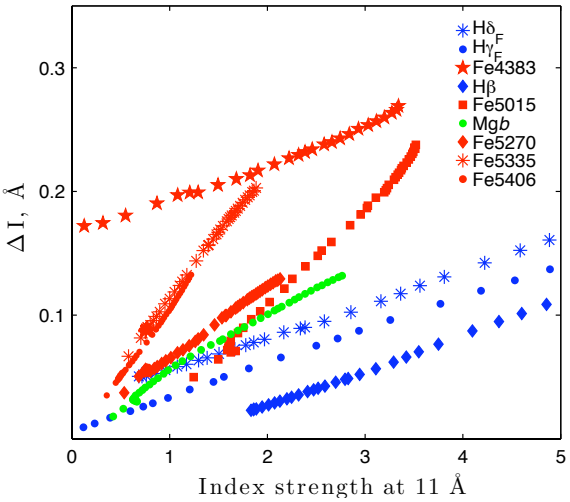

Figure 3.11: The deviation of index values after changing the resolution from 9 Å to 11 Å as a function of measured index strength at 11 Å of AV/MILES model spectra.

In this section we investigate the behaviors of line indices at different resolutions, and provide corrections of our measured indices to the Lick system. We assess possible effects of a variation of the resolution on the ages and metallicities. For this purpose, we used AV/MILES model spectra. First, we degraded the model spectra to Lick resolution, since most studies in the literature are based on this resolution. For simplicity, however, we consider a fixed resolution of 9 Å, although the original Lick system varies from ~8.4 to 11.5 Å depending on wavelength. In addition, we computed another degraded version of the model spectra, adopting the resolution

of our data (11 Å). These two different resolutions are compared with each other in Figure 3.11, where we show the difference ΔI between the measured indices for the two resolutions (i.e., ΔI = Indices measured at 9 Å − 11 Å) as a function of index strength. We find that Fe5335 and Fe5406 suffer slightly more degradation in the strong absorption region than the Balmer lines (Hβ, Hγ_F, and Hδ_F) and the Mg indices. The percentage variations of these features are ∼10.5% for Fe5335 & Fe5406, ∼6% in case of Fe5270 & Fe5015 and Mgb, and even smaller for Hβ (i.e., ∼2%) and other higher order Balmer lines. Note that these systematic deviations in absorption line strengths are smaller than half of the typical (statistical) measurement error from our galaxy spectra. From the relations illustrated in Figure 3.11, we computed corrections for index strength for all the measured indices of our galaxy sample, in order to correct our data back to the Lick resolution (9 Å). This allows us to apply a separate correction for each galaxy, depending on its individual index strength. We then further corrected each index by applying the offsets between flux-calibrated spectra and the non-flux-calibrated original Lick/IDS system (see next Section 3.5.1).

3.5.1 Lick offsets

Table 3.3: Offsets to the Lick/IDS stellar library system derived from the MILES library.

Index (1)	Offset (2)	rms (3)	Number of stars (4)	A (5)	B (6)
CN_1	−0.008 ± 0.002	0.027	222	−0.008 ± 0.003	0.060 ± 0.014
CN_2	−0.003 ± 0.002	0.031	220	−0.005 ± 0.004	0.056 ± 0.015
Ca4227	0.06 ± 0.02	0.35	237	-	
G4300	−0.05 ± 0.04	0.62	238	−0.545 ± 0.050	0.108 ± 0.016
Fe4383	0.46 ± 0.05	0.74	237	-	
Ca4455	0.36 ± 0.02	0.33	237	-	
Fe4531	0.07 ± 0.03	0.49	237	−0.108 ± 0.047	0.064 ± 0.021
$C_2$4668	−0.23 ± 0.05	0.79	237	−0.423 ± 0.057	0.051 ± 0.013
Hβ	−0.09 ± 0.02	0.25	239	-	
Fe5015	0.40 ± 0.04	0.59	237	0.216 ± 0.044	0.048 ± 0.011
Mg_1	0.007 ± 0.001	0.013	239	0.004 ± 0.002	0.057 ± 0.009
Mg_2	0.019 ± 0.001	0.017	239	0.006 ± 0.003	0.078 ± 0.006
Mg b	0.03 ± 0.02	0.29	239	-	
Fe5270	0.07 ± 0.02	0.34	239	-	
Fe5335	−0.04 ± 0.02	0.32	239	-	
Fe5406	−0.07 ± 0.02	0.28	237	-	
Fe5709	0.05 ± 0.01	0.21	235	-	
Fe5782	0.03 ± 0.01	0.18	231	0.077 ± 0.022	−0.076 ± 0.025
Na D	0.17 ± 0.02	0.32	238	0.219 ± 0.026	−0.025 ± 0.010
TiO_1	0.009 ± 0.001	0.010	237	0.008 ± 0.001	0.084 ± 0.008
TiO_2	0.001 ± 0.001	0.010	216	−0.000 ± 0.002	0.037 ± 0.006
Hδ_A	−0.03 ± 0.05	0.75	212	−0.018 ± 0.049	0.033 ± 0.012
Hγ_A	0.08 ± 0.04	0.67	237	0.166 ± 0.040	0.021 ± 0.008
Hδ_F	−0.01 ± 0.03	0.46	212	-	
Hγ_F	0.05 ± 0.02	0.38	237	-	

Note. Column (1) gives the index name, while column (2) gives the mean offset (Lick - MILES) to the Lick/IDS system. Column (3) gives a robust estimate of the 1σ scatter and column (4) shows th number of stars used in the comparison for each index. Columns (5) and (6) give the coefficents of a linear fit to (Lick - MILES) = $A + B \times$ Lick where a significant slope was found.

In this work, we derived offsets from the Lick star spectra of the MILES library. For this project

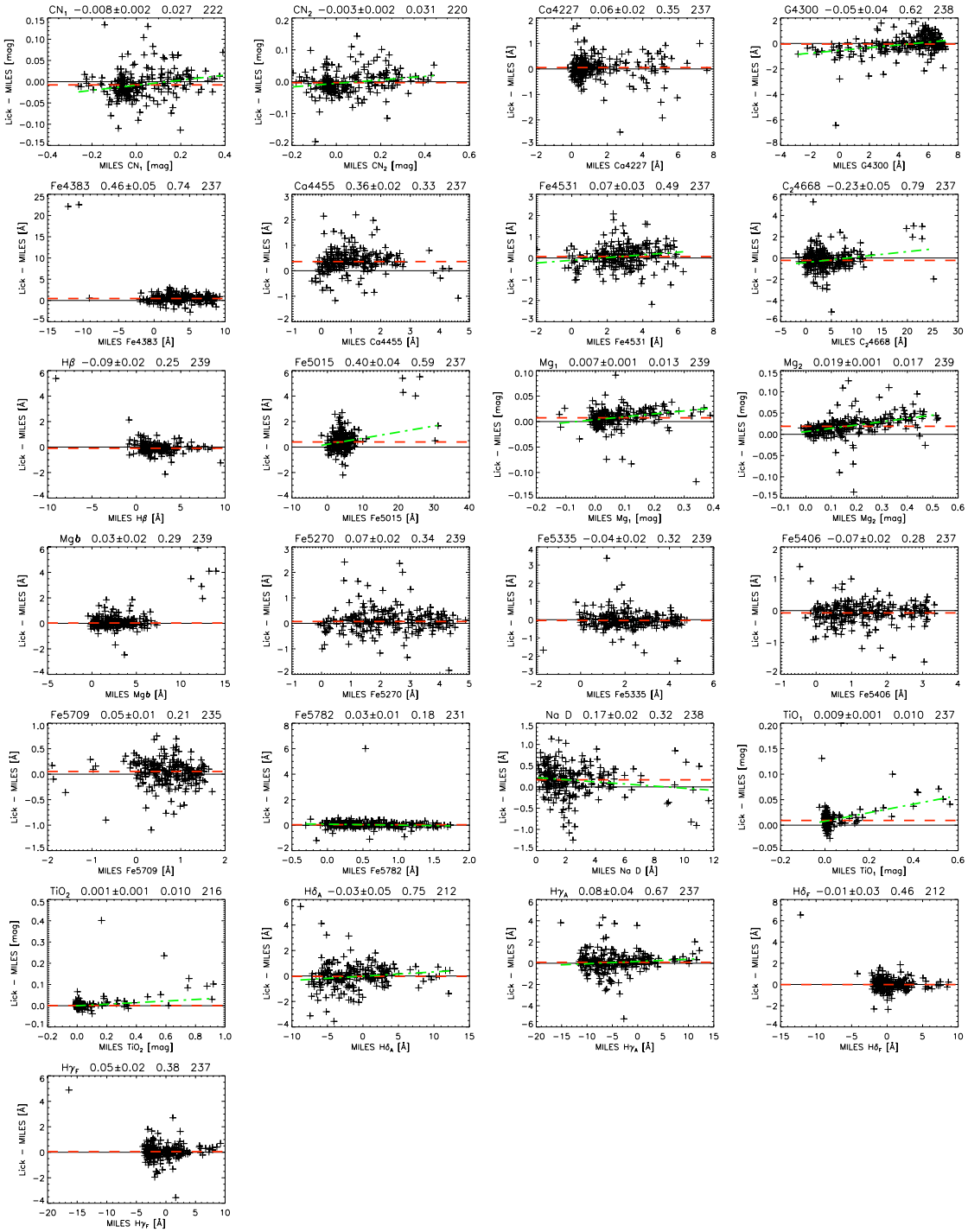

Figure 3.12: Comparison of Lick/IDS index measurements with the MILES stellar library (Sánchez-Blázquez et al., 2006) for stars in common (plus signs). The red dashed line in each panel shows the mean offset derived by a biweight estimator (see also Table 3.3). In the title of each panel we list the index name, the index offset and associated error, a robust estimate of the 1σ scatter and the number of stars used in the comparison. A subset of the indices shows evidence for line-strength dependent offset. For indices where this is a significant effect (2σ), we also show a robust fit to the relation (green dash-dotted line). See text for details.

and instrument configuration there were no stars observed in common with the original Lick/IDS stellar library (Worthey et al., 1994a) which is the standard way to calibrate the index measurements to the Lick system by deriving small offsets (Worthey & Ottaviani, 1997). However, we made use of the MILES stellar library (Sánchez-Blázquez et al., 2006) to determine the offsets to indices measured in flux calibrated spectra from the original Lick/IDS system, assuming that the MILES library and our data are well flux-calibrated.

The spectra were first broadened to the Lick/IDS resolution with a wavelength-dependent Gaussian assuming a spectral resolution of the MILES library of 2.3 Å (FWHM). Then, we compared the index measurements in common with the Lick stellar library for up to 239 stars depending on the availability of the measurements. The offsets and associated errors (see Figure 3.12 and Table 3.3) were derived with an outlier resistant biweight estimator (IDL Astronomy library[5] `biweight_mean.pro`). The offsets are generally small (<0.2 Å) but some individual indices show larger offsets (e.g., Fe4383, Fe5015). Additionally, several indices show evidence for line-strength dependent offsets (e.g., CN_2, G4300, Mg_2; see also Vazdekis & Arimoto 1999). We used an outlier-resistant two-variable linear regression method (IDL Astronomy library `robust_linefit.pro`) to investigate the significance of such trends. For indices where we find a slope different from zero with more than 2σ significance we show the fit in Figure 3.12 with a green dash-dotted line and give the fit parameters in Table 3.3.

We note that previous attempts to establish Lick offsets with the Jones 1997 stellar library (Norris et al. 2006;Worthey & Ottaviani 1997) have resulted in significantly different offsets for some indices, perhaps most notably the higher order Balmer lines. We ascribe the differences in offsets to an imperfect flux calibration of the Jones library. Recently, Sanchez-Blazquez et al. (2009) also used the MILES library to derive Lick offsets and find similar results. However, significant differences remain for individual indices (e.g., Mg*b*) where we favour our outlier robust analysis.

For the present study, we apply the offsets listed in Table 3.3 (column 2). Only one of the indices (Fe5015) used in this study to derive the stellar population parameter estimates shows evidence for a line-strength dependent offset. Since the trend is very weak in the range of observed line-strength for this index we apply only a normal offset.

With these corrections, our data qualify for comparisons with various models based on the Lick resolution. We are thus in the position to compare our data to the TMB03 models, which provide tabulated values of Lick indices as a function of age, [Z/H] and abundance ratio [α/Fe].

3.5.2 Comparison of measured indices

To examine the robustness of our approach for correcting the indices back to the Lick system, we compare the final corrected values of those galaxies common to Geha et al. (2003) and M08 with their published values. In Figure 3.13, we find that these adopted corrections give results consistent with the previously published data. Therefore, our further analyses (i.e., index analysis, comparison to models, and extraction of age and metallicity) are done using the Lick system, unless explicitely stated otherwise.

[5] http://idlastro.gsfc.nasa.gov/

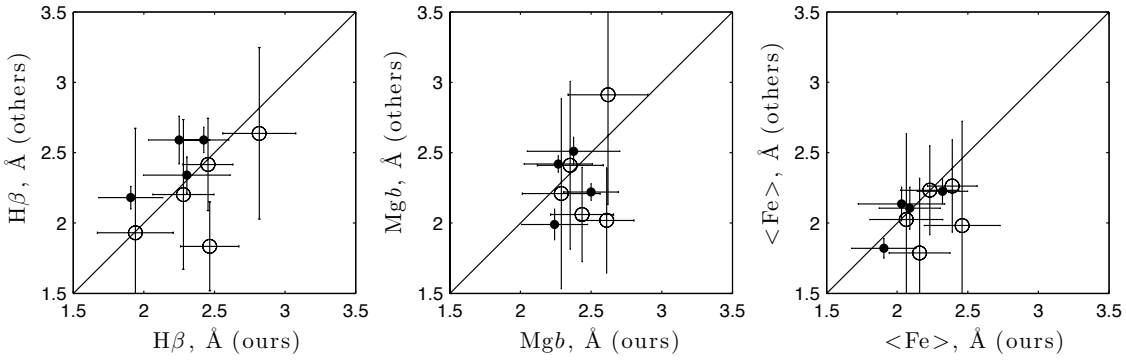

Figure 3.13: Comparison of our Lick indices, corrected back to the Lick system, with previously published data. Open circles represent the galaxies in common with the M08 sample and filled circles stand for the data of Geha et al. (2003).

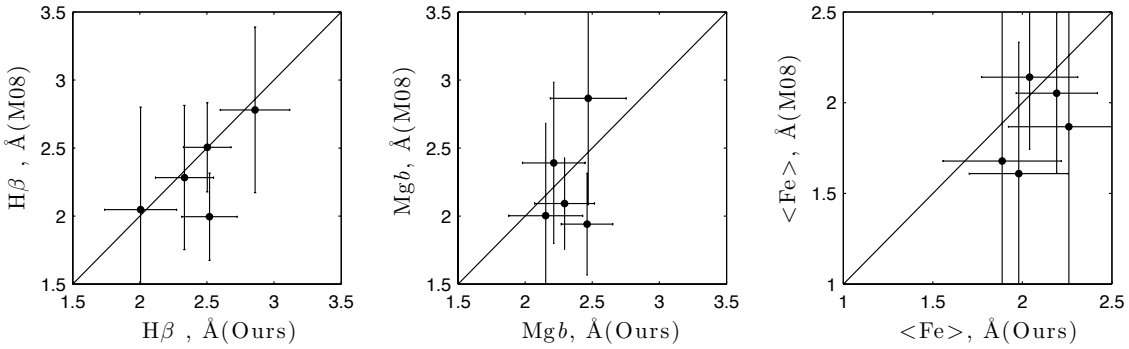

Figure 3.14: Comparison between the Lick indices measured from our and the M08 sample for the galaxies common to both samples, at the resolution 11Å.

4

Stellar populations of Virgo cluster early-type dwarf galaxies with and without discs: a dichotomy in age?

Abstract

Using high signal-to-noise ratio VLT/FORS2 spectroscopy, we have studied the properties of the central stellar populations and ages of a sample of 26 dEs in the Virgo Cluster. We conformed that these galaxies do not exhibit same stellar population for different morphology. The nucleated galaxy, which are distributed more dense region of the cluster are old (with mean age $9.61^{+14.21}_{-10.59}$ Gyr) and metal poor (with mean $\log(Z/Z_{\odot}) = -0.83^{+0.44}_{-0.44}$). On the other hand disc shaped dEs, which are distributed relatively farther region from the cluster center, have intermediate age and slightly enhanced metallicity of average $3.71^{+3.35}_{-1.96}$ Gyr & $\log(Z/Z_{\odot}) = -0.5^{+0.39}_{-0.36}$ respectively. We also found a week correlations between the luminosity weighted-mean age Vs over-density and anti-correlation of metallicity with over-density. We thus argue that the environment does play a crucial role during the evolution of dwarf galaxy and conclude that these galaxies cannot originate from same evolutionary history for different morphology. Old and metal poor dEs could have early termination of star formation activity with infall of primordial galaxy in the cluster potential are normal nucleated. By contrast, the discy galaxy, which are metal rich and relatively young, must have undergone through structural transformation of a late-type spiral into a spheroidal system.

Result published on S. Paudel et al., MNRAS, 405, 800, 2010.

Contents

Figures

4.1 Introduction

In previous chapter, we introduced some basic characteristics of our original early-type dwarf galaxies (dEs) sample. We already explained the important steps of data reduction procedure and the procedure that followed towards the Lick index measurement, including consistency checks of the models used, as well as tests and comparisons of Lick indices at different spectral resolutions. We will now concentrate on the derivation of stellar population parameters from well measured and calibrated absorption line strengths. As we described in chapter 2, we will use the stellar population model of TMB03 to derive age, metallicity and α-abundant ratio, however we use other models BC03 and AV/MILES to test the consistency of estimated stellar population parameters.

This Chapter particularly focuses on the variation of stellar population properties among the different morphological types of dEs. This chapter is organized as follows: In Section 4.2, we provide an overview of morphological diversity in dEs. Section 4.3 describes an extended sample of dEs, which we have obtained by adding the dEs sample of Michielsen et al. (2008): hereafter M08. Since, we already have described the data reduction and calibration of measured absorption line strength in the Lick system in Chapter 3, we only describe the derivation of stellar population parameters in Section 4.4. The results from our analysis are presented in Section 4.5, separating the actual index measurements (Section 4.5.1) and the subsequently derived ages and metallicities (Section 4.5.2). Finally, Section 4.6 presents the discussion of the results, and our conclusions.

4.2 A morphological diversity in dEs

The discovery of the substructures and morphological inhomogeneity in the dEs has been one major achievement since special image analysis techniques have been introduced to study the morphological properties of dEs. Pioneering contribution by Jerjen et al. (2000); Barazza et al. (2002) and extensive study of Lisker et al. (2006) later made clear, in fact, that dEs can not be regarded as homogeneous stellar system in the sense of color and substructure. These features can actually be seen in the dEs over a large range of magnitude. However, luminous populations seem to host more frequently than faint dEs.

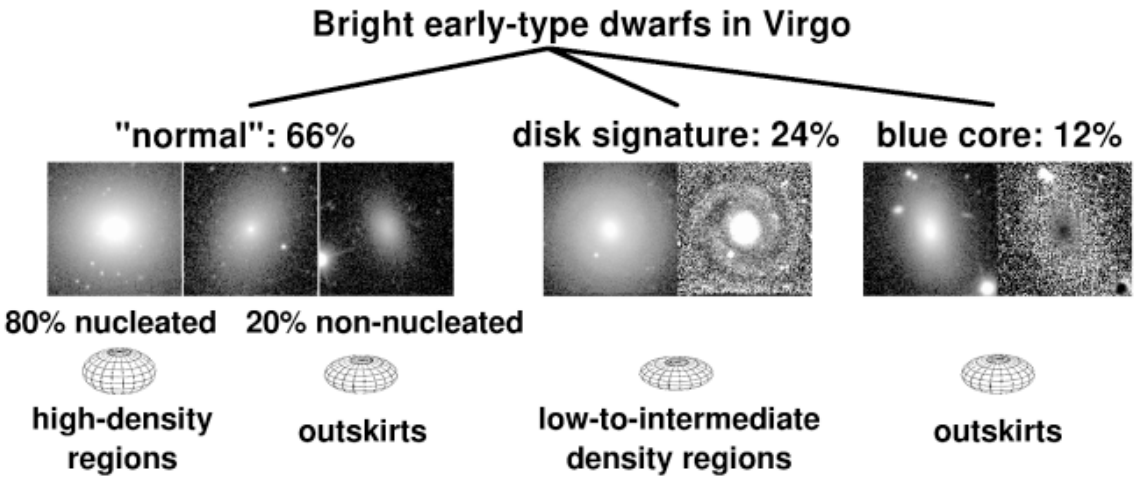

Figure 4.1: A morphological diversity in dEs: Lisker et al. (2007)

A recent systematic study by Lisker et al. (2006, 2007, hereafter L06 and L07, respectively) revealed a striking heterogeneity of the class of early-type dwarfs. They found different subclasses, with significantly different shapes, colors, and spatial distributions. Analyzing a large sample of dEs, Lisker et al classified the dEs mainly in three different morphological types: (1) dEs with disc features like spiral arms or bars dE(di), (2) dEs with central bright nucleus dE(N) (3) dEs without any prominent central nucleus dE(nN): see Figure 4.1. In addition, some dEs have central blue color excess classified as blue-centre dEs i.e. dE(bc). However, these classifications are not straightforward, there are some dEs with disc feature and blue color excess in the centre. Therefore, for the shake of simplicity Lisker et al purpose a cumulative way of classification i.e. a nucleated, discy and blue centre dE can be classified as a dE(N,di,bc) and non-nucleated but with disc feature are represented with dE(nN,di). The classification of a dE as nucleated and non-nucleated is not unambiguous. Many Virgo dEs that were classified as non-nucleated in the VCC actually host a faint nucleus that was hardly detectable with the VCC data (Grant et al., 2005; Côté et al., 2006). A more appropriate term might be *dEs without a nucleus of significant relative brightness* as compared to the central galaxy light. Grant et al. (2005) pointed out that dEs classified as nucleated and non-nucleated might actually form a continuum with respect to relative nucleus brightness.

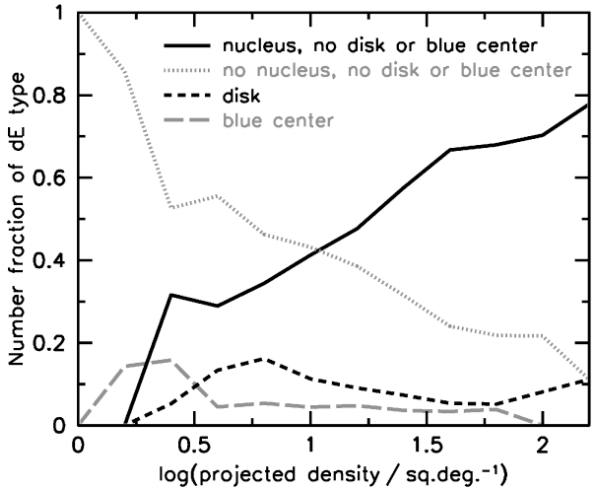

Figure 4.2: Morphology-density relation within the dE class: Lisker (2009)

The dEs with disc feature are preferentially distributed in the cluster outskirts. On the other hand, nucleated smooth dEs are mainly found in dense cluster center and they are relatively red in color than dEs with disc feature: see Figure 4.2 for morphology-density relation within the dE class in Virgo cluster. Lisker et al. also show that almost a quarter of dEs in their sample host disc features and it arises with the fraction of 50% at the bight end. The analysis of the projected axial ratio of dEs shows the non-nucleated dEs are flatter than the nucleated ones. From the distributions of projected axial ratios, Lisker et al. (2007) estimated intrinsic axial ratio distributions for the different subclasses, which are illustrated in Figure 4.1:. dE(nN)s are flatter than dE(N)s (the difference disappears towards fainter magnitudes), dE(bc)s have similarly flat shapes as the dE(nN)s, and dE(di)s are the flattest population (Lisker, 2009).

These morphologically different dEs, with significantly different in colors and spatial distributions, could have gone through different evolutionary processes. Those dEs with a disk component have a flat shape and are predominantly found in the outskirts of the cluster, suggesting that they – or their progenitors – might have just recently fallen into the cluster environment. In contrast, dEs with a compact stellar nucleus follow the classical picture of dwarf ellipticals: they are spheroidal objects that are preferentially found in the dense cluster center. Thus, given the structural heterogeneity and the scatter in their stellar population characteristics, the question

arises whether they have a similar or different formation history? Here we address this question with exploring the relation between their stellar populations, structural parameters and the environment.

4.3 The sample

Table 4.1: Galaxies from Michielsen et al. (2008) incorporated in our extended sample.

Name	RA	Dec	Type	M_r	Density[a]	R_{eff}	RV	Remark
VCC0021	12:10:23.15	10:11:19.04	bc,N	−17.01	1.8	15.2	486 ± 25	
VCC0397	12:20:12.18	06:37:23.56	di,N	−16.76	—	12.4	2471 ± 46	poss. mem.
VCC0523	12:22:04.14	12:47:14.60	di,N	−18.57	20.2	25.7	1981 ± 20	
VCC0917	12:26:32.39	13:34:43.54	-	−16.55	45.9	9.2	1238 ± 20	removed
VCC1087	12:28:14.90	11:47:23.58	N	−18.50	54.9	28.4	675 ± 12	
VCC1122	12:28:41.71	12:54:57.08	N	−17.13	66.0	19.1	476 ± 10	
VCC1183	12:29:22.51	11:26:01.73	di,N	−17.82	28.2	19.6	1335 ± 12	
VCC1431	12:32:23.41	11:15:46.94	N	−17.72	30.2	9.3	1505 ± 21	
VCC1549	12:34:14.83	11:04:17.51	N	−17.24	28.3	10.9	1357 ± 37	
VCC1695	12:36:54.85	12:31:11.93	di	−17.63	21.4	22.8	1547 ± 29	
VCC1910	12:42:08.67	11:45:15.19	di,N	−17.86	28.1	13.6	206 ± 26	
VCC1912	12:42:09.07	12:35:47.93	bc,N	−17.83	19.6	22.3	−169 ± 28	
VCC1947	12:42:56.37	03:40:36.12	di,N	−17.61	—	9.4	974 ± 19	poss. mem.

[a]Local projected galaxy number density

We build an extended sample by adding Virgo dEs from the M08 sample whose morphology is defined in L06. The MAGPOP ITP[1] provide us flux calibrated spectra of their sample dEs. M08 selected their galaxies to be brighter than $m_B <\sim 15$ mag, with high central surface brightness, and all hosting a central nucleus. In total, our extended sample thus comprises three dE(bc)s (of which one also hosts a disc, as mentioned above), 13 dE(di)s, and 22 dE(N)s that do not show disc features, which comprises disky versus non-disky ratio $\sim \frac{1}{2}$ with the fairly large density range ∼3 to ∼70. Note that we removed VCC 0917 from M08 sample because it has a different subclass, as this galaxy is neither discy, nucleated, nor blue-centered according to L06.

We believe that this is a representative sample of bright-nucleated early-type dwarf galaxies in the Virgo cluster with different sub-structural types. Table 4.1 lists the M08 sample galaxies and some of their basic properties.

For this work, we use central four arc-sec aperture, which corresponding to 320 pc with a distance modulus $m - M = 31.09$ (16.5 Mpc, Mei et al. 2007), to extract the one dimensional spectra. This is done in order to guarantee that the resulting Lick indices will have sufficiently small errors to allow a precise stellar population analysis, and to enable a direct comparison with the sample of M08, who used the same extraction aperture.

4.4 Extraction of stellar population parameters from model fitting

As the aim of our work is to understand the star formation and evolutionary history of dwarf galaxies, we extract stellar population characteristics from those indices, and combinations of

[1]http://www.astro.rug.nl/~peletier/MAGPOP_ITP.html

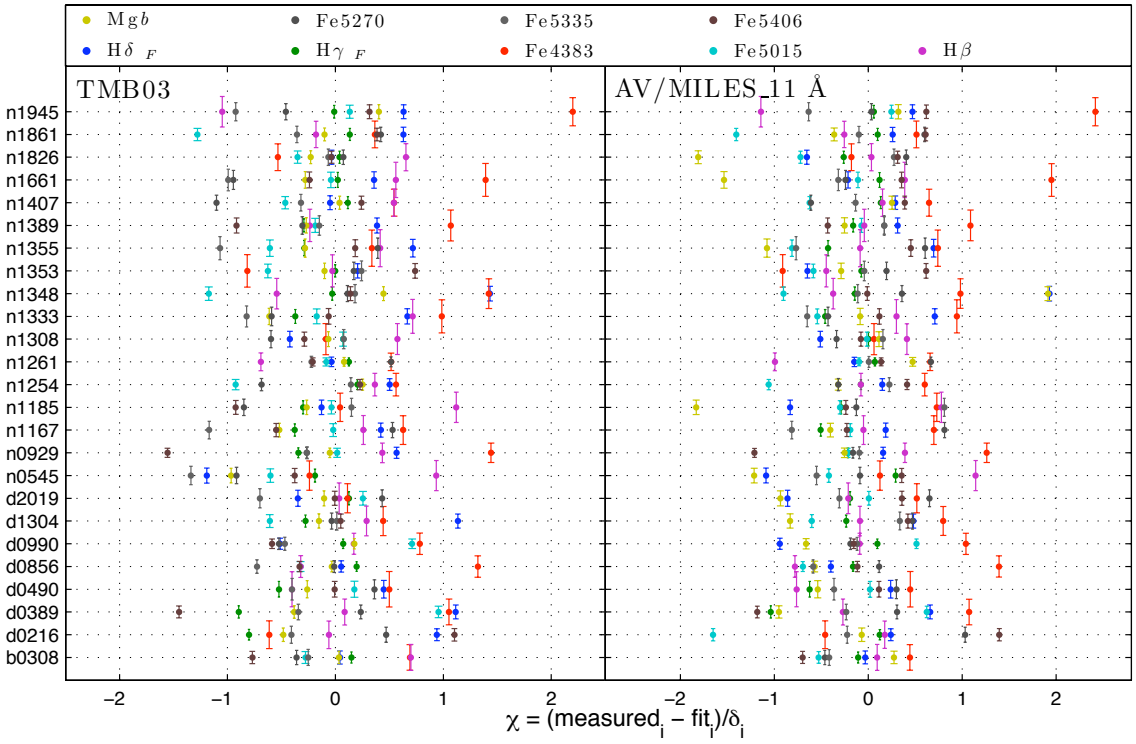

Figure 4.3: Distribution of the deviation of indices from the best fit model point. The Y-axis is labeled with the VCC number of our target galaxies preceded by a letter indicating their galaxy type.

indices, that are sensitive to age, metallicity, or the relative abundance of different metals. Population synthesis models then provide us with SSP-equivalent, or mean luminosity-weighted, ages and metallicities. It is necessary to mention that the SSP-equivalent ages are biased towards younger ages (Trager et al., 2000a, 2005) since in the optical, most of the light comes from the youngest component of the stellar population, and the age correlates most strongly with last star formation activity. Therefore, the measured age is influenced to a large extent by the last star formation activity in the galaxy. However, the SSP-equivalent metallicity is an excellent tracer of the light-weighted metallicity (Trager & Somerville, 2009). This is because hot, young stars contribute little to the metal lines in a composite spectrum (Trager et al., 2005; Serra & Trager, 2007).

To convert our measured indices to ages and metallicities, we used the χ^2-minimization method as suggested by Proctor et al. (2004). In this method, we have the advantage to use a large set of indices to get the best fitting stellar population parameters. Therefore, it makes better use of the information that directly depends on age, metallicity and $\alpha-$element abundance ratio, as compared to an analysis of single indices or index pairs. To perform the model fits, we first interpolated the model grid of TMB03 to a finer grid. The actual χ^2-minimization was then performed on the age, [Z/H], and [α/Fe] parameter space. While the method allows us to use as many indices as possible, we used only the nine indices with the best measurement quality (Hδ_F, Hγ_F, Fe4383, Hβ, Fe5015, Mgb, Fe5270, Fe5335 & Fe5406) among the measured Lick indices from our spectra, which are tabulated in Table 4.2. To calculate the uncertainties in the stellar population parameters, we transformed the index error to the stellar population error contours and obtained the maximum of the error from that.

In Figure 4.4, we show the comparison of derived ages and metallicities using different SSP models (TMB03 & AV/MILES). We derived TMB03 ages and metallicities by correcting our

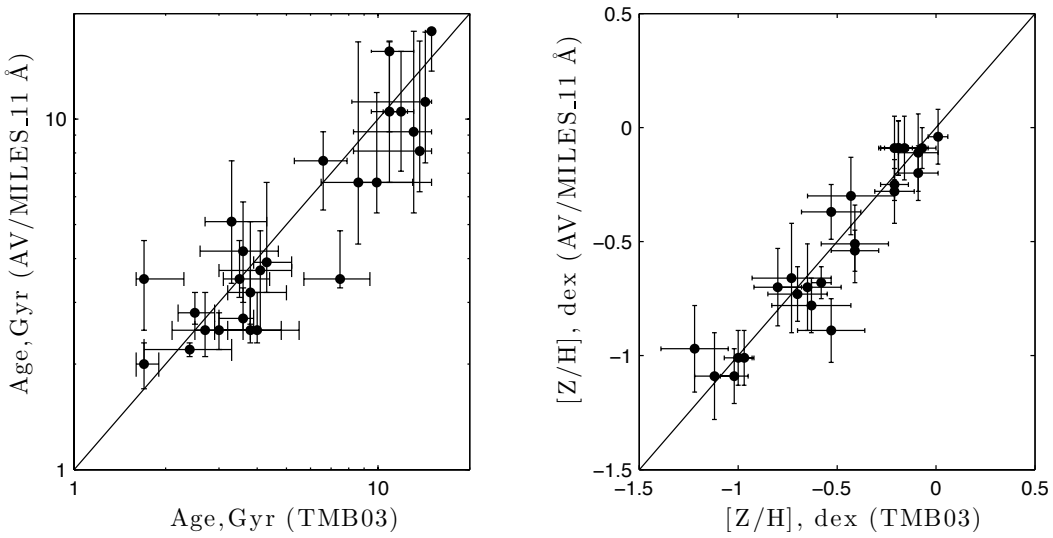

Figure 4.4: Comparison between derived age & metallicity using the TMB03 model at Lick resolution and the AV/MILES model at our resolution, i.e., 11 Å.

data to the Lick system as described above, while AV/MILES ages and metallicities were obtained directly at the resolution of our data (11 Å), by degrading the AV/MILES model down to this resolution prior to the model fitting. We use the same set of nine indices in both cases. Although, the measured age and metallicity agree well within the error limit, it seems that the majority of derived ages are overestimated, when we used the model TMB03. As a further test to check the source of this slight offset, we compared the estimated SSP parameters from the model AV/MILES at different resolutions (i.e., at 9 Å and 11 Å) for the M08 sample. While no strong deviation is seen, there might be a small systematic bias of having younger ages when we degrade the resolution, Figure 4.5). In any case, the estimated ages at different resolution agree well within the errors.

The behavior of the nine well-measured indices with respect to the best-fit model index value is shown in Figure 4.3. Each color represents a different index; the galaxy number along with its subtype label is provided as y-axis. Clearly, the index values lie well within the 2σ uncertainty range, and surprisingly, in the vast majority of cases even within the 1σ limit. It is interesting that the deviation of the Mg*b* indices for the AV/MILES model is systematically negative in almost all cases, and only for VCC 1348 it shows a significantly positive deviation. This galaxy has the highest $\alpha-$element abundance among our sample (see Table 4.4). On the other hand, for the TMB03 model, the distribution of Mg*b* indices is rather symmetric, and all lie within the 1σ error limit. Therefore the asymmetric distribution of Mg*b* for the AV/MILES model can be interpreted as an effect of having a fixed solar $\alpha-$element abundance ratio. We also note that the deviations of Fe5015 and Fe4383 are mostly positive, while Fe5335 and Fe5406 have negative deviations in most cases. However, the overall mean of the deviations for all indices is always less than half of sigma for the model TMB03.

The derived values of age and metallicity for our dEs, along with their uncertainties, using the TMB03 model, are tabulated in Table 4.4. We also remeasured age and metallicity for the spectral sample of M08, using the same nine indices as in our sample. This guarantees a proper comparison, because M08 have used a different approach (i.e. quadratic interpolation over the nearest SSP model grid points in the Hβ-[MgFe] diagram, as suggested by the method of Cardiel et al. 2003). Interestingly, we obtain a smaller error on age and metallicity, as compared to their measurement. Nevertheless, the measured ages and metallicities match very well (see Figure

4.5 left panel).

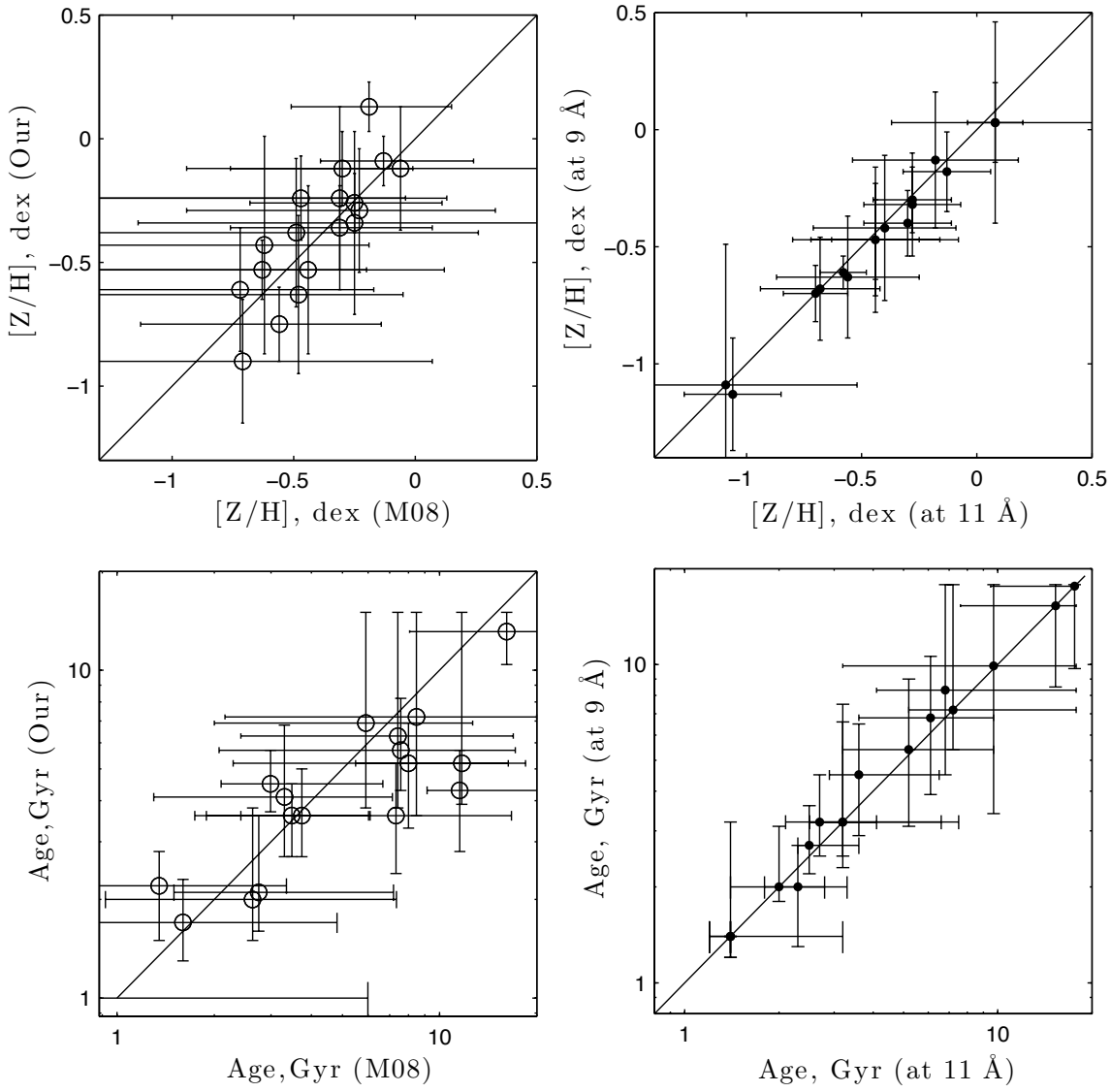

Figure 4.5: Left: Comparison between the derived metallicity (top) and age (bottom) with TMB03 for our sample and that of M08. We use different approaches, i.e. following Proctor et al. (2004) and Cardiel et al. (2003) by us and by M08, respectively.
Right: Comparison of derived stellar population parameters from the AV/MILES model at different resolutions for the M08 sample.

4.5 Results

In this section, we first show the measured indices directly, in correlations with galaxy absolute magnitude, and in simple diagnostic index versus index plots, which compare them to model grids of age and metallicity. Finally, we analyze the stellar population results obtained from model fitting.

4.5.1 Lick indices for Virgo dEs

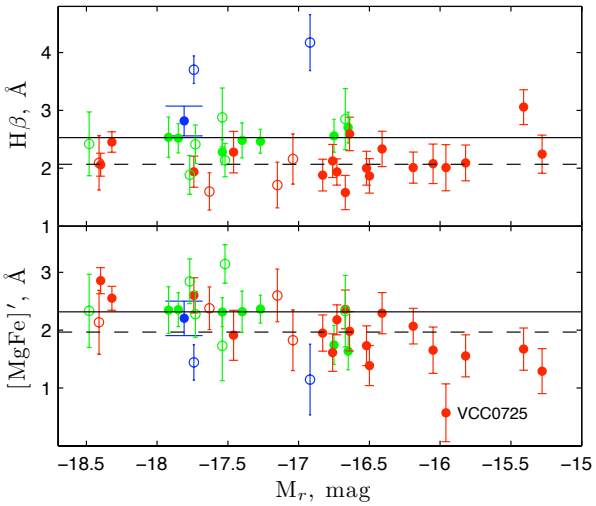

Figure 4.6: Relations between M$_r$ and the indices used as age and metallicity indicators (dE(bc): blue, dE(di): green, dE(N): red). Open circles represent dEs from the M08 sample. The median of the indices is represented by the dashed horizontal line for the dE(N)s and by the solid line for the dE(di)s.

The relation of the galaxy magnitude and the indices that are widely used as age and metallicity indicators (i.e. Hβ as good age indicator and [MgFe]′ as good mean metallicity indicator, with [MgFe]′ = $\sqrt{\text{Mg}b \times (0.72 \times \text{Fe5270} + 0.28 \times \text{Fe5335})}$ (Thomas et al. 2003)) are shown in Figure 4.6. It is remarkable that we do not see any correlation between the age sensitive index Hβ and magnitude, while a small but clear offset between nucleated early-type dwarfs with and without discs (dE(di) and dE(N), respectively) is seen. On the other hand, the metallicity sensitive index [MgFe]′ shows a weak anti-correlation with M$_r$, from the brighter dE(di)s down to the fainter dE(N)s. As we know (Worthey et al., 1994a), there are no such pure indices which only depend on either age or metallicity. Therefore, the exploration of age and metallicity by comparing the indices or their combinations to model predictions is presented further below.

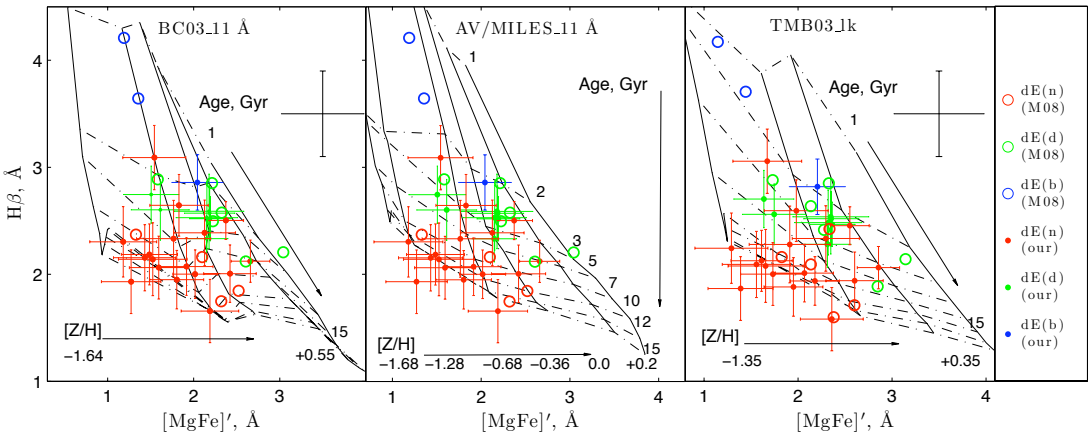

Figure 4.7: The age-sensitive index Hβ as a function of the metallicity-sensitive index [MgFe]′. Overplotted grid lines are the stellar population models of BC03(left), AV/MILES (middle) & TMB03 with [α/Fe] = 0.0 dex (right). The points without error bars are from the M08 sample; the mean error for these data is shown as a cross in the upper right corner of each panel. Colors and symbols are the same as in Figure 4.6.

Note VCC 0725 is an outlier, due to its fairly low Mgb content (see 4.2). This galaxy is one of the faintest among our sample and there is almost no galaxy light beyond the central nucleus. Therefore, we suspect that a fairly large domination of the residual sky noise within the four-

arcsec aperture could produce such an effect. Hence, we remove this galaxy from the sample during the subsequent analysis.

Figure 4.7 shows the distribution in Hβ versus [MgFe]′ of dEs and a grid of simple stellar population models of BC03, AV/MILES & TMB03 (with [α/Fe] = 0.0 dex). We use [MgFe]′ as a metallicity indicator, which is considered independent of [α/Fe]-abundance, and Hβ as age indicator, because its age sensitivity is greater and it is less degenerate with metallicity or abundance ratio variations than the other Balmer indices (Korn et al., 2005). The solid lines, which are close to vertical, are of constant metallicity, whereas the dashed lines, which are close to horizontal, connect constant-age models (from top to bottom: 1, 2, 3, 5, 7, 10, 12, & 15 Gyr). All three panels appear to be fairly consistent with each other. However, there are some galaxies that lie outside of the model grid, located at low Hβ, i.e., at the bottom left corner of the grid. Nevertheless, when taking into account their errorbars, they could still lie within the grid region. Moreover, it is not surprising that some galaxies (particularly dEs) fall outside of model grid. The same problem has already been noticed in the similar type of study of the dEs in the Coma cluster by Poggianti et al. (2001). This can be an issue of how the mass loss along the red giant branch is treated in the models, as discussed by Maraston et al. (2003).

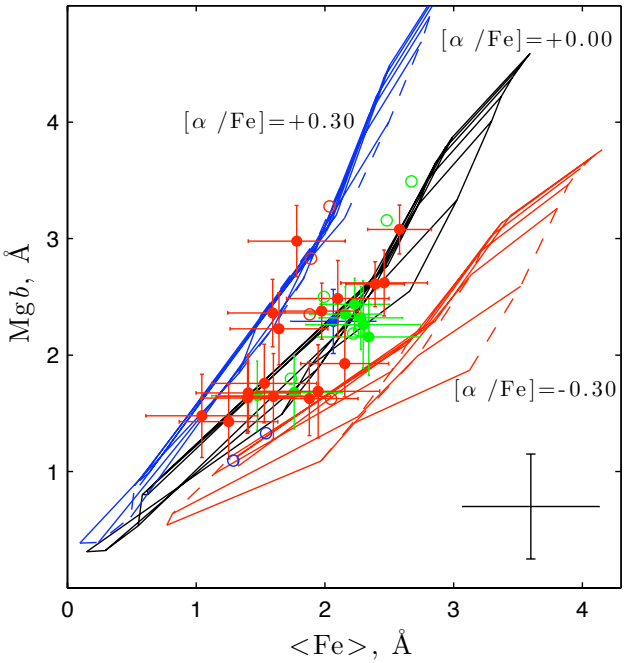

Figure 4.8: Central Mg versus <Fe> indices after correcting back to Lick resolution, superimposed on the TMB03 model with different ages, metallicities, and abundance ratios. The symbols are the same as in Figure 4.7.

We can see that most of the dEs appear to have sub-solar metallicity, supporting the results of van Zee et al. (2004), M08, Geha et al. (2003), Koleva et al. (2009) . On the other hand, their ages span a wide range. It is apparent that all dEs with blue central colors (dE(bc), blue symbols) are located towards fairly young ages, falling above the 3 Gyr line in the figure. There is almost no overlap between the dE(bc) and the dE(N) (red symbols), except for VCC 1353. Furthermore, most of the discy dEs (dE(di), green in color) lie in between dE(N) and dE(bc).

Thus, a clear division of the different subclasses in terms of age is present, with low, intermediate and high ages for dE(bc), dE(di) and dE(N), respectively. Despite of having a much larger spread, the dE(N)s are clustered in the bottom left corner of the grid – or even below the grid in some cases – centered on the low metallicity region. Interestingly, only three dE(di)s fall left of the metallicity line of [Z/H] = −0.36 dex.

Figure 4.8 presents the Mgb vs <Fe> diagram, where the data are superimposed on the TMB03

Table 4.2: Measured central line-strength indices corrected to the Lick/IDS system, measured in the central 4 arcsec with one sigma error

Galaxy VCC	Hδ_F Å	Hγ_F Å	Fe4383 Å	Hβ Å	Fe5015 Å	Mgb Å	Fe5270 Å	Fe5335 Å	Fe5406 Å
0308	2.29 ± 0.28	1.66 ± 0.24	3.46 ± 0.56	2.82 ± 0.26	4.78 ± 0.57	2.29 ± 0.28	2.20 ± 0.31	1.93 ± 0.35	1.07 ± 0.27
0216	3.73 ± 0.26	2.75 ± 0.23	1.07 ± 0.61	2.70 ± 0.27	3.19 ± 0.60	1.65 ± 0.30	1.81 ± 0.33	1.14 ± 0.38	1.12 ± 0.27
0389	1.57 ± 0.30	0.09 ± 0.27	4.38 ± 0.56	2.52 ± 0.25	4.61 ± 0.57	2.32 ± 0.27	2.53 ± 0.30	2.03 ± 0.34	0.99 ± 0.26
0490	1.72 ± 0.39	0.56 ± 0.34	4.07 ± 0.78	2.54 ± 0.35	4.30 ± 0.77	2.26 ± 0.38	2.62 ± 0.42	1.98 ± 0.47	1.38 ± 0.35
0856	1.39 ± 0.25	0.57 ± 0.21	4.26 ± 0.47	2.28 ± 0.22	4.36 ± 0.48	2.35 ± 0.23	2.42 ± 0.26	1.90 ± 0.29	1.27 ± 0.23
0990	1.13 ± 0.25	0.40 ± 0.21	4.26 ± 0.47	2.47 ± 0.21	4.73 ± 0.46	2.44 ± 0.22	2.38 ± 0.25	2.09 ± 0.28	1.29 ± 0.21
1304	2.66 ± 0.31	1.60 ± 0.27	2.68 ± 0.64	2.56 ± 0.28	3.66 ± 0.65	1.68 ± 0.31	1.89 ± 0.35	1.64 ± 0.39	1.02 ± 0.31
2019	1.24 ± 0.35	0.63 ± 0.29	3.98 ± 0.64	2.48 ± 0.30	4.70 ± 0.68	2.16 ± 0.33	2.70 ± 0.37	1.98 ± 0.42	1.45 ± 0.31
0545	1.14 ± 0.33	0.61 ± 0.29	2.44 ± 0.65	1.87 ± 0.30	3.74 ± 0.66	1.43 ± 0.32	1.48 ± 0.36	1.03 ± 0.40	0.83 ± 0.31
0725	2.51 ± 0.39	1.27 ± 0.36	1.55 ± 0.85	2.01 ± 0.40	3.46 ± 0.88	0.19 ± 0.45	1.74 ± 0.48	1.37 ± 0.55	0.75 ± 0.40
0929	0.80 ± 0.24	-0.59 ± 0.21	5.38 ± 0.43	2.06 ± 0.20	5.44 ± 0.43	3.08 ± 0.21	2.74 ± 0.23	2.42 ± 0.26	1.29 ± 0.20
1167	1.86 ± 0.31	0.71 ± 0.27	2.68 ± 0.63	2.13 ± 0.29	3.11 ± 0.63	1.63 ± 0.30	1.84 ± 0.34	0.96 ± 0.39	0.67 ± 0.29
1185	1.16 ± 0.32	0.27 ± 0.29	3.29 ± 0.62	2.00 ± 0.29	4.33 ± 0.67	1.63 ± 0.32	1.80 ± 0.36	1.96 ± 0.40	0.89 ± 0.30
1254	1.36 ± 0.26	0.28 ± 0.22	3.62 ± 0.50	1.94 ± 0.23	4.24 ± 0.49	2.38 ± 0.24	2.03 ± 0.27	1.92 ± 0.30	1.24 ± 0.22
1261	1.50 ± 0.21	0.66 ± 0.18	3.99 ± 0.38	2.45 ± 0.18	4.48 ± 0.39	2.61 ± 0.19	2.63 ± 0.21	2.15 ± 0.24	1.37 ± 0.18
1308	1.22 ± 0.34	0.46 ± 0.30	3.48 ± 0.68	2.33 ± 0.31	4.85 ± 0.68	2.49 ± 0.33	2.14 ± 0.38	2.06 ± 0.42	1.20 ± 0.31
1333	2.58 ± 0.34	1.33 ± 0.30	2.51 ± 0.73	2.24 ± 0.33	3.14 ± 0.74	1.48 ± 0.36	1.23 ± 0.41	0.85 ± 0.46	0.69 ± 0.34
1348	1.83 ± 0.32	-0.08 ± 0.29	3.70 ± 0.65	1.58 ± 0.30	3.31 ± 0.67	2.98 ± 0.31	1.98 ± 0.35	1.58 ± 0.40	0.98 ± 0.30
1353	3.34 ± 0.31	2.69 ± 0.27	0.89 ± 0.72	3.06 ± 0.30	3.12 ± 0.71	1.76 ± 0.34	1.68 ± 0.38	1.38 ± 0.43	1.03 ± 0.32
1355	1.98 ± 0.39	0.97 ± 0.34	3.50 ± 0.80	2.28 ± 0.36	4.41 ± 0.82	1.69 ± 0.40	2.44 ± 0.45	1.46 ± 0.51	1.34 ± 0.37
1389	1.92 ± 0.33	0.79 ± 0.29	2.91 ± 0.68	2.09 ± 0.31	2.71 ± 0.71	1.67 ± 0.33	1.50 ± 0.38	1.30 ± 0.43	0.50 ± 0.33
1407	1.46 ± 0.30	0.31 ± 0.27	3.27 ± 0.59	1.88 ± 0.27	3.90 ± 0.60	2.36 ± 0.29	1.64 ± 0.33	1.55 ± 0.37	1.10 ± 0.28
1661	1.39 ± 0.36	0.44 ± 0.33	4.29 ± 0.72	2.08 ± 0.34	4.12 ± 0.77	1.65 ± 0.37	1.75 ± 0.42	1.46 ± 0.47	1.11 ± 0.35
1826	1.12 ± 0.31	0.26 ± 0.26	3.25 ± 0.59	2.01 ± 0.27	4.40 ± 0.59	1.93 ± 0.29	2.31 ± 0.32	2.00 ± 0.36	1.26 ± 0.27
1861	1.34 ± 0.31	0.23 ± 0.27	4.35 ± 0.59	1.94 ± 0.27	4.78 ± 0.58	2.62 ± 0.28	2.74 ± 0.32	2.18 ± 0.36	1.58 ± 0.28
1945	2.13 ± 0.31	1.17 ± 0.28	4.12 ± 0.62	2.59 ± 0.29	3.20 ± 0.67	2.23 ± 0.31	1.92 ± 0.36	1.37 ± 0.40	1.20 ± 0.30

Table 4.3: Measured central line-strength indices corrected to the Lick/IDS system, measured in the central 4 arcsec with one sigma error

VCC	Ca4227	Ca4455	CN1	CN2	Fe4531	C4668	Fe5709	Fe5782	G4300	Mg1	Mg2
No.	Å	Å	mag	mag	Å	Å	Å	Å	Å	mag	mag
0308	0.77 ± 0.21	0.57 ± 0.29	-0.06 ± 0.01	-0.02 ± 0.01	2.51 ± 0.43	2.90 ± 0.67	0.73 ± 0.19	0.43 ± 0.19	3.06 ± 0.39	0.03 ± 0.006	0.119 ± 0.007
0216	0.52 ± 0.22	0.12 ± 0.30	-0.10 ± 0.01	-0.07 ± 0.01	1.70 ± 0.45	2.04 ± 0.69	0.49 ± 0.21	0.41 ± 0.20	1.76 ± 0.41	0.02 ± 0.006	0.090 ± 0.007
0389	0.59 ± 0.23	0.49 ± 0.29	-0.01 ± 0.01	0.00 ± 0.01	2.56 ± 0.43	3.54 ± 0.67	0.59 ± 0.19	0.50 ± 0.18	3.84 ± 0.39	0.04 ± 0.006	0.147 ± 0.007
0490	1.27 ± 0.28	0.82 ± 0.39	-0.06 ± 0.01	-0.01 ± 0.02	2.75 ± 0.59	3.85 ± 0.89	0.75 ± 0.26	0.39 ± 0.25	3.57 ± 0.53	0.04 ± 0.008	0.130 ± 0.010
0856	0.61 ± 0.25	0.99 ± 0.33	-0.07 ± 0.01	-0.04 ± 0.01	1.61 ± 0.51	2.34 ± 0.78	0.80 ± 0.22	0.26 ± 0.21	3.40 ± 0.43	0.03 ± 0.007	0.121 ± 0.008
0990	1.28 ± 0.17	0.99 ± 0.24	-0.06 ± 0.01	-0.02 ± 0.01	2.23 ± 0.37	3.49 ± 0.55	0.74 ± 0.16	0.71 ± 0.16	4.33 ± 0.31	0.04 ± 0.005	0.135 ± 0.006
1304	0.88 ± 0.18	0.99 ± 0.23	-0.03 ± 0.01	0.00 ± 0.01	2.70 ± 0.35	3.53 ± 0.54	0.76 ± 0.16	0.58 ± 0.15	4.23 ± 0.31	0.03 ± 0.005	0.135 ± 0.006
2019	0.82 ± 0.24	0.39 ± 0.33	-0.09 ± 0.01	-0.05 ± 0.01	1.94 ± 0.50	2.01 ± 0.77	0.61 ± 0.22	0.31 ± 0.21	2.62 ± 0.45	0.02 ± 0.007	0.089 ± 0.008
0545	0.97 ± 0.25	0.62 ± 0.34	-0.02 ± 0.01	0.00 ± 0.01	2.90 ± 0.50	3.68 ± 0.77	0.70 ± 0.24	0.51 ± 0.23	4.07 ± 0.44	0.03 ± 0.007	0.133 ± 0.008
0725	0.39 ± 0.32	0.43 ± 0.43	-0.10 ± 0.01	-0.06 ± 0.02	1.62 ± 0.65	1.98 ± 1.03	0.28 ± 0.30	0.38 ± 0.27	3.31 ± 0.57	0.02 ± 0.009	0.078 ± 0.011
0929	1.33 ± 0.17	1.16 ± 0.22	-0.04 ± 0.01	-0.00 ± 0.01	2.81 ± 0.32	4.94 ± 0.51	0.81 ± 0.15	0.45 ± 0.14	5.14 ± 0.29	0.05 ± 0.005	0.169 ± 0.006
1167	0.54 ± 0.24	0.11 ± 0.32	-0.03 ± 0.01	-0.00 ± 0.01	2.06 ± 0.46	1.76 ± 0.74	0.26 ± 0.21	0.13 ± 0.20	3.33 ± 0.43	0.03 ± 0.007	0.119 ± 0.008
1185	0.67 ± 0.25	0.83 ± 0.32	-0.03 ± 0.01	-0.01 ± 0.01	1.94 ± 0.50	2.20 ± 0.78	0.45 ± 0.22	0.46 ± 0.21	4.21 ± 0.42	0.03 ± 0.007	0.110 ± 0.008
1254	0.92 ± 0.18	0.70 ± 0.25	0.02 ± 0.01	0.06 ± 0.01	2.38 ± 0.38	2.44 ± 0.58	0.48 ± 0.17	0.35 ± 0.16	3.92 ± 0.33	0.04 ± 0.005	0.141 ± 0.006
1261	0.93 ± 0.15	0.85 ± 0.20	-0.04 ± 0.00	-0.00 ± 0.01	2.86 ± 0.30	3.79 ± 0.45	0.84 ± 0.14	0.47 ± 0.13	3.85 ± 0.26	0.03 ± 0.004	0.133 ± 0.005
1308	0.95 ± 0.25	0.90 ± 0.34	-0.04 ± 0.01	0.00 ± 0.01	2.70 ± 0.51	3.10 ± 0.79	0.64 ± 0.23	0.45 ± 0.22	4.24 ± 0.45	0.03 ± 0.007	0.129 ± 0.009
1333	0.68 ± 0.27	0.82 ± 0.37	-0.11 ± 0.01	-0.06 ± 0.01	1.01 ± 0.58	0.79 ± 0.88	0.21 ± 0.25	0.01 ± 0.24	2.93 ± 0.49	0.02 ± 0.008	0.082 ± 0.009
1348	0.78 ± 0.24	0.59 ± 0.33	0.00 ± 0.01	0.06 ± 0.01	2.66 ± 0.48	2.82 ± 0.78	0.34 ± 0.22	0.43 ± 0.21	4.78 ± 0.42	0.06 ± 0.007	0.161 ± 0.008
1353	0.56 ± 0.26	0.29 ± 0.35	-0.10 ± 0.01	-0.06 ± 0.01	2.04 ± 0.54	2.03 ± 0.83	0.59 ± 0.23	0.21 ± 0.23	1.67 ± 0.49	0.01 ± 0.008	0.083 ± 0.009
1355	0.64 ± 0.30	0.50 ± 0.40	-0.06 ± 0.01	-0.03 ± 0.02	2.40 ± 0.59	3.92 ± 0.96	0.42 ± 0.29	0.49 ± 0.26	3.89 ± 0.53	0.04 ± 0.009	0.125 ± 0.010
1389	0.50 ± 0.26	0.45 ± 0.35	-0.03 ± 0.01	-0.00 ± 0.01	1.89 ± 0.51	1.15 ± 0.83	0.48 ± 0.23	0.13 ± 0.23	3.09 ± 0.46	0.02 ± 0.008	0.087 ± 0.009
1407	0.73 ± 0.22	0.63 ± 0.30	-0.01 ± 0.01	0.01 ± 0.01	2.32 ± 0.47	2.22 ± 0.71	0.49 ± 0.21	0.30 ± 0.20	4.18 ± 0.40	0.04 ± 0.007	0.140 ± 0.008
1661	0.71 ± 0.28	0.60 ± 0.39	0.02 ± 0.01	0.06 ± 0.01	2.03 ± 0.58	1.10 ± 0.93	0.60 ± 0.24	0.11 ± 0.23	3.41 ± 0.49	0.04 ± 0.008	0.116 ± 0.009
1826	0.84 ± 0.22	0.61 ± 0.30	-0.08 ± 0.01	-0.05 ± 0.01	2.42 ± 0.44	3.06 ± 0.70	0.69 ± 0.21	0.51 ± 0.19	4.17 ± 0.39	0.02 ± 0.006	0.119 ± 0.007
1861	1.11 ± 0.22	0.71 ± 0.30	-0.02 ± 0.01	0.00 ± 0.01	2.87 ± 0.44	3.57 ± 0.68	0.88 ± 0.21	0.45 ± 0.19	4.57 ± 0.40	0.04 ± 0.006	0.146 ± 0.007
1945	0.90 ± 0.24	0.55 ± 0.33	-0.02 ± 0.01	0.02 ± 0.01	2.41 ± 0.48	2.04 ± 0.78	0.64 ± 0.21	0.45 ± 0.20	3.80 ± 0.42	0.03 ± 0.007	0.106 ± 0.008

model with various $\alpha-$element abundance ratios: [α/Fe]= −0.3, 0.0, and +0.3 dex. The results from previous studies of the stellar populations of low-mass systems (Gorgas et al., 1997; Geha et al., 2003; Thomas et al., 2003), that the $\alpha-$element abundance of dEs is consistent with solar, seem to be in agreement with our study. However, the scatter is fairly large for the dE(N)s, and on average they might be slightly more $\alpha-$enhanced than the dE(di)s.

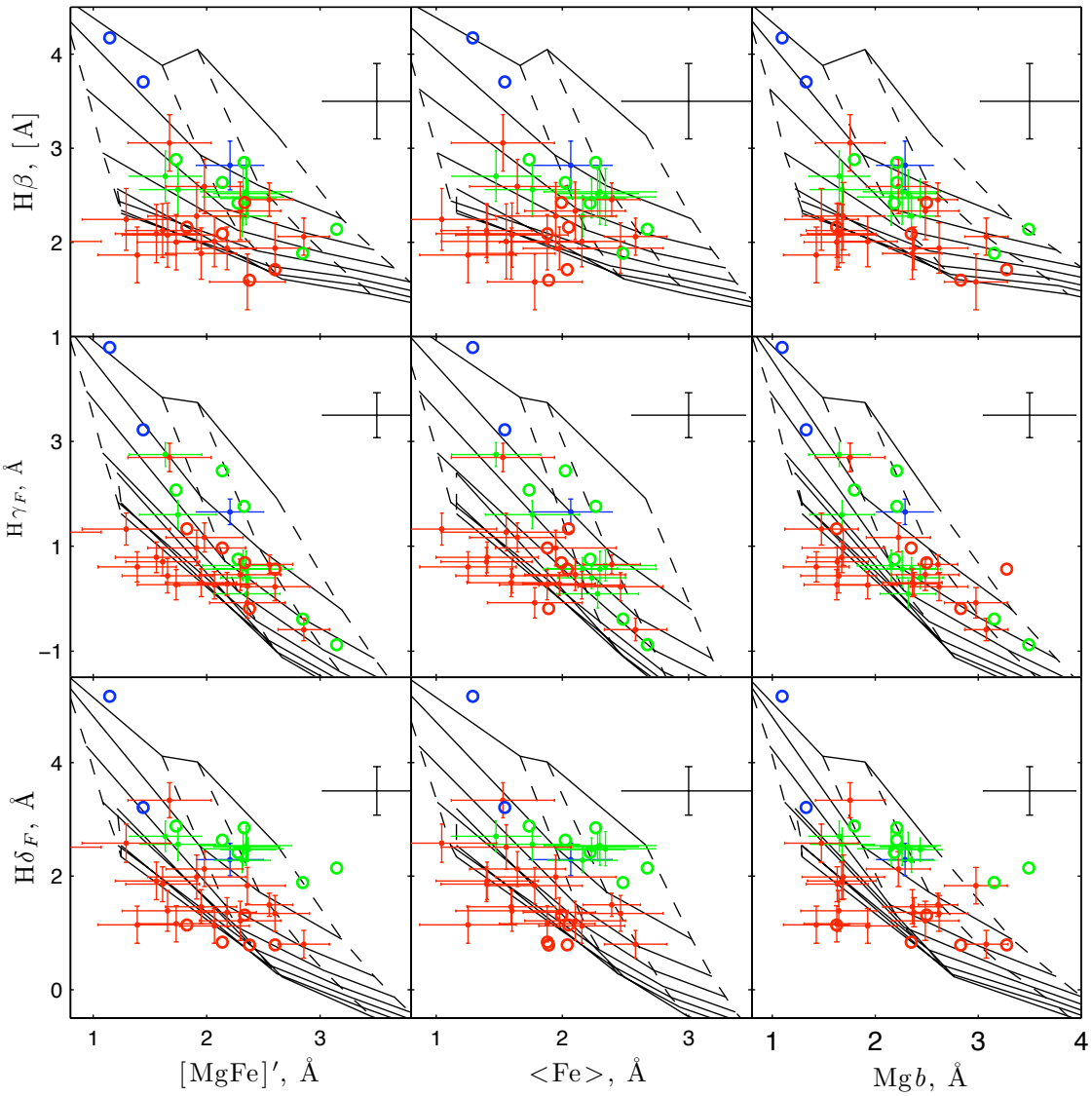

Figure 4.9: Lick/IDS index−index diagrams of the age-sensitive Balmer indices Hβ, Hγ_F and Hδ_F versus the metallicity sensitive indices Mgb,<Fe> and [MgFe]′, with over plotted model grids of TMB03

4.5.2 Age, metallicity and abundance ratios

Using the combined sample of our galaxies and the re-measurement of the M08 galaxies' spectra with the method of the χ^2-minimization, we find a mean age of 3.0 ±0.8 Gyr and a mean metallicity of [Z/H] = −0.31 ±0.10 dex for the dE(di)s. In contrast, the mean values for the dE(N)s are 7.5 ±1.9 Gyr and [Z/H] = −0.54 ±0.14 dex. The dE(bc)s have comparatively young

ages (i.e. less than 3 Gyr). Two of them show a rather low metallicity (−0.90 ±0.25 dex for VCC0021 and −0.75 ±0.15 dex for VCC1912), while the third one also belongs to the discy subclass (VCC 0308), and indeed has a significantly larger metallicity (i.e. −0.09 ±0.10 dex), consistent with the other dE(di)s.

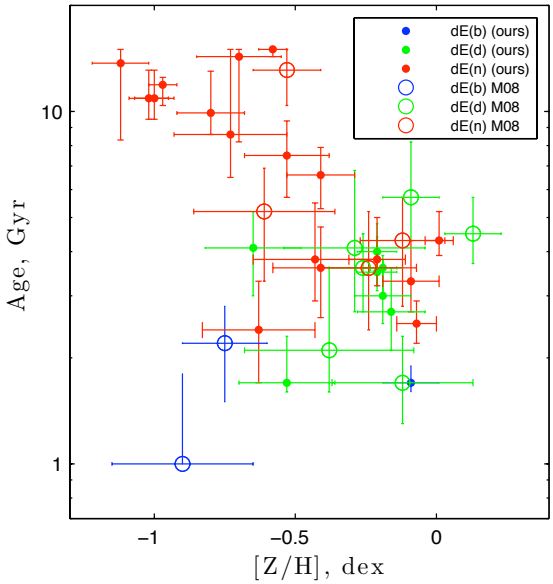

Figure 4.10: Age versus metallicity [Z/H]. Here color and symbols are the same as in Figure4.6.

As a statistical comparison, we have used the Kolmogorov-Smirnov test for the goodness of fit with the null hypothesis that two observed distributions are from the same continuous distribution. The estimated probability P_{KS} that the difference is at least as large as observed if they had been drawn from the same population, is P_{KS} = 0.01, 0.03 and 0.15 for the age, metallicity, and [α/Fe]-abundance distributions, respectively, of dE(N)s and dE(di)s. This apparently confirms that the age and metallicity differ significantly for dEs with and without discs. However, this interpretation is challenged when the stellar population characteristics are considered with respect to galaxy luminosity; details are given at the end of this section.

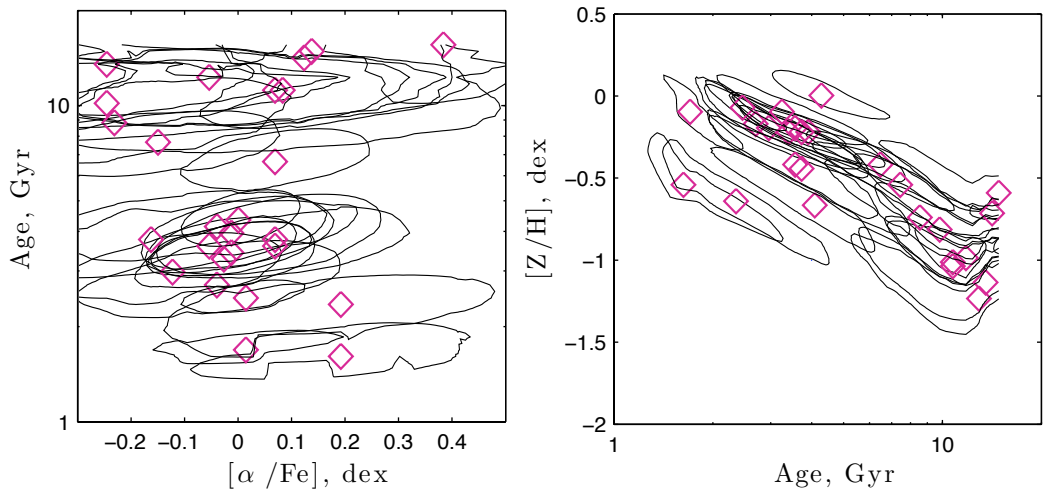

Figure 4.11: Error contours in different projection planes of age, metallicity and [α/Fe]-abundance space.

The galaxies in our sample follow a general trend linking age and metallicity: as displayed in Figure 4.10, we see that the derived ages are decreasing with increasing metallicity of the dEs,

The estimated stellar population parameters using the model TMB03 at the Lick standard resolution.

VCC	Age	[Z/H]	[α/Fe]
No.	Gyr	dex	dex
0308	$01.7^{+0.2}_{-0.1}$	-0.09 ± 0.10	0.01 ± 0.07
0216	$01.7^{+0.6}_{-0.1}$	-0.53 ± 0.17	0.19 ± 0.13
0389	$04.0^{+0.8}_{-0.8}$	-0.21 ± 0.07	-0.01 ± 0.08
0490	$02.7^{+0.9}_{-0.6}$	-0.16 ± 0.12	-0.04 ± 0.11
0856	$03.5^{+0.9}_{-0.4}$	-0.21 ± 0.07	-0.01 ± 0.08
0990	$03.6^{+0.3}_{-0.6}$	-0.19 ± 0.07	-0.06 ± 0.08
1304	$04.1^{+1.1}_{-1.1}$	-0.65 ± 0.17	-0.04 ± 0.18
2019	$03.0^{+0.8}_{-0.5}$	-0.19 ± 0.10	-0.12 ± 0.11
0545	$11.9^{+0.6}_{-1.5}$	-0.97 ± 0.05	-0.06 ± 0.22
0929	$04.3^{+0.9}_{-0.4}$	0.01 ± 0.05	0.00 ± 0.05
1167	$10.9^{+2.2}_{-1.4}$	-1.00 ± 0.07	0.07 ± 0.16
1185	$09.9^{+3.1}_{-1.3}$	-0.80 ± 0.12	-0.25 ± 0.16
1254	$06.6^{+1.3}_{-1.3}$	-0.41 ± 0.12	0.07 ± 0.08
1261	$02.5^{+0.4}_{-0.3}$	-0.07 ± 0.07	0.01 ± 0.05
1308	$03.8^{+1.2}_{-0.6}$	-0.21 ± 0.10	0.07 ± 0.09
1333	$13.7^{+1.3}_{-5.4}$	-1.12 ± 0.10	0.12 ± 0.23
1348	$15.0^{+0.0}_{-0.7}$	-0.58 ± 0.05	0.38 ± 0.09
1353	$02.4^{+0.9}_{-0.7}$	-0.63 ± 0.20	0.19 ± 0.22
1355	$03.8^{+1.7}_{-0.9}$	-0.43 ± 0.22	-0.16 ± 0.16
1389	$10.9^{+2.2}_{-1.4}$	-1.02 ± 0.07	0.08 ± 0.18
1407	$14.3^{+0.7}_{-6.1}$	-0.70 ± 0.15	0.13 ± 0.13
1661	$08.6^{+6.4}_{-2.1}$	-0.73 ± 0.20	-0.23 ± 0.16
1826	$07.5^{+1.9}_{-1.8}$	-0.53 ± 0.15	-0.15 ± 0.14
1861	$03.3^{+1.0}_{-0.6}$	-0.09 ± 0.10	-0.03 ± 0.08
1945	$03.6^{+1.1}_{-1}$	-0.41 ± 0.17	0.07 ± 0.12
Galaxies from M08			
0021	$01.0^{+0.8}_{-0.0}$	-0.90 ± 0.25	0.00 ± 0.30
1912	$02.2^{+0.6}_{-0.7}$	-0.75 ± 0.15	-0.11 ± 0.19
0397	$01.7^{+0.6}_{-0.4}$	-0.12 ± 0.25	-0.04 ± 0.16
0523	$04.1^{+2.7}_{-1.4}$	-0.29 ± 0.25	0.15 ± 0.18
1183	$03.6^{+0.9}_{-0.9}$	-0.26 ± 0.12	-0.06 ± 0.11
1695	$02.1^{+1.5}_{-0.5}$	-0.38 ± 0.30	0.04 ± 0.26
1910	$05.7^{+2.5}_{-1.4}$	-0.09 ± 0.10	0.05 ± 0.08
1947	$04.5^{+1.2}_{-0.8}$	0.13 ± 0.10	0.09 ± 0.07
1087	$03.6^{+1.6}_{-1.2}$	-0.24 ± 0.17	-0.12 ± 0.16
1122	$05.2^{+1.7}_{-1.9}$	-0.61 ± 0.25	-0.29 ± 0.20
1431	$13.1^{+1.9}_{-2.7}$	-0.53 ± 0.12	0.28 ± 0.12
1549	$04.3^{+1.4}_{-1.5}$	-0.12 ± 0.15	0.19 ± 0.11

The estimated stellar population parameters for original sample using the AV/MILES model at the resolution of 11 ÅFWHM.

VCC	Age	[Z/H]
no	Gyr	dex
0308	$1.8^{+0.1}_{-0.3}$	-0.01 ± 0.17
0216	$2.2^{+0.0}_{-0.0}$	-0.85 ± 0.05
0389	$3^{+0.4}_{-0.2}$	-0.16 ± 0.09
0490	$2.5^{+0.3}_{-0.2}$	-0.06 ± 0.17
0856	$2.8^{+0.2}_{-0.0}$	-0.16 ± 0.09
0990	$3^{+0.2}_{-0.2}$	-0.16 ± 0.07
1304	$2.7^{+1.0}_{-0.3}$	-0.68 ± 0.14
2019	$2.7^{+0.2}_{-0.2}$	-0.11 ± 0.09
0545	$15.6^{+0.0}_{-5.1}$	-1.06 ± 0.12
0725	$7.1^{+2.1}_{-0.4}$	-1.20 ± 0.14
0929	$3.7^{+1.1}_{-0.5}$	-0.01 ± 0.09
1167	$7.6^{+9.1}_{-0.5}$	-0.97 ± 0.14
1185	$7.1^{+4.9}_{-0.9}$	-0.70 ± 0.19
1254	$5.1^{+0.7}_{-0.6}$	-0.47 ± 0.07
1261	$2.7^{+0.0}_{-0.2}$	-0.09 ± 0.10
1308	$3.2^{+1.3}_{-0.4}$	-0.28 ± 0.14
1333	$6.2^{+11.6}_{-1.1}$	-1.06 ± 0.24
1348	$17.8^{+0.0}_{-10.2}$	-0.82 ± 0.21
1353	$2^{+0.1}_{-0.1}$	-0.68 ± 0.14
1355	$2.5^{+0.5}_{-0.2}$	-0.35 ± 0.17
1389	$16.7^{+1.1}_{-9.6}$	-1.13 ± 0.19
1407	$7.6^{+1.1}_{-1.7}$	-0.70 ± 0.12
1661	$6.6^{+1.4}_{-2.2}$	-0.68 ± 0.22
1826	$4.8^{+0.7}_{-1.3}$	-0.42 ± 0.14
1861	$3^{+0.2}_{-0.4}$	-0.09 ± 0.12
1945	$3^{+1.2}_{-0.5}$	-0.54 ± 0.12

Table 4.4

similar to the observation of Rakos et al. 2001 for Fornax dEs. Interestingly, we see that an age-metallicity anti-correlation is present for the dE(N)s, even tighter than previously noticed by Poggianti et al. (2001) for Coma cluster dEs. Such an age-metallicity anti-correlation is also found for giant early-type galaxies, but it is under debate because of the correlation of the metallicity and age errors (Trager et al., 2000a; Kuntschner et al., 2001). Nevertheless, together with the dE(di)s, it can be noticed that the brighter dEs might even follow an opposite trend of increasing metallicity with increasing age. It needs to be mentioned, however, that the scatter of values is fairly large.

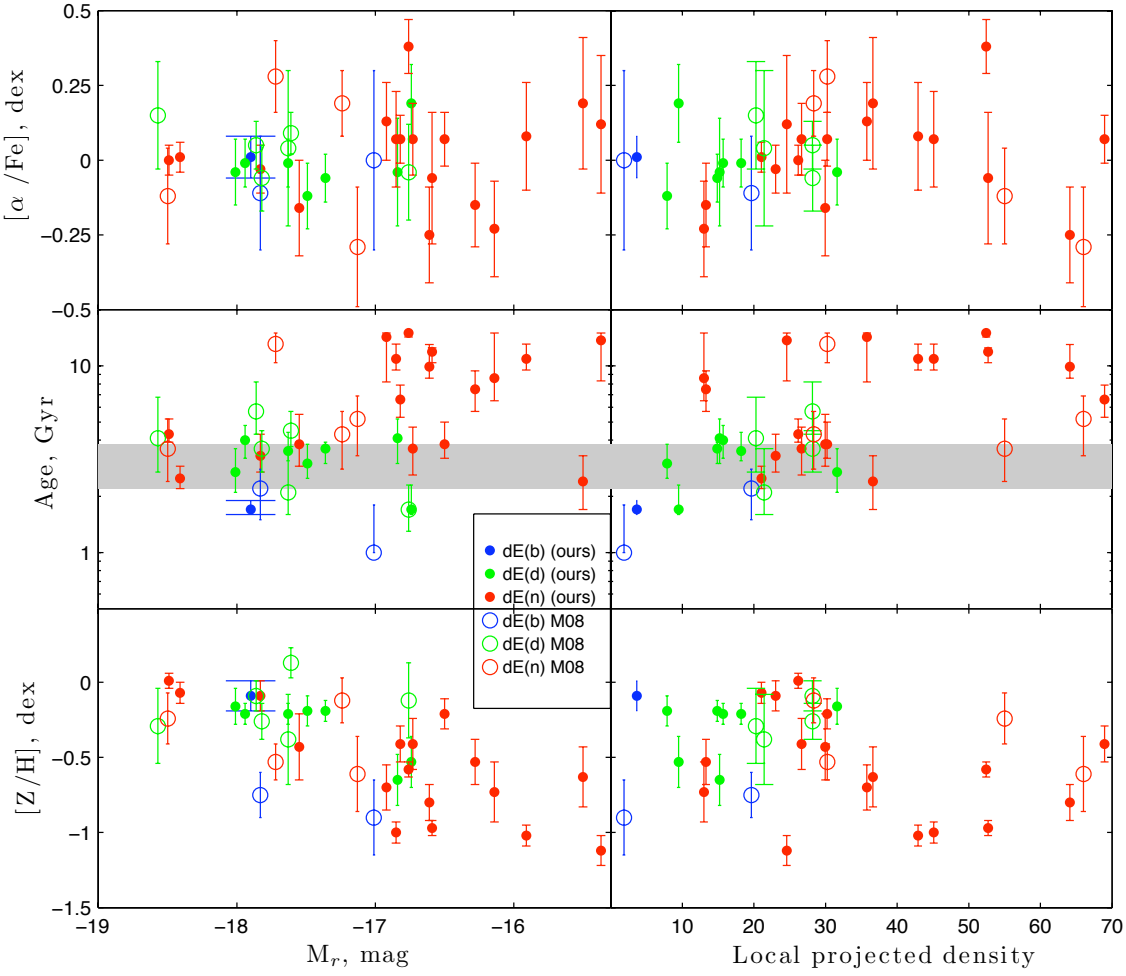

Figure 4.12: The derived ages (top), metallicities (middle) and [α/Fe]-abundance (bottom), plotted against r band absolute magnitude (left), and against local projected density (right, number per sq.deg.). Colors and symbols are the same as in Figure 4.6. The gray shaded region represents the mean $\pm\sigma$ age and metallicity of dEs(di)

In addition, we provide a plot with the error ellipses (Figure 4.11), to better illustrate the behavior of our measurements with respect to the age and metallicity anti-correlation. Kuntschner et al. 2001 suggest that, when the measurement errors in the line strength are not negligible, the tilt of the model grid leads to the correlated errors in age and metallicity, as visualized by the error contours in the age metallicity plane in Figure 4.11.

The luminosity-weighted metallicities derived from the well measured nine indices are shown as a function of galaxy absolute magnitude in Figure 4.12 (bottom left). Both dE(di)s and dE(N)s follow the well known metallicity−luminosity relation (Poggianti et al., 2001). In contrast,

we do not see any strong correlation between measured metallicity and local projected galaxy density (bottom right). In the top panel of the Figure, one can see that the dEs in general are consistent with solar [α/Fe]-abundance, and we do not see any relation with luminosity or local density.

Unlike the correlation of metallicity and luminosity, the measured ages show an aniti-correlation with the luminosity, and correlation with local projected density, although the latter trend is not as strong as the former. It appears that this might be the cause of the apparent age difference between dEs with and without discs, since in addition to the relation with magnitude, the dE(N)s are situated in the denser cluster regions as compared to the dE(di)s. Thus, taking the left and right panels in Figure 4.12 together, no significant difference is seen between dE(di)s and dE(N)s in either age or metallicity, *as long as they are compared at the same magnitude and local density*.

On the other hand, the bimodality in the age distribution is quite prominent. Interestingly, the majority of those dEs belonging to the group with lower ages lie consistently within the one-sigma area of the dE(di)s (gray-shaded region in Figure 4.12). But we do not see any such strong bimodality in the metallicity distribution.

4.6 Discussion and conclusion

We have undertaken a spectroscopic investigation of Virgo cluster dEs, deriving ages, metallicities and $\alpha-$element abundance ratios for 38 dEs of different types, i.e., dEs with and without discs, and examined the variation of their stellar populations according to their morphology. We have established that the mean ages and metallicities of different types of dEs are different.

This result mostly represents the central part of the galaxy, as we used a central fixed aperture to extract the one-dimensional spectra of the galaxies, in order to optimize the SNR for our Lick index analysis. We expect that having a wider aperture effectively minimize the influence of central nucleus. In a worst-case scenario, for those dEs that have a relatively low surface brightness, i.e., a rather faint stellar envelope compared to the nucleus, it is not unquestionable whether our extracted spectra do really represent the galaxies as a whole, or the nuclei only. Interestingly, though, we found that most of the faint nucleated dEs have a fairly old stellar population, and that typically, the nuclei tend to be younger than their host galaxies (Paudel & Lisker, 2009). This appears consistent with the studies of Chilingarian (2009) for Virgo dEs and Koleva et al. (2009) for Fornax cluster dEs: both concluded that the central part of the galaxies are relatively younger and more metal-rich than the outer part. In that respect, we can argue that having a strong effect of the central nucleus in the spectral extraction process does not bias our conclusions. If anything, our result of old galaxy ages at fainter magnitudes could only become somewhat more pronounced by removing the nucleus contribution.

It was known before that the different dE subclasses, in particular those with and without discs, exhibit differences in their colors, magnitude, and the local environment in which they reside(Lisker et al., 2007). The dE(di)s were found to have, on average, slightly bluer colors than the dE(N)s, and Lisker et al. interpreted this color difference with either older age or higher metallicity of the dE(N)s. By combining our sample with that of M08, and therefore reaching statistically significant subsample sizes, we see that the color offset is mainly an effect of age rather than metallicity. However, it is not straightforward to tell which governing factor is most responsible for this apparent correlation of galaxy substructure and stellar population characteristics. As noted above, we find correlations of age with both magnitude and local density,

and we know that the dE(di)s are relatively bright and typically located in less dense cluster regions than the dE(N)s; the combination thus shows that no significant difference between the stellar population of dE(di)s and dE(N)s can be claimed. This is interesting, since Lisker et al. (2008) pointed out that the fairly wide (estimated) distribution of intrinsic axial ratios of the dE(N)s would be consistent with assuming that the dE(di)s – most of which are nucleated – are simply the flat tail of this distribution. The location in regions of comparatively lower density could then be interpreted such that discs in dwarfs can only survive for a reasonably long time if the amount of dynamical heating due to tidal forces is low (also see Mastropietro et al., 2005), and therefore, dEs with discs are preferentially found outside of the cluster center. Moreover, L06 noted that there could still be a significant fraction of objects that have discs, but that were simply not found by their analysis of SDSS images, due to low SNR or the lack of disc features like spiral arms or bars. We see in our data that a handful of dE(N)s are as young and metal rich as the dE(di)s, and interestingly, they also lie in a low density region. So maybe, just as a possibility, these could be those dE(N)s that actually host discs, but were not identified as such — which would then also explain the bimodality when compared to the fainter ones.

Furthermore, an apparent inconsistency is observed in the relation between age and luminosity: previous studies provided evidence for a continuously later formation epoch and/or a longer duration of star formation when going from the massive ellipticals to the dwarfs (see, e.g., Gavazzi et al., 2002; Boselli et al., 2005; Lisker & Han, 2008), which apparently is at variance with our findings. On the other hand, this trend is unlikely to continue to even fainter magnitudes, since most of the Local Group dwarf Spheroidal (dSph) galaxies are know to be dominated by old populations (e.g. Grebel, 1999). It seems that, the fainter dEs are significantly older than the brighter ones, no matter at which density they are located. To statistically confirm this result, we divide the total sample in two groups: those being fainter and brighter than the mean magnitude $M_r = -17.22$ mag. We obtain a mean age of 3.9 Gyr and 7.4 Gyr for the brighter and fainter group, respectively, which is very similar to the mean ages of the discy and nucleated subsamples (3.0 and 7.5 Gyr). Furthermore, the K-S test supports our finding that a dichotomy in the distribution of ages can be seen not only with respect to different morphology but also different luminosity, as we get a K-S test probability of 0.01 for the null hypothesis that the age distributions of the fainter and brighter group are not different.

The ages of 10 Gyr and above indeed appear more comparable to the Local Group dSphs. In that sense, we find a discontinuity in the trend of stellar population characteristics with luminosity, and we can speculate that the fainter dEs might be a different species than the brighter ones or simply were not able to sustain star formation for as long a period as the more luminous and presumably more massive dEs.

In comparison to previous stellar population studies of dEs in different clusters, unlike Chilingarian et al. (2008) who found a correlation of [α/Fe] with the projected distance in the Abell496 cluster – although only in the very central part – and the study of Smith et al. (2009) for Coma, we do not find any correlation between α-element abundance ratio with environmental density. This could also be due to differences between the clusters, in the sense that Coma is a more virialized cluster of higher richness class than Virgo. Nevertheless, our range of age and metallicity roughly agrees with their ranges. Another study byGeha et al. (2003), focusing on the stellar populations of rotating and non-rotating Virgo dEs, resulted in no difference between them. On the other hand, a recent, more extensive study by Toloba et al. (2009) finds that rotating Virgo dEs are typically located further from the cluster center and have younger stellar population ages. We have only six dEs in common with these studies (counting only those for which tabulated values were published). Three of them (VCC 0308, VCC 0856 & VCC 1947) have disc substructure and are rotating, while for three (VCC 1254, VCC 1261 & VCC 1308) no disc

features were identified and they are non-rotating according to Geha et al.. Note, though, that VCC 1261 is clearly rotating from the analysis of dE globular clusters of Beasley et al. (2009). Chilingarian (2009) shows that this galaxy contains a rotating kinematically decoupled core, indicating the difficulties in drawing robust conclusions on the global rotation of a dE from the inner stellar kinematics. We also find that the overall stellar populations are quite mixed within these six galaxies, as has already been noted by van Zee et al. (2004) in their study of (non-)rotating dEs.

There have been numerous discussions on the origin of the passive dwarf galaxies. The key issue is whether cluster dwarfs are *primordial*, having formed from the highest density peaks in the proto-cluster (Tully et al., 2002) and avoiding subsequent merging, or originating from transformation of late-type disc galaxies through the interaction with the cluster environment (e.g. Boselli & Gavazzi, 2006). However, to explain the formation of dEs, using such single scenarios may be too simplistic, and it is likely that both scenarios operate at some level. Furthermore, the question is how to find unique features for such a process that dominates in a given mass regime, a given environment, and for a given morphological subclass of dwarfs.

Our results promote the idea of different scenarios for different morphology and/or different luminosity of dEs, although the physical mechanisms responsible for the quenching of the star formation activity in the galaxies are not easy to understand from the stellar population properties. The observed systematic difference in age & metallicity between different types of dEs support the finding of L07. The typical age range of the brighter dEs of less than 5 Gyr indicates that the star formation activity ceased at $z < 0.5$. The younger age, higher metallicity and consistency with solar $\alpha-$element abundance would suggest that a discy dE can indeed form through the structural transformation of a late-type spiral into a spheroidal system, triggered by the popular scenario of strong tidal interactions with massive cluster galaxies. A stellar disc component (which has rather high metallicity) may survive and form a bar and spiral features that can be retained for some time depending on the tidal heating of the galaxy (Mastropietro et al. 2005; also see Lisker & Fuchs 2009). This "galaxy harassment" process could thus produce disc-shaped dEs.

On the other hand, the fainter dE(N)s, with their older ages, might be a different class of objects with a different formation scenario. The poorer metal content supports the idea that they might be primordial objects, as suggested by Rakos & Schombert (2004); they might have either suffered early infall into the cluster potential, or formed together with cluster itself. The generally low surface brightness of dEs suggests that whichever mechanism is responsible for the halting the star formation activity; it must have been rather efficient. The common idea is that internal feedback might be responsible for their cessation of star formation activity at such early epochs. We can speculate that the slightly higher mean [α/Fe] as compared to the dE(di)s could indicate a more efficient star formation activity than their discy counterparts before the quenching. High-efficiency star formation has also been suggested as an explanation for the comparatively high metallicity of the old populations of Local group dSph as compared to dIrr populations of the same age, i.e., as an explanation for the offset along the metallicity−luminosity relation (Grebel et al., 2003). However, further dynamical studies of these fainter galaxies are needed to prove whether the removal of gas by internal feedback processes is efficient or not, since it has been pointed out that it is difficult to really eject the gas from a dwarf galaxy by supernovae explosions unless the dwarfs have masses less than 10^7 solar masses (Mac Low & Ferrara, 1999).

5

Nuclei of early-type dwarf galaxies: insights from stellar populations

Abstract

We present a comprehensive analysis of the spatially resolved stellar population properties of 26 early-type dwarf (dE) galaxies in the Virgo cluster. Using the number of line strength index measured in the Lick/IDS system we estimate the simple stellar population-equivalent (SSP-equivalent) age, metallicity and abundance ratio [α/Fe]. In particular, we focus on the comparison of the stellar populations between the central nucleus and the surrounding galactic main body of our sample galaxies. Our estimated ages of the nuclei are lower than those of the respective galactic main bodies for most dEs with an average of 3.5 Gyr age difference. We find only five dEs with significantly older nuclei than their galactic main bodies. Furthermore, we observe the dE nuclei to be more metal rich compared to their host galaxies, and more or less all dEs brighter than $M_r = -17$ mag exhibit such a differences in age and metallicity between galactic main body and nucleus of dEs. The metallicity of both nucleus and galactic main body of dEs correlates with the total luminosity of dEs. However, nucleus metallicity cover lager range (+0.18 to −1.22 dex) than galactic main body, and the all dEs galactic main bodies have sub-solar metallicity. The Spearman rank order test confirmed that the SSP-equivalent ages of nuclei of dEs correlate with the local projected density of galaxy cluster. The alpha-element abundance ratios are consistent with the solar value for both components (i.e, nucleus and galactic main body) of the dEs. We also examine the presence of gradients in SSP parameters for the 13 brightest dEs, which permit us to measure the absorption line strengths with sufficient signal-to-noise ratio up to 1.2 kpc (15 arc-sec) radial distance from the center. We notice that different behaviour of SSP gradient in dEs, i.e., both flat and steeper profile are frequent, however the observed overall trend of increasing age and decreasing metallicity with the radius is consistent with earlier studies. Estimates of the α-abundance ratio as function of radius are consistent with no gradient along the major axis.

Result published on S. Paudel et al., 2011 MNRAS in press.

Contents

Figures

5.1 Introduction

EARLY-type dwarf galaxies (dEs, M_B > -18) are the numerically dominant population in the present-day Universe (Sandage et al., 1985; Binggeli et al., 1987; Ferguson & Binggeli, 1994). They also exhibit strong clustering, being found predominantly in the close vicinity of giant galaxies, either as satellites of individual giants, or as members of galaxy clusters (Ferguson & Sandage, 1989). Although the dEs are characterized by their smooth appearance, having no recent or ongoing star formation and apparently no gas or dust content, the understanding of their origin and evolution remain major challenges for extragalactic astronomy. Stellar population studies show that dEs exhibit on average younger ages as compared to their giant counterparts, and also a lower metal content according to the correlation of metallicity and luminosity (Michielsen et al., 2008). However, past studies provided a wide range of ages (e.g., Poggianti et al. 2001; Rakos et al. 2001; Caldwell et al. 2003; Geha et al. 2003; van Zee et al. 2004), from as old as being primordial objects to dEs with recently formed young stellar populations.

It appears that dEs themselves are not a homogeneous class of objects. Sub-structures such as stellar disks, faint spiral arms or bars are quite frequent among the brighter dEs (Lisker et al., 2006, 2007). Many dEs are found to contain a central surface brightness enhancement consistent with a point source on top of the galactic main body (e.g. Binggeli & Cameron, 1991, 1993), referred to as so-called nucleated dEs, see Figure 5.1 as an example. The studies from the HST/ACS Virgo cluster survey (Côté et al., 2006), with their high angular resolution, not only verified the presence of such a distinct nucleus but also showed that nuclei are ubiquitous in bright dEs, covering a range in nucleus brightness and reaching up to 10% of the total light of the parent galaxy. Interestingly, dEs with comparably faint nuclei that had not been identified before Côté et al. (2006) show several systematically different properties as compared to dEs with bright nuclei (Lisker et al., 2007, 2008).

5.1.1 Properties of dEs nuclei

Different studies of dE nuclei from different data sets found several contradictory properties for the nuclei (Grant et al., 2005; Lotz et al., 2004; Côté et al., 2006). Particularly, the ground and space based data sets yielded different results. Grant et al. (2005) found that the nuclei are on average redder than their surrounding galactic main body. On the other hand, studies using HST observations (Côté et al., 2006; Lotz et al., 2004) measured the dE nuclei to be slightly bluer than the galactic part. Furthermore, Côté et al. (2006), who used high quality data sets from the ACS Virgo Cluster Survey, proposed that the nuclei rather closely match the nuclear clusters of late type spiral galaxies in terms of size, luminosity and overall frequency. Another related scenario is also emerging: the recently discovered new (candidate) type of extremely small dwarf galaxies, the UCDs (Ultra Compact Dwarfs) with typical magnitudes of $-13 < M_b < -11$ (Hilker et al., 1999; Phillipps et al., 2001), might be the remnant nuclei of tidally stripped dwarf galaxies (Bekki et al., 2003; Drinkwater et al., 2003; Goerdt et al., 2008).

The formation mechanisms of the nuclei of dEs are poorly understood and various possibilities have been proposed, also depending on the evolution and formation of dEs as a whole. As the nucleated dEs are preferentially rounder in shape, van den Bergh (1986) proposed that the nuclei of dEs could have formed from the gas that sank to the centre of the more slowly rotating objects. Since they predominantly appear in highly dense environments, like the centre of a cluster of galaxies, the pressure from the surrounding inter-galactic medium may allow dwarf

galaxies to retain their gas during star formation and produce multiple generation of stars (Silk et al., 1987; Babul & Rees, 1992), forming nuclei in the process. In both proposed scenarios the nuclei are formed along with the evolution of the galaxy itself, i.e., continuous star formation activity occurs at the dE centre as time passes. Unlike that, Oh & Lin (2000) suggested that dE nuclei might have formed in a different way, namely through subsequent migration or orbital decay of several globular clusters towards the centre of their host dE.

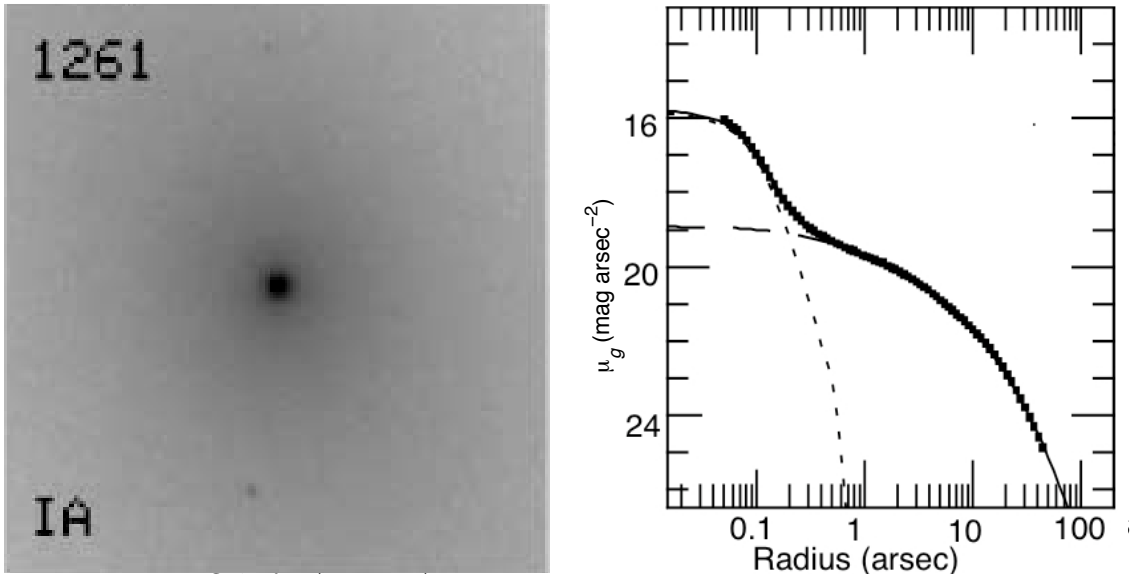

Figure 5.1: F475W-band images of VCC1261 from the ACS Virgo Cluster Survey (Côté et al., 2006), the nucleus is prominently seen in the centre. The surface brightness profile is on right side, where we can clearly see the two components in the light profile i.e for the nucleus and galactic main body.

It is difficult to provide a definitive observational test of these different scenarios for nucleus formation. Nevertheless, we can gain some insight by comparing the different observational properties, in particular relative ages and chemical enrichment characteristics, of the nuclei with their galactic main bodies, as well as with UCDs as their possible descendants. However, we need to bear mind that there may be a mixture of different formation scenarios.

Our previous study based on this dataset (Paudel et al., 2010, hereafter Paper I) has focused on the analysis of the inner stellar populations of dEs as a whole, without separating nuclei and galactic main bodies. Instead, our intention was to see the variation of the inner stellar population properties with different morphological subclasses of dEs (cf. Lisker et al., 2007), using a much larger sample of Virgo dEs than in previous Lick index studies. We showed that dEs with different substructure properties (with/without disk features, Lisker et al. 2006) have significantly different stellar populations: dEs with disk features are younger and more metal rich than dEs without disks. Therefore we concluded that these dEs probably do not have the same origin, as they also differ in their distribution with local environmental density in which they reside. By selection, all dEs in our sample contain a central nucleus, therefore it seems important to see the nature of the stellar populations of the nuclei and the surrounding galactic main bodies separately. And since there are different possibilities for the processes that form nuclei and also dEs themselves, we ask: can the nuclei thus tell us something about the formation history of dEs?

This Chapter is organized as follows. In Section 5.2, we describe the sample of Virgo cluster dEs, observation and data reduction in brief. In section 5.3, we describe the measurement of line-strength indices in the Lick/IDS system and extraction of stellar population parameters from the

absorption line-strength indices. Our main results from the stellar population parameters are given in Section 5.4 and are discussed in Section 5.5. Finally, we summarize our findings in Section 5.6.

5.2 The sample, observation and data reduction

In this study, we use our original sample of 26 nucleated dEs in the Virgo cluster. The sample properties such as position in the color magnitude relation, total galactic luminosity, radial velocity and their local projected density within the Virgo cluster are described in Chapter 3. The sample covers the full range of local density and includes the different morphological dE subtypes, i.e., 8 dEs with disks (dE(di)s) and 18 dEs without disks, which we hereafter simply refer to as dE(N)s. One dE(di) (VCC0308) contains a weak blue color excess in the centre, thus being referred to as a blue-centre dE (cf. Lisker et al., 2006).

The observations were carried out at ESO-Very Large Telescope (VLT) with FORS2 instrument. The 1" slit and V300 grism provide the resolution of 11 Å FWHM. The other basic observational properties and the data reduction processes are described in Chapter 3. Only the change for dEs introduce at this level is a new criterion for the binning process, following the separate extraction of the spectra for the nucleus and the underlying galactic body from the different parts of the dEs. Since, we aim to perform the separate analysis of stellar populations of nuclei and galactic body with the reduction of the galactic contamination on the nuclei spectra. Additionally, the possible gradient of SSP parameters in our sample dEs is also explored if SNR permits us.

We carefully checked the issue of scattered light during the reduction of the data, since the presence of a significant amount of scattered light could produce an artificial gradient in the measured line indices. Fortunately, our MOS-MXU setup utilized in this investigation provides the opportunity to quantify it. There are always free intra-slit regions where no light enters directly from the sky. After the bias subtraction these regions should not contain any flux, unless scattered light were present. We thus calculate the average amount of light within such regions manually. We find that the mean is zero within the uncertainties, which are of the order of some hundredths of a count (see Figure 5.2). The FORS2 pipeline reduction produces the same result. It therefore confirms that there is no scattered light left in the spectra.

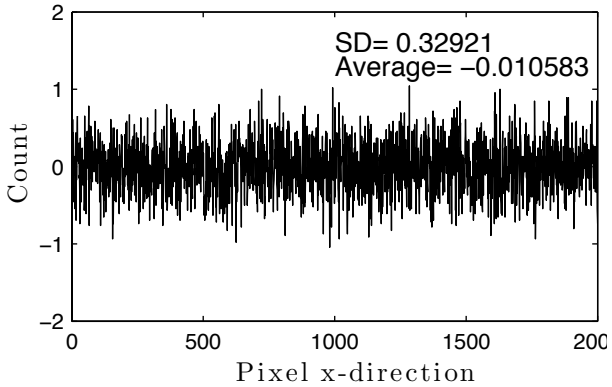

Figure 5.2: The noise level of CCD after the bias subtraction.

In a different way, there is still the probability of mixing the nucleus light out to far beyond the central nucleus in case of bad seeing or instrumental blurring. To examine this effect, we also observed a star in an additional slit along with each target-field. Then, through the light profile of this star, we quantify the amount of such light at a radius of 3" beyond the centre. Our measurements show that spread nuclear light is less than 1% of galactic light at 3" distance from

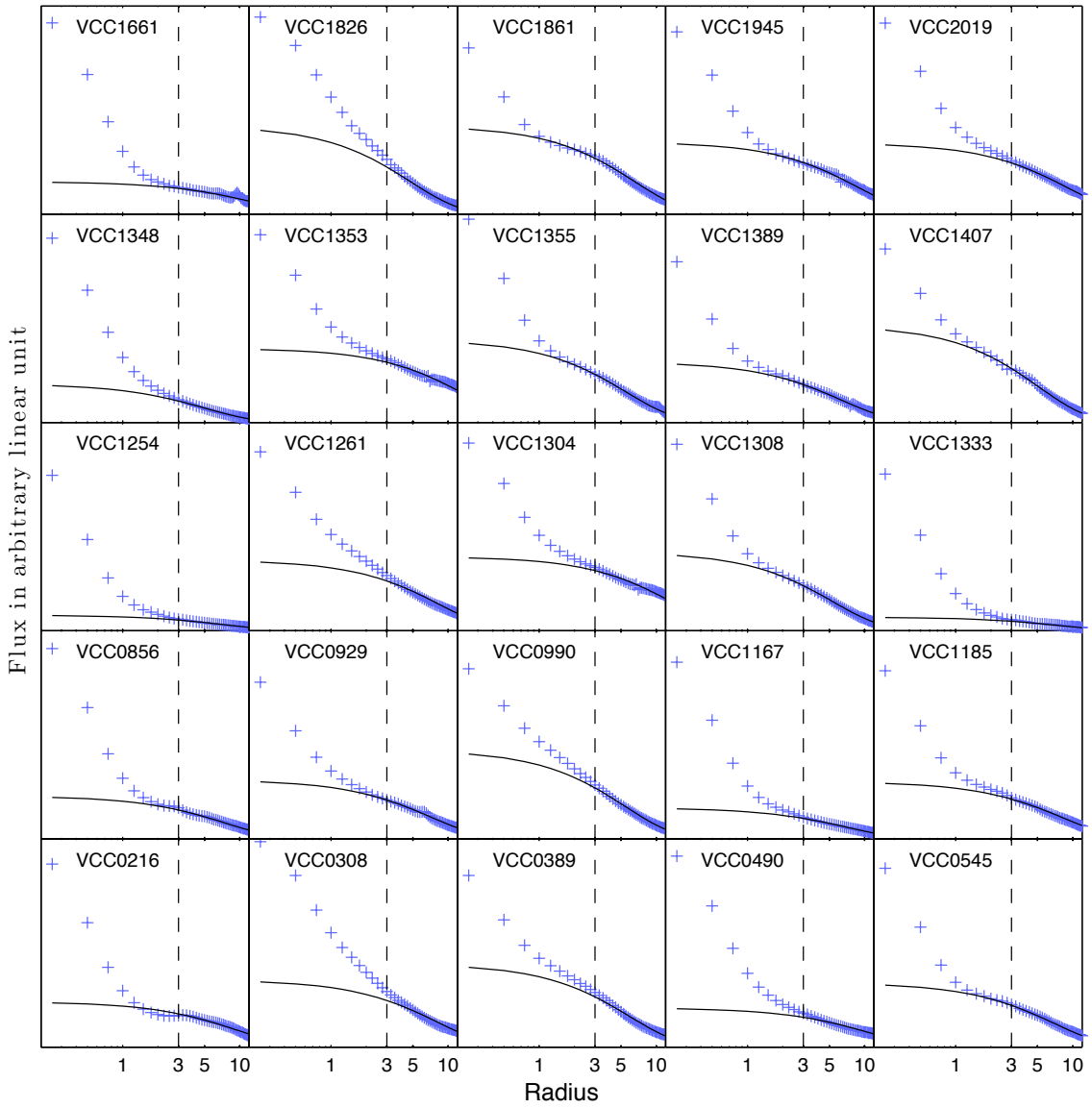

Figure 5.3: The light profile of dEs. The crosses represent the observed flux along the slit, and the solid line is the fitted exponential profile beyond 3” and extrapolated to the centre.

the galaxy centre. The observed FWHM of the stars is always ∼1”.3 or less, consistent with this negligible fraction of starlight at 3” from the centre.

5.2.1 Extraction of nuclear spectra and analysis of light profile

Our goals in this investigation are the measurement of simple stellar population (SSP) equivalent parameters (see Trager et al. 2008) of dE nuclei and a comparison with the SSPs of the surrounding galactic main bodies. Additionally, if the signal-to-noise ratio (hereafter SNR) permits us, we wish to explore gradients in the SSP parameters, which help to determine whether the SSP of the nuclei is very different from the rest of the galaxy or is just a continuity of a smooth SSP gradient at the centre of dEs. Although there is no precise definition for what a nucleus is, the working definition used by several studies is that an excess of light from the smooth exponential (or higher order Sérsic) profile of the rest of the galactic part is observed,

Table 5.1: The measured signal-to-noise ratio (SNR) per pixel at 5000 Å.

Galaxy Name	Nuc. SNR) pix^{-1}	Gal. SNR pix^{-1}	Reff arc-sec	M_r Total mag	m_r Nuc mag	Light fraction in %
VCC0216	47	30	13.3	−16.78	19.510	22
VCC0308	35	31	18.7	−17.95	19.185	40
VCC0389	32	30	17.2	−18.00	18.498	48
VCC0490	32	23	27.6	−18.09	18.658	25
VCC0545	33	30	13.3	−16.61	19.384	35
VCC0725	23	–	25.2	−16.19	20.923	–
VCC0856	56	35	15.9	−17.71	18.355	23
VCC0929	56	34	20.5	−18.58	17.961	33
VCC0990	35	33	09.9	−17.39	18.572	53
VCC1167	46	30	27.3	−16.95	19.078	17
VCC1185	33	50	19.3	−16.65	20.332	30
VCC1254	67	31	14.9	−17.17	17.784	09
VCC1261	50	42	22.5	−18.47	18.563	42
VCC1304	35	31	16.2	−16.86	18.859	33
VCC1308	39	27	11.4	−16.50	19.774	44
VCC1333	41	28	18.5	−15.44	19.329	10
VCC1348	42	25	13.1	−16.94	18.257	23
VCC1353	28	31	08.8	−15.51	20.452	53
VCC1355	24	28	29.6	−17.59	20.130	57
VCC1389	30	31	12.8	−15.98	20.314	36
VCC1407	27	31	11.8	−16.95	20.098	52
VCC1661	34	29	18.9	−16.18	19.911	16
VCC1826	23	31	07.8	−16.30	19.179	56
VCC1861	30	31	18.4	−17.78	19.263	47
VCC1945	31	38	21.5	−17.11	19.432	35
VCC2019	31	29	18.1	−17.53	19.747	37

.

The second and third columns are the measured SNR from the galactic-light-subtracted nuclear spectra and from the galactic main body spectra respectively. Fourth and fifth columns are total galactic and nucleus magnitude of dEs derived from the SDSS r_band images. Nucleus magnitudes are derived as follows. First, a Sérsic fit to the radial profile of the galaxy is done. From this fit, a two-dimensional elliptical model image, taking into account the median SDSS PSF of 1".4 FWHM, is created and subtracted from the original image, leaving only the nucleus in the center. The nucleus magnitude is then measured by circular aperture photometry with r = 2". Our estimated error in the magnitude error is 0.2 mag, which is consistent with the RMS scattering of Côté et al. (2006). The last column represents the amount (in fraction of total light of the central aperture) of light subtracted from the central nucleus.

looking like a compact source sitting at the centre of the galaxy. Because of its compactness, it is considered as a point source and represented with a seeing convolved Gaussian light profile. Likewise, the study of Grant et al. 2005 represents the nuclei as a point source convolved with Gaussian seeing. Côté et al. 2006 used a slightly different approach, by fitting a two component core-Sérsic model (Graham & Guzmán, 2003). In Figure 5.3 we can clearly see for most dEs the change in the light profile at the centre (e.g. VCC0216, VCC0856, VCC0545, VCC1353 and VCC1945). On the other hand, VCC0308, VCC0990, VCC1261 and VCC1826 exhibit a rather smooth light profile. There may be several factors which produce such differences in the light profile even though all dEs in this sample are confirmed as nucleated from other photometric studies (Binggeli et al., 1985; Lisker et al., 2007). Insufficient spatial resolution or observed seeing which might blur the steeper light profile of the nuclei makes it harder to separate the galactic light profile. However, Côté et al. (2006) have observed the existence of a profile break in the case of VCC0856, VCC1261, VCC1355, VCC1407, VCC1661 and VCC2019, reconfirming the existence of a nucleus at the centre of dEs with HST high resolution surface photometry.

It is rather difficult to carry out an analysis of the stellar populations of nuclei *alone*, because the nuclei are always situated on top of the underlying galactic main bodies. It is also hard to separate the galactic light from the central nucleus of such a faint object. The studies that have been done by Chilingarian (2009) and Koleva et al. (2009) provide results without galactic light subtraction from the nucleus. Although there is, in our sample, typically a fairly large domination of light from the nucleus as compared to galactic light at the photometric centre of the dEs, still a considerable amount of underlying light of the host galaxy can alter the observed properties of the nuclei. We therefore aim to reduce the galactic light contamination in the nucleus spectra, attempting a separate extraction of spectra for the nucleus and the galactic part. See next Section.

5.2.2 Subtraction of galactic light from the nucleus

In order to subtract the galaxy light from the nucleus, we determine a scaling factor by fitting the galactic main body's light profile (measured along the slit) by an exponential profile and extrapolating it to the very centre, yielding the amount of galaxy light contained in the nucleus aperture. The Figure 5.4 provides a schematic view of the subtraction of galactic light from the central nucleus. First, we average the galaxy frame in the wavelength direction between 4000 Å to 5500 Å, assuming that there is not any severe change in light profile from exponential with the wavelength. The fitting of the galaxy light profile with an exponential has been done only considering the galaxy light beyond the 3" from the centre, because we assume that the light from the nucleus should not be spread out to these distances, as the mean FWHM is 1".25 for our observations.

The scaling of the galactic light to match the centre of the galaxy has been done by extrapolation of the light profile to the centre of dEs. The scale factor C has been calculated using the following equation,

$$C = \frac{\sum_{i=-1}^{1} F_i^g}{\sum_{i=13}^{32} F_i^g} \tag{5.1}$$

where F^g is the flux from the best fitted galaxy profile (solid line in Figure 5.4), and i is in pixel

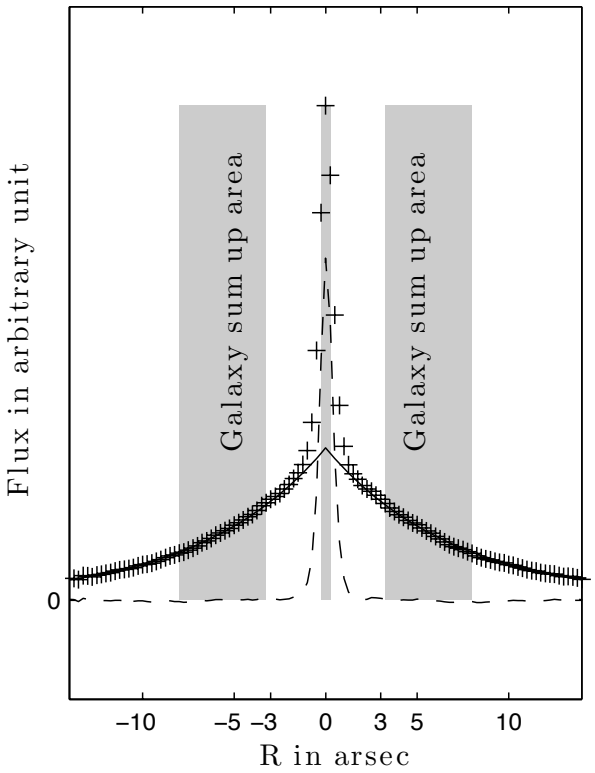

Figure 5.4: A schematic view of the fitting of the light profile for VCC0490 and the binning processes. The cross symbol represents the distribution of the observed total light (i.e galaxy + nucleus) and solid line represents the exponentially fitted light profile of the galaxy. The dashed line is the residual nucleus after the subtraction of galaxy light, which represents the pure nuclear light profile.

scale (i.e., 0".25) with the origin at the central peak of the observed slit profile of the galaxies. Then we subtract the galaxy light from the nucleus using

$$F_{\lambda}^{nuc} = \sum_{i=-1}^{1} F_{\lambda i}^{o} - C \sum_{i=13}^{32} F_{\lambda i}^{o} \tag{5.2}$$

here, F^{o} is the observed light in the frame.

Although our exponential profiles of the galaxies are in good agreement with the observed profiles (see Figure 5.3), some dEs have steeper profiles than exponential (Janz & Lisker, 2008) - VCC0389, VCC0929, VCC1167, VCC1254, VCC1348 and VCC1861 have n ≈2. Note, however, this finding is based on fitting a much larger radial interval from the imaging data. In these cases, we again derived the galactic light profile for n = 2, which produced a better match for VCC0929. However, the calculated difference of the amount of galaxy light which might be left at the centre when using n = 1 was less than 30% of the total central light when compared to n = 2. Therefore, we always used the exponential profile for scaling the galactic light to the centre for all dEs.

Given the above considerations about the difficulty of separating nucleus and galaxy, we point out that our approach ensures the removal of a *significant part*, yet probably not 100% of galaxy light contamination. For those few cases where the central light profile looks rather smooth with ground-based data, and can only be disentangled with space-based photometry, our "nucleus" spectrum thus needs to be considered representative for the combination of nucleus *and* galactic central light.

We extract the nucleus spectra from the central 0".75 (i.e., 3 pixels). The region between 0".75 and 3" is not used for this extraction, to avoid any effects of nucleus light in the spectra of the galactic main body. We then integrate over the interval 3" to 8" from each side of the nucleus to

extract the spectra of the galactic main body. The individual spectra of galactic main body from the different side of nucleus were then co-added to produce a spectrum of higher SNR.

Before co-adding the spectra from the different sides of the galaxies, we analyze their slit profile to check for inconsistencies or asymmetries, e.g. by contaminating objects on the slit. We find only one galaxy, VCC1945, has an asymmetric profile that deviates from a smooth exponential profile on one side. We noticed that a bright point source (foreground/background or intra-galactic globular cluster) lies on one side of the slit. Therefore, we remove the spectrum from this side. For completeness, we also compare the spectra from the different sides of the galaxy before co-adding them, and we always find good agreement. Finally, the measured SNR at 5000 Å for both the galaxy-subtracted nucleus spectra and the combined galaxy spectra is given in Table 5.1.

5.3 Line strength measurements

Before measuring the Lick absorption line indices from the flux calibrated spectra of the galactic main bodies and nuclei, we also carefully checked whether any emission lines are present, particularly since some dEs show a fairly young nucleus. However, we do not detect any [OIII] emission, thus we do not correct the Hβ absorption for possible contamination by emission. If such emission were present, it would make the measured Hβ absorption smaller, and therefore derived ages older. On the other hand, it could be possible that we do not see any emission lines because of the low spectral resolution. To quantify what strength of an emission line in a high-resolution spectrum (i.e, model of Vazdekis et al., 2010) would be smeared out in a low-resolution like ours, such that it is not recognized visually, we select a model spectrum of age 2 Gyr, and added an emission of Hβ. We then degrade the spectrum to the low-resolution of 11 Å. We find that the added emission line could have an effect of up to 12% on the measured absorption line strength, which reveals a relatively small effect on the age.

Note that we have not applied a velocity dispersion correction for the Lick indices, because the expected galactic velocity dispersion, $\sigma_{gal} \leq 50$ km s^{-1}, is significantly below our spectral resolution $\sigma_{instr} \sim 280$ km s^{-1}. Therefore these corrections are not necessary.

To measure the absorption line strengths from the spectra, we use the routine *Indexf*[1] developed by N. Cardiel. It uses the definition of the Lick indices from Trager et al. (1998) and also derives the uncertainty in measured strength using Monte-Carlo simulations. Calibrations of our measured line strengths to the actual Lick system have been done as described in Chapter 3. In Table 5.3 and 5.4 we list the measured indices for the nuclei and galactic main bodies, respectively. The comparisons of the estimated SSP parameters are shown in Figure 5.6 and 5.12.

5.3.1 Extraction of SSP parameters

We use the method of Lick indices (Burstein et al., 1984; Worthey et al., 1994b; Trager et al., 1998) as a tool for estimating the stellar population characteristics. We translate our Lick index measurements into SSP-equivalent ages, metallicities, and α-element abundance ratios by comparing them to the stellar population models of Thomas et al. (2003) by χ^2-minimization, following Proctor & Sansom (2002). For this we use the nine indices Hδ_F, Hγ_F, Fe4383, Hβ, Fe5015, Mgb , Fe5270, Fe5335 & Fe5406. Note that the SSP models assume all the stars were

[1] http://www.ucm.es/info/Astrof/software/indexf/indexf.html

formed in a single burst and have the same age and metallicity. In fact, the galaxies may be a composite stellar system formed during several episodic star formation events, with different chemical compositions in general. Therefore, our estimated stellar population parameters can be considered *SSP−equivalent stellar populations*. The correlation of age and metallicity in the model fitting is illustrated in next paragraph.

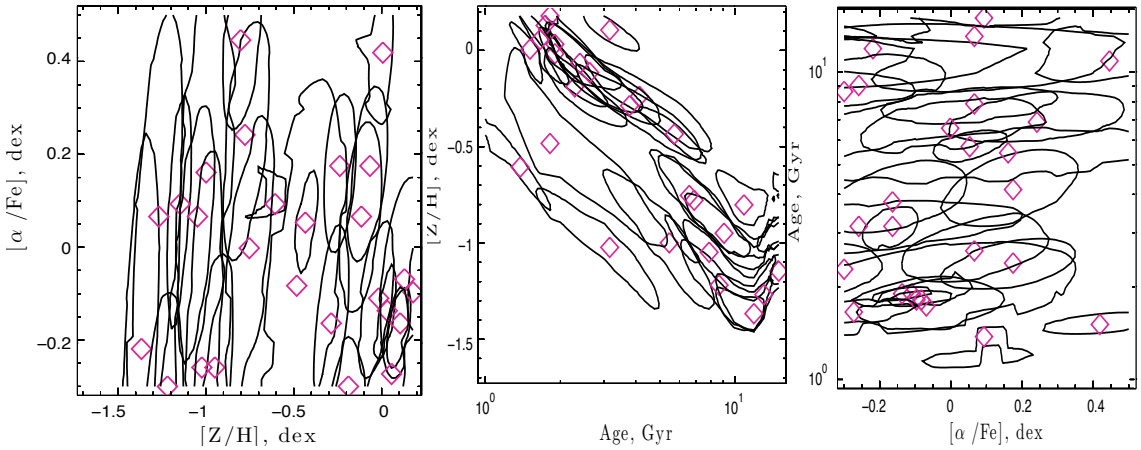

Figure 5.5: Examples of $\Delta\chi^2$ contours in different projection planes of age, metallicity and [α/Fe]-abundance space.

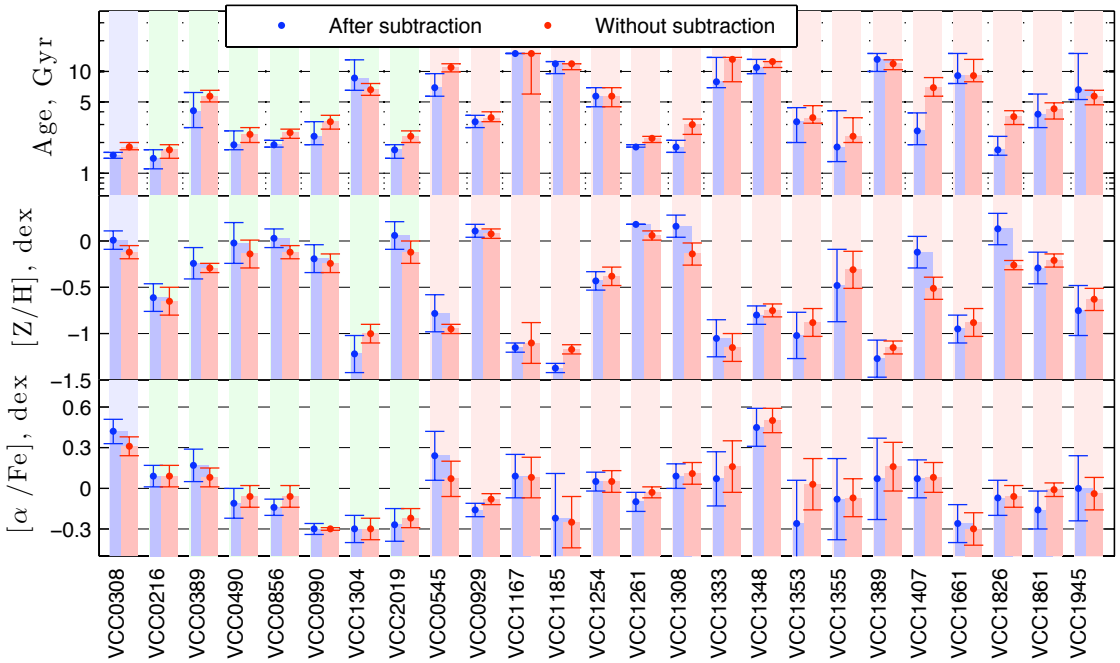

Figure 5.6: The comparison of the SSP-equivalent parameters after and before subtraction of galaxies' light from the nuclei spectra.

It is well known that the age-metallicity degeneracy is a difficult problem to estimate galaxy age and metallicity. However, there are several different methods have been suggested to cope with this complication. By using the large number of indices and adopting the technique of Proctor & Sansom (2002), the effect of this degeneracy on the estimates of SSP parameters can be minimized. Figure 5.5, shows examples of the of $\Delta\chi^2$ contours obtained with the method we have used to derive the SSP parameters, indicating the minimum with a diamond symbol. The

contours are drawn with $\Delta\chi^2 = 2.3$ (i.e., errors including 2 degrees of freedom (Press et al., 1992, Section 15.6)). This shows that the typical 1σ uncertainties we obtain on the SSP parameters are of the order of 0.1 dex. The effect of the age-metallicity degeneracy (e.g. Worthey et al., 1994b) can be recognized in the tilt of the contours in the age versus metallicity plot.

5.4 Results: sges, metallicities and α-abundance ratios

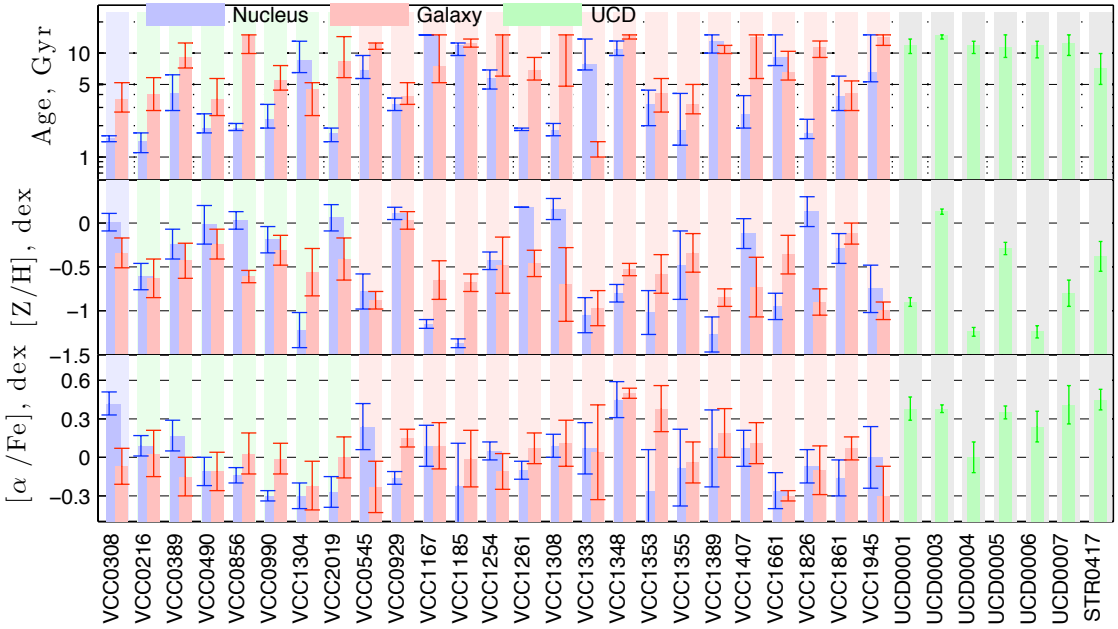

Figure 5.7: A comparison of stellar population parameters. The SSPs from the different parts of the dEs are represented with vertical bars of different color: blue for the nuclei and red for the galactic main bodies. The faint background colors indicate the dE subtype: blue for the nucleated dE with disk and blue centre, green for the nucleated dEs with disks, and red for the nucleated dEs without disk features. The Virgo UCDs are represented by the green vertical bars with gray background. For the UCDs, we used published values of line strengths from Evstigneeva et al. (2007) to derive the stellar population parameters (see text).

In this section, we present the SSP-equivalent ages, metallicities and α-abundance ratios of our sample dEs (Table 5.2). Note that, in case of the least luminous dE, VCC0725, we find that the sky noise becomes dominant beyond the central aperture. Hence, we remove its galactic part from the sample and therefore provide no SSP parameters for the galactic main body of this dE.

We can clearly see that the ages of the nuclei are significantly lower than the ages of the surrounding galactic main bodies (Figure 5.7). The differences are more prominent in the discy dEs: only VCC1304 has a nucleus that is older than the galactic part. Moreover, we find that only four other non-discy dE(N)s (VCC1167, VCC1333, VCC1389 and VCC1661 – see Section 5.2) have nuclei with significantly larger ages than the galactic main bodies. The median difference in age between the galactic main bodies and nuclei is 3.5 Gyr. Examining the Figure 5.7 individually galaxy by galaxy, one can see that VCC0856 shows the largest difference (>10 Gyr) in age between the nucleus and the galactic part. The nucleus of the blue centre dE VCC0308, while having a young age, does not show up as being special, having an age of 1.5 ±0.1 Gyr, similar to other dE nuclei such as VCC0216, VCC2019 and VCC1826.

The metallicity distributions of the nuclei and the surrounding galactic main bodies also differ:

Table 5.2: SSP-equivalent stellar population parameters for the nuclei and the galactic main bodies.

VCC	Age, Gyr		[Z/H], dex		[α/Fe], dex	
no.	Nuc.	Gal.	Nuc.	Gal.	Nuc.	Gal.
0216	$1.4^{+0.3}_{-0.3}$	$4.0^{+1.8}_{-1.2}$	-0.61 ± 0.15	-0.63 ± 0.22	0.09 ± 0.08	0.03 ± 0.18
0308	$1.5^{+0.1}_{-0.1}$	$3.6^{+1.6}_{-0.9}$	0.01 ± 0.10	-0.34 ± 0.17	0.42 ± 0.09	-0.07 ± 0.14
0389	$4.1^{+2.1}_{-1.3}$	$9.1^{+3.4}_{-1.9}$	-0.24 ± 0.17	-0.43 ± 0.20	0.17 ± 0.12	-0.15 ± 0.15
0490	$1.9^{+0.7}_{-0.2}$	$3.6^{+2.1}_{-1.1}$	-0.02 ± 0.22	-0.24 ± 0.17	-0.11 ± 0.11	-0.11 ± 0.15
0545	$6.9^{+2.6}_{-1.2}$	$12.5^{+0.0}_{-1.6}$	-0.78 ± 0.20	-0.88 ± 0.10	0.24 ± 0.18	-0.23 ± 0.20
0725[a]	$5.5^{+1.4}_{-1.7}$	– –	-1.00 ± 0.25	-- –	0.16 ± 0.38	– –
0856	$1.9^{+0.2}_{-0.1}$	$15.0^{+0.0}_{-5.1}$	0.03 ± 0.10	-0.61 ± 0.07	-0.14 ± 0.06	0.03 ± 0.16
0929	$3.2^{+0.5}_{-0.4}$	$3.8^{+1.4}_{-0.6}$	0.11 ± 0.07	0.03 ± 0.10	-0.16 ± 0.05	0.15 ± 0.07
0990	$2.3^{+0.9}_{-0.4}$	$5.5^{+2.1}_{-1.1}$	-0.19 ± 0.15	-0.31 ± 0.17	-0.30 ± 0.04	-0.01 ± 0.12
1167	$15^{+0.0}_{-0.0}$	$7.5^{+7.5}_{-2.3}$	-1.15 ± 0.05	-0.65 ± 0.22	0.09 ± 0.16	0.09 ± 0.18
1185	$11.9^{+0.6}_{-2.4}$	$12.5^{+1.2}_{-1.1}$	-1.37 ± 0.05	-0.68 ± 0.10	-0.22 ± 0.33	-0.01 ± 0.22
1254	$5.7^{+1.2}_{-1.2}$	$15.0^{+0.0}_{-9.0}$	-0.43 ± 0.10	-0.48 ± 0.32	0.05 ± 0.07	-0.11 ± 0.14
1261	$1.8^{+0.1}_{-0.0}$	$6.9^{+2.2}_{-1.4}$	0.18 ± 0.00	-0.46 ± 0.15	-0.10 ± 0.07	0.07 ± 0.12
1304	$8.6^{+4.4}_{-2.1}$	$4.5^{+0.7}_{-2.0}$	-1.22 ± 0.20	-0.56 ± 0.27	-0.30 ± 0.10	-0.22 ± 0.19
1308	$1.8^{+0.3}_{-0.2}$	$15.0^{+0.0}_{-10.2}$	$+0.16 \pm 0.12$	-0.70 ± 0.42	0.09 ± 0.09	0.11 ± 0.18
1333	$7.9^{+5.8}_{-1.0}$	$1.0^{+0.4}_{-0.0}$	-1.05 ± 0.20	-0.97 ± 0.20	0.07 ± 0.20	0.04 ± 0.37
1348	$10.9^{+2.2}_{-1.4}$	$15.0^{+0.0}_{-1.3}$	-0.80 ± 0.10	-0.53 ± 0.07	0.45 ± 0.14	0.50 ± 0.04
1353	$3.2^{+1.2}_{-1.2}$	$4.1^{+1.6}_{-1.4}$	-1.02 ± 0.25	-0.58 ± 0.22	-0.26 ± 0.32	0.38 ± 0.18
1355	$1.8^{+2.3}_{-0.5}$	$3.2^{+1.8}_{-0.6}$	-0.48 ± 0.39	-0.34 ± 0.22	-0.08 ± 0.30	-0.04 ± 0.16
1389	$13.1^{+1.9}_{-3.1}$	$11.9^{+0.0}_{-2.0}$	-1.27 ± 0.20	-0.85 ± 0.10	0.07 ± 0.30	0.19 ± 0.19
1407	$2.6^{+1.3}_{-0.7}$	$14.3^{+0.7}_{-8.6}$	-0.12 ± 0.17	-0.73 ± 0.34	0.07 ± 0.14	0.11 ± 0.16
1661	$9.1^{+5.9}_{-1.5}$	$6.6^{+3.8}_{-1.1}$	-0.95 ± 0.15	-0.36 ± 0.22	-0.26 ± 0.14	-0.30 ± 0.04
1826	$1.7^{+0.6}_{-0.2}$	$11.4^{+1.7}_{-2.3}$	$+0.13 \pm 0.17$	-0.90 ± 0.15	-0.07 ± 0.13	-0.10 ± 0.19
1861	$3.8^{+2.2}_{-1.0}$	$4.1^{+1.3}_{-1.3}$	-0.29 ± 0.17	-0.12 ± 0.12	-0.16 ± 0.14	0.07 ± 0.09
1945	$6.6^{+8.4}_{-1.3}$	$14.3^{+0.7}_{-2.4}$	-0.75 ± 0.27	-1.00 ± 0.10	0.00 ± 0.24	-0.30 ± 0.23
2019	$1.7^{+0.2}_{-0.3}$	$8.3^{+6.1}_{-2.5}$	$+0.06 \pm 0.15$	-0.41 ± 0.24	-0.27 ± 0.12	0.00 ± 0.16

[a] without subtraction of galactic light and does not have a measurement of SSPs from the galactic main body (see text).

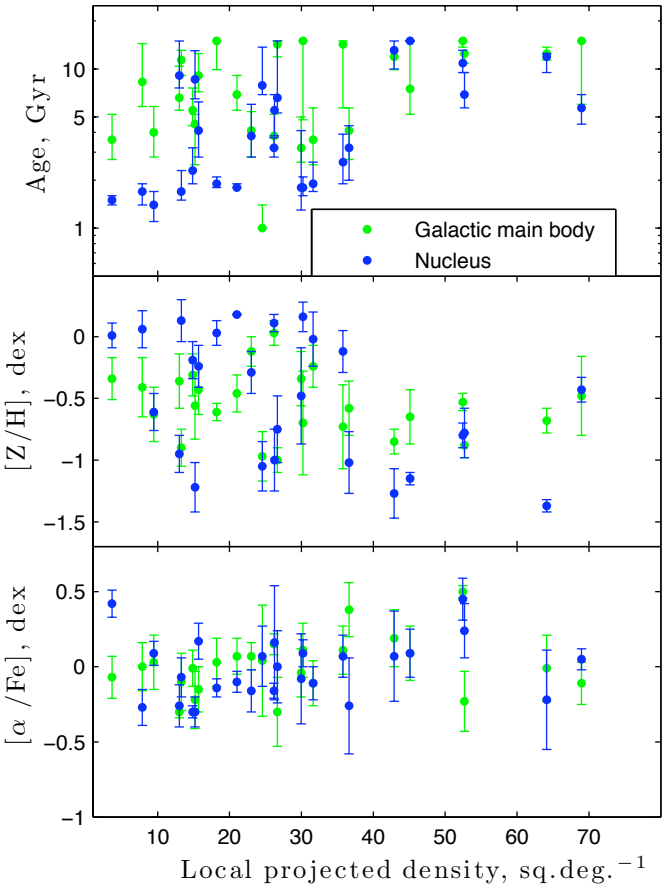

Figure 5.8: The age, metallicity and [α/Fe] versus local projected density. Green color represents the galactic main body and blue indicates the nucleus.

the majority of the nuclei are relatively metal enhanced as compared to the galactic main bodies. However, it is remarkable that those nuclei that are older or equally old as the galactic part are also less metal rich than the latter. We find that the nucleus of VCC1308 has the highest metallicity of +0.16 ±0.12 dex. For all dEs, the galactic main bodies have sub-solar metallicity. The α-abundance ratio from nuclei and galactic main bodies show a wide distribution. The nuclei of three dEs (i.e., VCC0308, VCC0389 and VCC0545) show significant α-enhancement as compared to their galactic part. On the contrary, four dEs, VCC0990, VCC0929, VCC1353 and VCC1861, exhibit a significantly enhanced α-abundance in the galactic part as compared to their nucleus.

In the right part of Figure 5.7, the green vertical bars present, for comparison, the derived stellar population parameters of the UCD sample of Evstigneeva et al. (2007). Note that we only use the published four indices (Hβ, Mgb, Fe5270 and Fe5335). However, we use the same method of estimation for the stellar population parameters. The UCD ages and metallicities are consistent with old and metal poor stellar populations. Almost all UCDs have ages ∼10 Gyr and metallicities vary between −1.25 to 0.13 dex. The [α/Fe]−abundances are always super solar in case of the UCDs, with a mean of 0.31 dex, which is 0.34 dex higher than the mean [α/Fe] of the dE nuclei.

The relation between the stellar population parameters and the local projected number density of galaxies in the cluster is plotted in Figure 6.5. The local projected density has been calculated from a circular projected area enclosing the 10th neighbor. It seems that there is a correlation between the local projected density and the ages of the nuclei. The Spearman rank order test shows a weak correlation of the ages and metallicities of the dE nuclei with the local projected

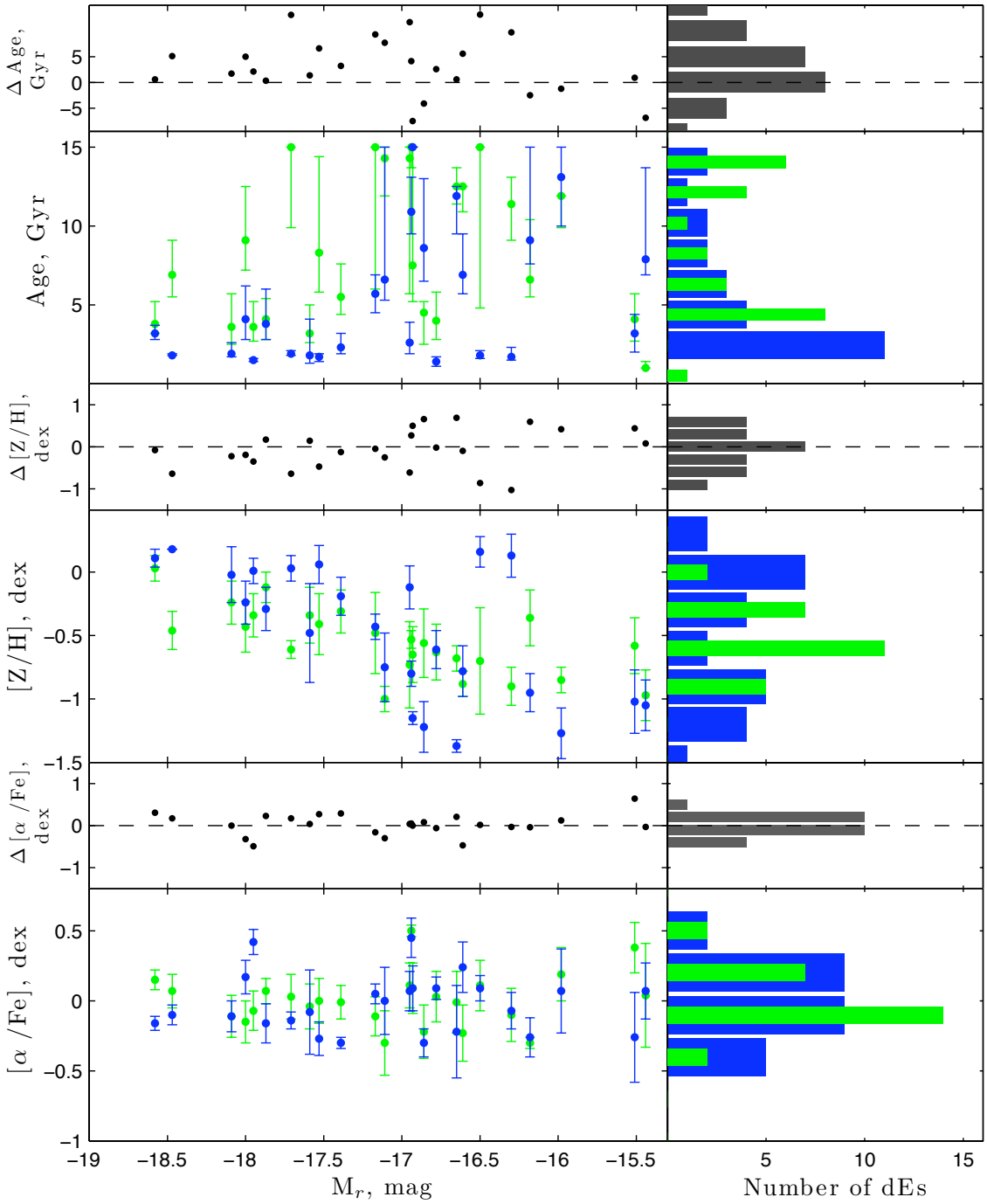

Figure 5.9: The derived ages (top), metallicities (middle) and [α/Fe]-abundance (bottom), plotted against $r-$band absolute magnitude (left). The blue color represents the nuclei and green color indicates the galactic main body. On top of each panel, we also show the difference in the SSP parameters, i.e. galactic part − nucleus. In the right panel, we provide the number distribution of the parameters.

densities. The correlation coefficients are 0.5 and −0.4, and the probabilities of the null hypothesis that there is no correlation are 0.2% and 4% for the age and metallicity, respectively. Unlike this, a similar test shows that the SSPs of the galactic main body do not have any relation with local projected densities.

The relations between the stellar population parameters and the total galactic luminosity are presented in Figure 5.9. At the top of each panel, we also provide the trend of the differences in the SSP parameters between the galactic main bodies and the nuclei. It is clearly recognized that almost all dEs brighter than $M_r = -17$ mag have younger and more metal-rich nuclei than the galactic main bodies. On the other hand, there is a relatively large scatter in the low luminosity region, and we can see that some of the nuclei are as old and metal poor as the galactic main bodies. However, the sign of the differences in age and metallicity between galactic main body and nucleus are completely opposite at the fainter and brighter end of the plot. As there exists a well-known metallicity-luminosity relation in early type galaxies (Poggianti et al., 2001), our sample also follows this relation for both nuclei and galaxies, i.e., the metallicity decreases with decreasing total galactic luminosity. The derived [α/Fe] values are fairly consistent with a roughly solar value for both nuclei and galactic main bodies.

In the right panels of Figure 5.9, we provide the number distribution (in the histogram) of stellar population parameters of the nuclei (in blue color) and the galactic main bodies (in green color). It seems that the ages of the galactic main bodies have a bimodal distribution, but the small number of data points in each bin and the fairly large errors in the age measurement increase the uncertainty; the bimodality thus remains a qualitative impression. The age distribution of the nuclei is highly dominated by nuclei of younger ages. The metallicity distribution however appears much broader in case of nuclei than galactic main body. The nucleus metallicity ranges from slightly super-solar (+0.18 dex) to strongly sub-solar values (−1.22 dex), and interestingly all dE galactic main bodies have sub-solar metallicity.

5.4.1 Stellar population gradients

Due to the low brightness of dEs, it is always challenging to get spectra from their outer part with sufficient SNR to study stellar population gradients. Some attempts have been made to derive the stellar population gradients in the different cluster dEs (Chilingarian 2009 for Virgo, Koleva et al. 2009 for Fornax). These studies used different methods to obtain SSP parameters, namely through spectral fitting with SSP models. Chilingarian (2009) observed either flat or negative radial gradients in metallicity in his sample. However, due to the relatively high uncertainty in the age estimation, he did not draw any conclusions on the radial behavior of ages. The study of Koleva et al. (2009) reconfirmed the result of the existence of negative metallicity gradients and found radial age gradients in the dEs, with older ages at larger radii.

In Figure 5.10−5.11, we present the radial profiles of SSP-equivalent age, metallicity and abundance ratio, measured in bins along the major axis of the dEs. It is interesting that we can divide these trends of SSPs in two groups. The first group dEs are those which exhibit a smooth trend of increasing the age and decreasing metallicity with radius, beginning from the nucleus, such as VCC0308, VCC0490, VCC0929, VCC1261 and VCC2019. In contrast, the second group shows a break in the SSP profile when going from the nucleus to the surrounding galactic part, with the latter having a nearly flat gradient, like e.g. for VCC0216, VCC0856, VCC1304 and VCC1355.

Three dEs, VCC2019, VCC1261 and VCC0308, show a significant gradient in age and metallicity, having a relatively young and metal enhanced nucleus. Likewise, the ages of VCC0389,

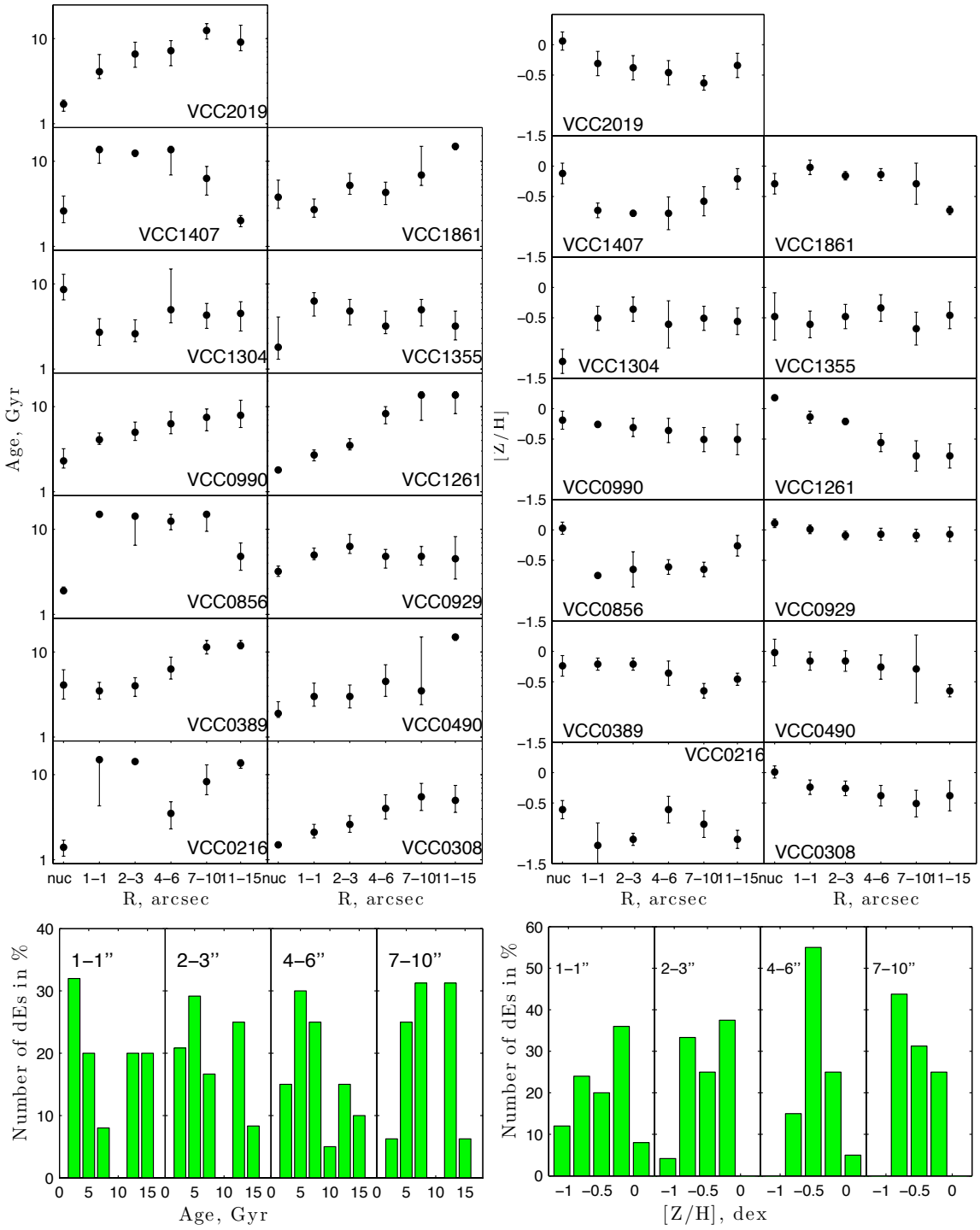

Figure 5.10: The radial age profiles of selected dEs (here we select those dEs which have sufficient SNR at the last radial bin, 11” to 15”). The age and metallicity distribution at different radial bins.

VCC0490, VCC0990, VCC0929 and VCC1407 also seem to correlate with the radius. Our derived ages for VCC0856 agree with the result of Chilingarian (2009) that this galaxy has a flat distribution of ages beyond the central nucleus. In addition to that, we can also see such a flatness in the age distribution of VCC1355. VCC1261 presents the largest gradient in metallicity starting from slightly super solar down to a sub-solar value of −0.75 dex. Although we do not see any strong trend of [α/Fe] with radius in most of the cases, VCC0216 and VCC2019 display the opposite trend of decreasing and increasing of [α/Fe] with radius, respectively.

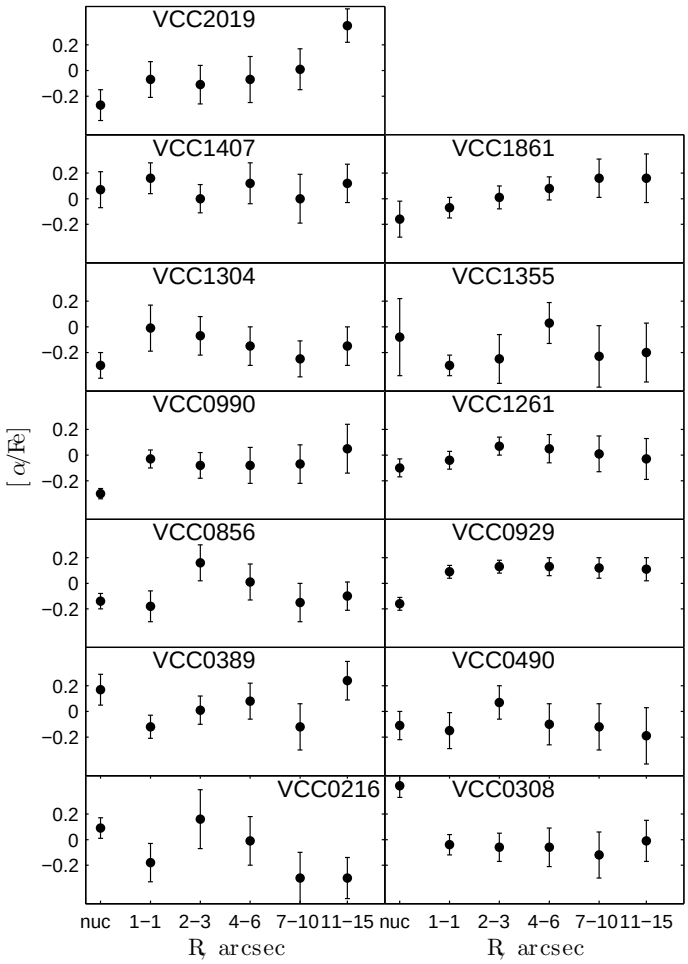

Figure 5.11: The radial profile of the α-abundance ratios of the dEs, selected as in Figure 5.10.

In bottom panel of Figure 5.10 we show the age and metallicity distribution of our dEs in the different radial bins. Note that there is not always the same number of dEs in each radial bin: due to insufficient SNR in the outer radii for some dEs, those were omitted from the respective bins. The first 1" bin contains 25 dEs, and the second, third and fourth bin contains 24, 20 and 16 dEs, respectively. Therefore, the y-axis represents the normalized fraction in percent. It is easily noticeable that the distributions change with radius: the inner bin is dominated by young ages and shows a broader metallicity distribution, and the fraction of old ages and low metallicities increases as we go outward, with the metallicity distribution becoming narrower.

5.5 Discussion

In this Chapter, we have characterized the stellar population parameters from the different parts of dEs: the nuclei and the surrounding galactic main bodies. Our primary motivation for this is to improve our understanding of the physical mechanisms responsible for the formation of dE nuclei and the subsequent evolution of dEs themselves. As we now discuss, our study makes two important contributions in this context: (i) to much more firmly establish the SSP-equivalent stellar population parameters of dEs and their nuclei (ii) to cast new light on the spatially re-

solved stellar population characteristics of dEs.

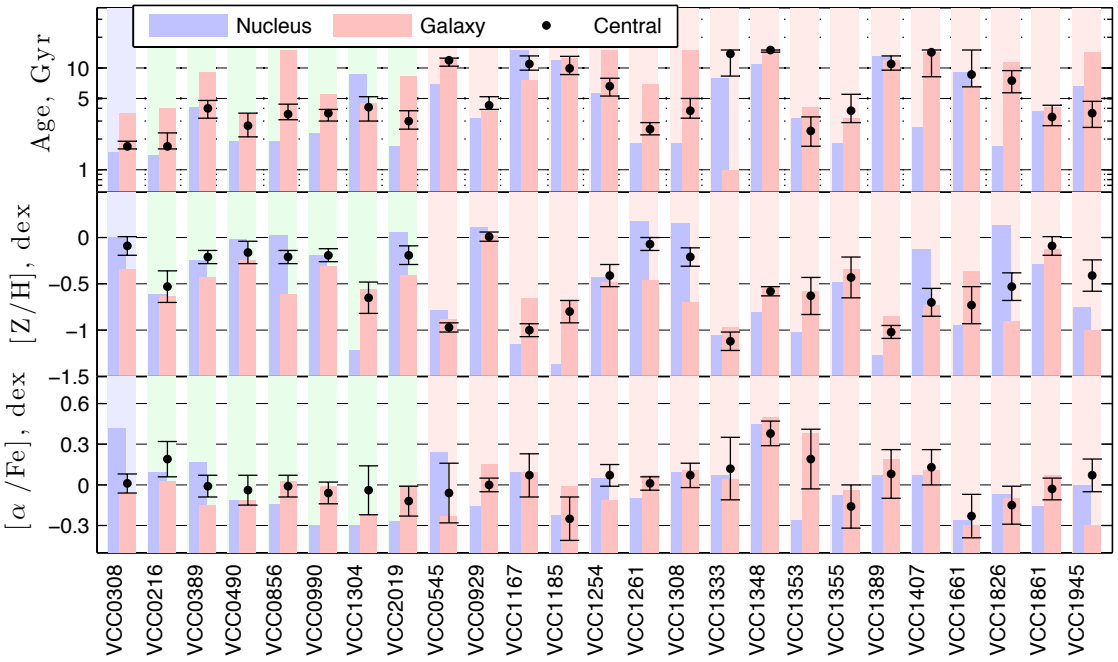

Figure 5.12: The comparison of the SSP-equivalent parameters of the galactic main bodies (red), nuclei of dEs (blue), and the result for the combined central light from Paper I (black), where a central spectrum was analyzed without separating nucleus and galactic main body.

The surrounding galactic main body is represented by extracting its spectrum from a 5" radial interval beyond 3" from the centre, avoiding any contamination with light from the nucleus. We expect that, due to our method of subtraction of the underlying galactic light from the nucleus spectra (see Section 5.2.2), we obtained comparatively clean spectra of the nuclei, with the derived stellar population properties from such spectra well representing the nucleus stellar population. Nevertheless, as outlined before, in the cases of weak nuclei there is still a chance that the remaining galactic light contributes significantly, such that the nuclear spectra represent the combination of nucleus and "central galaxy light". To test for a possible bias due to this effect, we select those dEs which have galactic light fraction (see Table 5.1) larger than 50% at the central aperture such as VCC0990, VCC1353, VCC1355, VCC1407 and VCC1826, but all these nuclei have ages less than 5 Gyr, and agree fairly well with the average age of the nuclei in total.

Generally speaking, stellar population gradients can be used as a proxy for the study of the evolutionary history of early type galaxies, since different formation models predict different gradients. In a nutshell, monolithic collapse models (Arimoto & Yoshii, 1987) predict slightly steeper gradients than the hierarchical merging model (White, 1980). These predictions, however, mainly apply to normal early-type galaxies (Es). In case of early-type dwarfs, different formation scenarios might be relevant, such as morphological transformation, or simply a primordial origin (also see the discussion in Chapter 4). Nevertheless, the overall distribution of age and metallicity at the different radial bins suggest that it occurs more frequently that the inner parts of dEs are younger and more metal enhanced than their outer parts, which is consistent with previous studies (Chilingarian, 2009; Koleva et al., 2009). We also see two distinct behaviours of radial SSP profiles; the presence of flat profiles may be due to a particular galaxy structure (i.e., a faint underlying disk) or may be an indication of a different origin. Among

the dEs with smooth SSP gradients, VCC0308 only has a very weak blue centre (Lisker et al., 2006), so it may well be that other galaxies have just a bit weaker color gradients and were thus not labeled "blue-centre dE" previously. On the other hand, VCC0216 and VCC0856 have a similarly young nucleus as VCC0308, but not an age gradient in the galaxy itself, which might lead to having no color gradient.

Another key result emerging from our study is a very clear picture of the differences between the stellar populations of the nuclei and the galactic main bodies of the dEs. To our knowledge, no spectroscopic study has yet performed such a comparison with a similar sample size. Studies based on color differences (Durrell 1997, Côté et al. 2006, and particularly Lotz et al. 2004) find slightly bluer nuclei. It is, however, not straightforward to interpret these color differences in the sense of stellar population properties, as we know that a degeneracy in the age and metallicity exists with color (see also Section 5.3.1). In contrast to the explanation of Lotz et al. (2004) of having more metal rich populations in the surrounding galactic main bodies, we find a metal poorer and older population in the galactic part on average. In addition to this, as Côté et al. (2006) note, there exists a color-luminosity relation for the nuclei. We also find that the metallicity of dE nuclei correlates with the total luminosity of dEs.

We have seen that there is almost no correlation between the ages of the galactic main bodies and the luminosity of the dEs. This might, at first glance, imply that the reason for the apparent age dichotomy in Paper I, finding a clear correlation with luminosity for the central stellar populations of dEs, was due to the nucleus contribution to the central aperture light. However, Figure 5.6 of the Appendix, which compares the SSPs resulting from the nucleus spectra before and after subtraction of the underlying galactic light, actually tells us that this conclusion is not true: if the very central stellar populations of the galaxies, whose pure light cannot be seen due to the superposed nucleus, would be so much older than the nucleus itself, the difference before/after subtraction would be quite significant, which is not found. Instead, the figure tells us that the very central part of the galaxy does also reach, in most cases, almost the young age of the nuclei. Thus, in many cases it is really the age gradient within the galaxy that makes the galactic part surrounding the nucleus appear significantly older than the nucleus itself in Figure 5.9.

5.5.1 Evolution of dEs and formation of nuclei

As we mentioned in the introduction, many studies have discussed the origin of the nuclei of dEs together with the evolution of dEs themselves. It is challenging to provide definitive observational tests of these different scenarios. Moreover, we argue in Paper I that not all dEs are the same class of object. The dichotomy in the age distribution of the galactic main bodies also supports the idea that one type of dEs may have a primordial origin (Rakos & Schombert, 2004), being relatively old and metal poor. These might have suffered either early infall into the cluster potential or formed together with the cluster itself. The common idea is that internal feedback might be responsible for the removal of gas, with the consequence that star formation activity ceases at such early epochs.

On the other hand, dEs with a relatively young and metal enhanced galactic main body likely have a different origin. As they are also preferentially brighter and often host disk-structure, they might have formed through the structural transformation of a late-type spiral into a spheroidal system, triggered by the popular scenario of strong tidal interactions with massive cluster galaxies. Simulations have shown that late-type galaxies entering in a rich cluster can undergo a significant morphological transformation into spheroidals by encounters with brighter galaxies and with the cluster's tidal field (Moore et al., 1996; Mastropietro et al., 2005). This scenario is unlikely to produce the observed radial SSP gradients: either metallicity gradients must have

formed in the late-type galaxies and somehow preserved during morphological transformation (see the discussion in Spolaor et al., 2010), or accretion of leftover gas towards the centre of the galaxy would have to be responsible for the creation of such gradients. However, the flat [α/Fe] profile implies a similar star formation time scale everywhere in the dEs.

As we discussed above, the fairly different types of dEs with and without disk structure might have a different origin. It is therefore even more difficult to explain the origin of the nuclei of these dEs with a single scenario. However, from this and previous studies, it is becoming clear that the majority of dE nuclei are unlikely to have formed through the merging of globular clusters: Côté et al. (2006) already explained the difficulty of this scenario with the luminosity differences, and additionally we find that most nuclei are fairly young and metal rich, at least in case of the brighter dEs ($M_r \leq -17.25$ mag). There are still the nuclei of some fainter dEs (i.e., $M_r > -17.25$ mag) which have fairly old and metal-poor populations, more resembling the stellar population properties of globular clusters. They might have formed through a different process as the nuclei of brighter dEs.

The younger and comparably metal-rich nuclei support the idea that the central stellar populations of dEs were governed by continuous infall and accretion of gas in the centre of the potential well, building the nuclei. The brighter dEs also host disk features (e.g. residual spiral arms/bars) and these dEs themselves might have been formed through the transformation of late-type spirals (Sc-Sd types). High resolution HST imaging has shown that such late-type objects frequently contain a compact nuclear cluster (Böker et al., 2002, 2004), and Côté et al. (2006) observed that such nuclear clusters have similar sizes to dE nuclei. Stellar population studies have shown that the majority of nuclear clusters have ages of few tens of Myr (Seth et al., 2006; Walcher et al., 2006) with episodic star formation activity. Following the simplest interpretation, it could be that the present day dE nuclei are simply the nuclear clusters of the transformed late-type galaxies, and their star formation activity faded with the morphological transformation of the host galaxies. However, this scenario again fails to explain the observed age difference between the nuclei and galactic main bodies, since late type disks are also considered to host star formation activity throughout the inner region and disk. Alternatively, the truncation of star formation in the disk due to interactions could be more efficient than in the nucleus, which eventually leads to the development of age/metallicity gradients in dEs and makes the central nucleus younger and metal richer than the galactic main body. In any case, more detailed numerical simulations are required to test these hypotheses.

We find that dE nuclei exhibit fairly different stellar populations than UCDs. Particularly, the relatively older population (larger than 8 Gyr) and slightly super-solar α-abundance of UCDs may seem to create an inconsistency in the idea of dE nuclei being the progenitors of UCDs. Nevertheless, the current sample of UCDs is limited, and the fairly large spread in the stellar population properties of dE nuclei may allow the possibility of UCD formation in the Virgo cluster by the stripping of such dEs whose nuclei have old and metal poor stellar populations (Paudel et al., 2010). Therefore, a larger sample of UCDs and perhaps a more rigorous comparison of SSP properties than this work is needed before any strong conclusions can be drawn.

5.6 Conclusions

We have investigated the stellar population properties of the central nucleus and the surrounding galactic main bodies for a sample of 26 dEs in the Virgo cluster and compared the SSP-equivalent stellar population parameters of the dE nuclei with the ones of a small sample of UCDs. In addition to this, we have derived the radial profiles for age, metallicity and [α/Fe]

abundance for 13 dEs. Our main findings can be summarized as follows:

- We find that for most of the dEs the nuclei are significantly younger (~3.5 Gyr) and more metal rich (~0.07 dex) as compared to the galactic main body of the galaxies. Only five dEs have significantly older nuclei than their galactic main bodies, and dEs with old and metal poor nuclei are more likely to be distributed in the dense region of the cluster than the dEs with young and metal-enhanced nuclei.
- The metallicity of dE nuclei correlates with the total luminosity of dEs, and the observed metallicities of the nuclei have a fairly large range (+0.18 to -1.22 dex). All galactic main bodies of the dEs have sub-solar metallicity.
- While we see two distinct behaviours of SSP profiles (with and without a break) the overall trend of increasing age and decreasing metallicity with the radius is consistent with earlier studies. The α-abundance is consistent to the solar value with no gradient along the major axis.
- These observed properties suggest that the merging of globular clusters might not be the appropriate scenario for the formation of nuclei in dEs, at least not for the brighter dEs. The younger and comparably metal-rich nuclei support the idea that the central stellar populations of dEs were governed by continuous infall/accretion of gas in the centre of the potential well, building the nuclei.
- The heterogeneous nature of the stellar population characteristics of dEs hints at different formation scenarios of dEs, similar to the conclusion of our previous study (Paudel et al., 2010). Our results suggest that the old, faint and metal-poor dEs are more likely to have a primordial origin, while those with relatively young ages and a higher metallicity and luminosity may have formed through morphological transformation.

5.7 Appendix

Table 5.3: Measured line strength indices from the nuclei of dEs after subtraction of galactic light and corrected to the Lick system.

VCC no.	Hδ_F Å	Hγ_F Å	Fe4383 Å	Hβ Å	Fe5015 Å	Mg$_b$ Å	Fe5270 Å	Fe5335 Å	Fe5406 Å
0216	4.75 ± 0.27	3.78 ± 0.24	0.06 ± 0.64	3.11 ± 0.28	3.82 ± 0.62	1.28 ± 0.31	1.69 ± 0.35	0.68 ± 0.39	1.44 ± 0.28
0308	2.95 ± 0.43	2.48 ± 0.35	4.08 ± 0.82	3.31 ± 0.36	4.49 ± 0.80	3.06 ± 0.38	0.84 ± 0.45	0.82 ± 0.53	0.72 ± 0.37
0389	2.78 ± 0.50	-0.20 ± 0.44	4.91 ± 0.91	2.39 ± 0.42	4.71 ± 0.90	2.41 ± 0.43	1.84 ± 0.48	2.00 ± 0.53	0.73 ± 0.42
0490	1.87 ± 0.47	0.94 ± 0.40	4.04 ± 0.87	2.89 ± 0.38	4.59 ± 0.83	2.17 ± 0.41	2.71 ± 0.45	2.10 ± 0.51	1.24 ± 0.37
0545	2.10 ± 0.44	0.79 ± 0.37	2.77 ± 0.86	2.84 ± 0.37	2.16 ± 0.85	2.00 ± 0.40	1.36 ± 0.45	1.00 ± 0.51	1.21 ± 0.38
0725[a]	2.01 ± 0.57	2.28 ± 0.50	2.16 ± 1.22	3.55 ± 0.52	2.55 ± 1.24	1.44 ± 0.57	1.16 ± 0.67	0.54 ± 0.77	0.39 ± 0.56
0856	1.76 ± 0.27	1.27 ± 0.22	4.81 ± 0.49	2.02 ± 0.23	5.17 ± 0.48	2.35 ± 0.24	2.69 ± 0.26	2.29 ± 0.29	1.40 ± 0.22
0929	0.04 ± 0.31	-0.28 ± 0.25	5.45 ± 0.51	2.35 ± 0.24	5.68 ± 0.50	2.82 ± 0.25	2.41 ± 0.28	3.15 ± 0.29	1.83 ± 0.22
0990	1.02 ± 0.59	1.01 ± 0.45	3.03 ± 0.97	2.94 ± 0.39	5.80 ± 0.82	1.33 ± 0.41	2.71 ± 0.44	1.25 ± 0.51	2.35 ± 0.36
1167	3.05 ± 0.30	1.45 ± 0.28	1.55 ± 0.62	2.58 ± 0.27	3.56 ± 0.61	1.38 ± 0.30	1.50 ± 0.33	1.13 ± 0.38	0.71 ± 0.28
1185	1.37 ± 0.44	2.05 ± 0.34	2.03 ± 0.85	2.17 ± 0.41	2.36 ± 0.90	1.04 ± 0.43	1.08 ± 0.48	0.48 ± 0.54	0.44 ± 0.41
1254	1.60 ± 0.23	0.60 ± 0.20	3.36 ± 0.43	1.93 ± 0.19	4.14 ± 0.42	2.31 ± 0.20	1.85 ± 0.23	2.06 ± 0.25	1.28 ± 0.19
1261	1.58 ± 0.32	0.45 ± 0.27	4.07 ± 0.59	2.77 ± 0.26	6.05 ± 0.55	2.76 ± 0.27	3.27 ± 0.30	2.95 ± 0.34	1.42 ± 0.25
1304	1.94 ± 0.41	1.75 ± 0.35	1.41 ± 0.85	2.46 ± 0.37	2.48 ± 0.85	0.82 ± 0.42	1.70 ± 0.45	1.57 ± 0.50	0.70 ± 0.39
1308	1.39 ± 0.58	1.28 ± 0.46	5.30 ± 1.00	2.55 ± 0.45	1.11 ± 1.10	3.11 ± 0.47	1.44 ± 0.55	2.24 ± 0.61	1.52 ± 0.46
1333	1.99 ± 0.34	1.72 ± 0.29	3.00 ± 0.70	2.20 ± 0.31	3.48 ± 0.69	1.61 ± 0.34	0.81 ± 0.38	0.99 ± 0.43	0.54 ± 0.32
1348	1.68 ± 0.36	0.29 ± 0.32	2.40 ± 0.69	2.16 ± 0.31	3.07 ± 0.68	2.26 ± 0.32	1.74 ± 0.36	0.85 ± 0.42	0.50 ± 0.31
1353	3.84 ± 0.47	3.50 ± 0.44	1.32 ± 1.10	3.00 ± 0.48	3.71 ± 1.06	1.13 ± 0.52	0.59 ± 0.60	1.62 ± 0.65	0.87 ± 0.51
1355	4.12 ± 0.75	1.72 ± 0.76	2.67 ± 1.76	2.75 ± 0.76	2.89 ± 1.74	1.44 ± 0.80	2.42 ± 0.89	1.66 ± 1.02	1.42 ± 0.75
1389	3.15 ± 0.47	1.27 ± 0.44	1.47 ± 1.01	1.65 ± 0.44	2.75 ± 0.98	1.37 ± 0.46	0.72 ± 0.52	1.33 ± 0.58	0.97 ± 0.42
1407	1.61 ± 0.70	0.69 ± 0.54	2.96 ± 1.25	2.52 ± 0.50	4.47 ± 1.05	2.64 ± 0.50	1.43 ± 0.57	2.42 ± 0.61	1.92 ± 0.46
1661	2.11 ± 0.41	0.35 ± 0.36	3.02 ± 0.82	2.49 ± 0.36	3.33 ± 0.82	1.09 ± 0.40	1.60 ± 0.44	1.12 ± 0.50	1.33 ± 0.36
1826	1.78 ± 1.62	0.75 ± 0.92	5.46 ± 1.59	3.01 ± 0.56	2.78 ± 1.26	2.65 ± 0.55	3.09 ± 0.59	2.34 ± 0.67	1.56 ± 0.49
1861	1.84 ± 0.50	0.52 ± 0.44	4.01 ± 0.93	1.78 ± 0.43	4.63 ± 0.90	2.00 ± 0.44	2.62 ± 0.48	1.92 ± 0.55	1.71 ± 0.42
1945	2.04 ± 0.43	0.88 ± 0.37	2.41 ± 0.87	2.29 ± 0.40	4.32 ± 0.89	1.66 ± 0.43	1.09 ± 0.50	1.17 ± 0.57	1.58 ± 0.41
2019	1.84 ± 0.52	1.24 ± 0.40	4.44 ± 0.91	2.95 ± 0.41	4.45 ± 0.90	2.00 ± 0.45	2.99 ± 0.49	2.34 ± 0.56	1.71 ± 0.43

[a] without subtraction of galactic light.

Table 5.4: Measured line strength indices from the galactic main body of dEs (i.e., 3 to 8 arcsec radial interval) and corrected to the Lick system.

VCC no.	$H\delta_F$ Å	$H\gamma_F$ Å	Fe4383 Å	$H\beta$ Å	Fe5015 Å	Mg_b Å	Fe5270 Å	Fe5335 Å	Fe5406 Å
0216	2.46 ± 0.38	1.87 ± 0.34	3.22 ± 0.80	2.35 ± 0.36	3.13 ± 0.84	2.02 ± 0.40	1.61 ± 0.46	1.35 ± 0.51	1.16 ± 0.38
0308	1.56 ± 0.38	0.85 ± 0.34	3.30 ± 0.78	2.46 ± 0.36	4.43 ± 0.81	2.00 ± 0.39	2.37 ± 0.44	2.06 ± 0.50	1.07 ± 0.37
0389	-0.57 ± 0.43	-0.06 ± 0.37	3.26 ± 0.79	2.49 ± 0.36	4.10 ± 0.81	2.22 ± 0.38	2.48 ± 0.43	1.89 ± 0.48	1.21 ± 0.37
0490	1.26 ± 0.53	0.64 ± 0.48	5.05 ± 1.04	2.26 ± 0.49	4.38 ± 1.10	2.23 ± 0.53	2.35 ± 0.60	1.87 ± 0.67	1.19 ± 0.49
0545	-0.05 ± 0.43	0.09 ± 0.37	2.51 ± 0.83	2.13 ± 0.38	3.82 ± 0.85	1.26 ± 0.42	0.78 ± 0.48	0.86 ± 0.53	1.16 ± 0.39
0856	1.39 ± 0.35	-0.48 ± 0.32	3.80 ± 0.70	1.94 ± 0.33	3.84 ± 0.73	2.11 ± 0.35	2.07 ± 0.39	1.84 ± 0.44	1.23 ± 0.33
0929	1.71 ± 0.32	-0.66 ± 0.31	5.48 ± 0.62	2.25 ± 0.30	4.40 ± 0.66	3.21 ± 0.31	2.78 ± 0.36	1.75 ± 0.40	1.43 ± 0.30
0990	0.88 ± 0.35	0.36 ± 0.31	4.18 ± 0.66	2.21 ± 0.30	4.52 ± 0.70	2.27 ± 0.32	2.12 ± 0.37	1.68 ± 0.42	1.31 ± 0.32
1167	1.79 ± 0.41	0.37 ± 0.39	3.41 ± 0.84	2.59 ± 0.39	3.07 ± 0.91	2.08 ± 0.43	1.75 ± 0.48	1.01 ± 0.58	1.41 ± 0.40
1185	1.50 ± 0.32	-0.88 ± 0.31	3.54 ± 0.65	1.53 ± 0.32	3.48 ± 0.69	1.59 ± 0.35	1.08 ± 0.39	2.12 ± 0.42	1.19 ± 0.32
1254	0.60 ± 0.45	-0.18 ± 0.39	5.24 ± 0.83	1.20 ± 0.41	3.84 ± 0.91	2.86 ± 0.42	1.86 ± 0.50	2.48 ± 0.55	2.09 ± 0.40
1261	1.20 ± 0.27	0.40 ± 0.25	3.61 ± 0.56	2.03 ± 0.26	3.66 ± 0.57	2.38 ± 0.28	2.16 ± 0.31	1.51 ± 0.36	1.37 ± 0.26
1304	2.31 ± 0.37	0.97 ± 0.36	3.88 ± 0.78	2.35 ± 0.37	4.14 ± 0.82	1.65 ± 0.40	2.31 ± 0.44	1.90 ± 0.49	1.06 ± 0.38
1308	1.72 ± 0.43	0.15 ± 0.40	2.38 ± 0.91	1.94 ± 0.41	4.91 ± 0.93	2.24 ± 0.43	1.86 ± 0.50	2.15 ± 0.56	1.16 ± 0.43
1333	6.16 ± 0.39	1.44 ± 0.50	1.13 ± 1.04	3.69 ± 0.44	1.94 ± 1.08	1.60 ± 0.51	1.48 ± 0.57	0.97 ± 0.67	1.29 ± 0.47
1348	2.56 ± 0.46	-1.30 ± 0.49	3.50 ± 0.98	1.94 ± 0.49	3.15 ± 1.06	3.14 ± 0.48	0.39 ± 0.59	1.00 ± 0.66	1.50 ± 0.47
1353	2.37 ± 0.37	1.52 ± 0.35	0.42 ± 0.85	2.78 ± 0.38	3.08 ± 0.86	2.21 ± 0.40	1.78 ± 0.46	1.14 ± 0.52	1.43 ± 0.40
1355	1.86 ± 0.43	1.08 ± 0.40	3.05 ± 0.90	2.45 ± 0.43	4.65 ± 0.97	1.93 ± 0.46	2.03 ± 0.52	1.46 ± 0.59	1.63 ± 0.44
1389	1.12 ± 0.39	0.18 ± 0.37	2.32 ± 0.80	2.15 ± 0.38	2.77 ± 0.90	1.83 ± 0.42	1.75 ± 0.47	1.19 ± 0.54	0.29 ± 0.41
1407	1.40 ± 0.39	0.55 ± 0.34	3.33 ± 0.78	1.90 ± 0.36	3.87 ± 0.80	2.34 ± 0.38	2.03 ± 0.43	1.51 ± 0.49	0.91 ± 0.37
1661	-0.04 ± 0.45	0.02 ± 0.40	4.31 ± 0.89	2.17 ± 0.42	5.75 ± 0.96	1.30 ± 0.46	1.10 ± 0.53	2.63 ± 0.57	1.63 ± 0.42
1826	1.85 ± 0.35	-0.13 ± 0.34	1.10 ± 0.75	2.02 ± 0.36	4.58 ± 0.82	1.34 ± 0.40	1.97 ± 0.45	1.91 ± 0.50	1.15 ± 0.37
1861	1.32 ± 0.39	-0.02 ± 0.36	4.58 ± 0.74	2.11 ± 0.35	4.68 ± 0.77	2.88 ± 0.37	1.92 ± 0.43	2.32 ± 0.47	1.56 ± 0.37
1945	1.96 ± 0.35	0.94 ± 0.33	6.20 ± 0.70	1.66 ± 0.36	2.89 ± 0.81	1.59 ± 0.39	1.46 ± 0.44	2.09 ± 0.49	1.23 ± 0.36
2019	0.68 ± 0.43	0.02 ± 0.37	3.97 ± 0.82	1.94 ± 0.39	4.63 ± 0.89	2.35 ± 0.42	2.12 ± 0.49	1.55 ± 0.56	1.36 ± 0.42

6

Nuclei of early-type dwarf galaxies: are they progenitors of UCDs?

Abstract

To address the question of whether the so-called ultra compact dwarf galaxies (UCDs) are the remnant nuclei of destroyed early-type dwarf galaxies (dEs), we analyze the stellar population parameters of the nuclei of 34 Virgo dEs, as well as ten Virgo UCDs, including one that we discovered and which we report on here. Based on absorption line strength (Lick index) measurements, we find that nuclei of Virgo dEs have younger stellar population ages than UCDs, with averages of 5 Gyr and >10 Gyr, respectively. In addition to this, the metallicity also differs: dE nuclei are on average more metal-rich than UCDs. On the other hand, comparing the stellar population parameters at the same local galaxy density, with UCDs being located in the high-density cluster regions, we do not find any difference in the stellar populations of dE nuclei and UCDs. In those regions, the dE nuclei are as old and as metal poor as UCDs. This evidence suggests that the Virgo UCDs may have formed through the stripping of dE nuclei.

Result published on S. Paudel et al., ApJ, 724L, 64P, 2010.

Contents

Figures

6.1 Introduction

In the previous two chapters, we studied the stellar population characteristics of early-type dwarfs (dEs). It revealed that dEs do not contain the homogenous stellar population properties, as they are heterogeneous in morphology. In addition, we saw a variation of their stellar population properties with radius, i.e. the centre of dEs has to be younger and metal enhanced than the outer part. And particularly, we found the nuclei of dEs are significantly younger than the galactic main body. In this Chapter, we focus on the recently discovered a type of galaxy called Ultra Compact Dwarf galaxy (UCD). We will derive the stellar population parameters (age, metallicity and α-abundant ratio) for a complete set of Virgo UCDs sample. Finally we will make a detail comparison between the stellar population properties of dEs nuclei and UCDs. The aim of the study is to check whether the nuclei of dEs are the progenitors of UCDs or not.

This Chapter is organized as follows: In Section 6.1.1, we provide an introductory of overview of UCDs. In Section 6.2, we describe sample, observation and data reduction. The next is results in Section 6.3 and finally the discussion and conclusions are presented in Section 6.4.

6.1.1 Ultra compact dwarf galaxies

The recently discovered Ultra Compact Dwarfs (UCDs) are the least luminous galaxies in the galaxy luminosity function. They are particularly found around the centre of nearby galaxy clusters (Hilker et al., 1999; Phillipps et al., 2001; Drinkwater et al., 2003). UCDs are compact stellar systems and more luminous than the typical globular clusters (GCs). They have properties intermediate between the dEs and GCs. Their sizes are typically three times larger than GCs. Deep imaging of the Fornax Cluster (Hilker et al., 2003) has established that the UCDs are not an extreme tail of the normal early-type dwarf galaxy population. But, Drinkwater et al. (2004) show that UCDs follow the Faber-Jaction relation which is defined by bright Es i.e. $L \propto \sigma^4$ (See Figure 6.1).

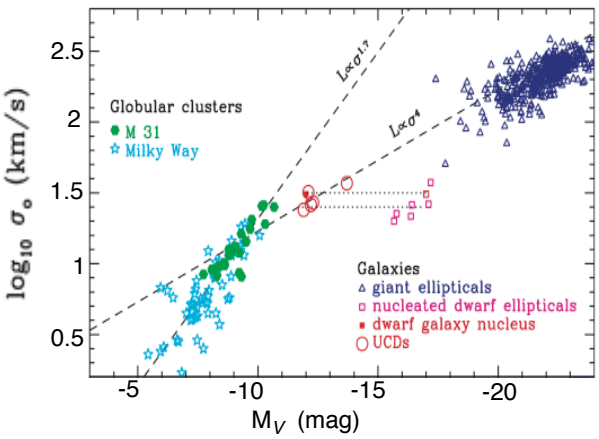

Figure 6.1: Faber-Jaction relation for early-type stellar systems, where UCDs fall along the line $L \propto \sigma^4$ and dEs deviate far from this line: (Drinkwater et al., 2004).

It seems that UCDs also can not be regarded as a homogenous stellar system (Hilker, 2009). A number of studies targeting various UCD samples in different galaxy clusters revealed the diverse nature of UCDs: Fornax UCDs are slightly redder on average than Virgo UCDs (Evstigneeva et al., 2008; Mieske et al., 2008, 2006). On the other hand, it is still a matter of debate whether or not UCDs contain the dark matter (Drinkwater et al., 2003; Haşegan et al., 2005; Hilker et al., 2007). This makes them very special objects to study in extragalactic astronomy. Their importance comes along with formation scenarios not only due to issue of dark mater, but also

the questions on their definition. In fact, this is related to the very defining properties of the galaxies i.e. in which conditions we should classify an object as a galaxy or not.

Overall it has been already noted that Virgo UCDs contain fairly old (age: > 8-10 Gyr) and metal poor (< −0.5 dex) stellar populations (Evstigneeva et al., 2007, hereafter E07). Therefore, it is also proposed that they could be very luminous intra-cluster GCs (Mieske et al., 2002). Another popular formation scenario is the threshing of nucleated dEs (Bassino et al., 1994). In this picture, UCDs are the remnants of galaxies that have been significantly stripped in the cluster environment. Numerical simulations (Bekki et al., 2003; Goerdt et al., 2008) have generally confirmed that the remnant nuclei resemble UCDs in their structural parameters. In Figure 6.1, the dotted lines show the path predicted by our threshing scenario for nucleated dwarfs being stripped to form UCDs (Drinkwater et al., 2003).

Stellar population studies of dEs provide evidence that the nuclei have intermediate ages and moderately metal-enriched stellar populations (Koleva et al., 2009; Chilingarian, 2009). In addition to this, since UCDs show slightly super solar [α/Fe] abundances, Evstigneeva et al. (2007) argued that the stellar population properties rather support the view that UCDs are luminous globular clusters than being nuclei of dEs.

In this work, we present a stellar population analysis based on absorption-line strengths (Lick indices, Burstein et al. 1984; Worthey et al. 1994b; Trager et al. 1998) of a fairly large sample of 34 nucleated dEs and 10 UCDs in the Virgo cluster. So far, studies comparing stellar population parameters derived from spectra used rather low numbers of objects. Moreover, the extraction of nuclear spectra has been made without subtracting the underlying galactic light, which can still contribute significantly at the photometric center of the dEs: see Chapter 5. We therefore apply a simple method to subtract most of this light (see Section 5.2.2), thus expecting that our measurements are representative for the stellar population properties of the nuclei themselves. Finally, we present the distributions of the stellar population parameters of dE nuclei and UCDs with respect to local galaxy density and to their luminosity, and we try to constrain possible formation scenarios of Virgo UCDs.

6.2 The sample, observations and data reduction

6.2.1 Sample selection and a new Virgo UCD

For this work, we extended the dEs sample by adding recently observed dEs. In total, dE sample comprises 34 nucleated dEs in the Virgo cluster (Virgo cluster catalog, VCC, Binggeli et al., 1985; Binggeli & Cameron, 1993), selected to have a relatively high "nucleus strength", which we define as the difference between the nucleus magnitude and the host galaxy effective surface brightness, $s_{r,\mathrm{nucleus}} = m_{r,\mathrm{nucleus}} - \mu_{r,\mathrm{eff,galaxy}}$, measured in SDSS r (see below). Thereby, $\mu_{r,\mathrm{eff,galaxy}}$ is a measure for the brightness of a unit area of the galaxy, determining the "contrast" between galaxy and nucleus (also see Lisker et al. 2007, their Figure 1). We select nuclei with $s_{r,\mathrm{nucleus}} < -1$ and $m_{r,\mathrm{nucleus}} < 21$ mag (see Figure 6.2).

Our UCD sample selection (see Table 1), is based on Evstigneeva et al. (2005) and Jones et al. (2006); our numbering follows the latter. Three of the nine Virgo UCDs of Jones et al. were not included in the Lick index study of Evstigneeva et al. (VUCD2, 8, and 9), so they were selected by us as targets. Three further UCDs were selected, since they fell in the same field-of-view as dE targets of our study. Due to the multi-slit observations, they could be easily included.

We also targeted a new Virgo UCD candidate, which we now indeed confirm as Virgo cluster

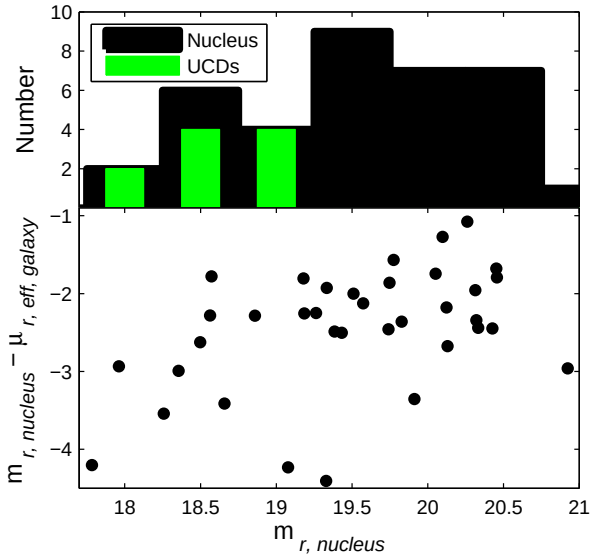

Figure 6.2: *Top:* Number distribution of dE nuclei and UCDs in our sample. *Bottom:* Our selection criteria for dE nuclei, limiting the nucleus magnitude $m_{r,\mathrm{nucleus}}$ to values brighter than 21 mag, and the "nucleus strength", i.e. the value of $m_{r,\mathrm{nucleus}} - \mu_{r,\mathrm{eff,galaxy}}$ to less than -1. Note that the nucleus sample is not complete within this parameter region, i.e. not all Virgo dE nuclei with these parameters have been observed.

member; it is named VUCD10 in Table 1. It was identified through a simple multiparameter selection procedure. From SDSS DR5 pipeline photometry, we obtained *ugriz* magnitudes and colors for all nine Virgo UCDs in Jones et al. (2006). When excluding VUCD7, which is clearly brighter than the others and appears to be an extended object in the SDSS images (also see Jones et al. 2006), the *r*-band magnitudes (SDSS "modelMag" values) lie within 18.0 to 19.1 mag. Their Petrosian radii in *r*, again excluding VUCD7, are below 2.2 arcsec. Their *u-r* colors, when excluding the much redder VUCD3, cover the range 1.8 to 2.4 mag (which includes VUCD7). Their *i-z* colors, again excluding VUCD3, lie between 0.1 and 0.25 mag (which again includes VUCD7). The right ascension and declination of all objects except VUCD3 and VUCD7 ranges from 187.5° to 188.1° and 11.9° to 12.7°, respectively. When querying the SDSS database for all objects fulfilling the above criteria of magnitude, radius, color, and position, 20 objects were identified that the SDSS classified as stars, among them VUCD1, 2, and 5. The same query, but for objects classified as galaxies, yielded only five objects: VUCD4, 6, 8, 9, and the new VUCD10, which we therefore included in our target sample.

With its radial velocity of 2425 km/s that we now measured from its spectrum, it is consistent with being a Virgo cluster member: in velocity space, Virgo member galaxies in the central cluster region reach velocities of 2600 km/s (Binggeli et al. 1987; Binggeli & Cameron 1993). It should be noted that many of the Virgo galaxies with velocities above ≈2000 km/s actually belong to one of the various "clouds" that might be located behind the main Virgo cluster aggregation (Binggeli et al., 1987) – however a membership in one of these clouds is ruled out by the projected position: VUCD lies close the central galaxy M87 and all clouds are located further away. And indeed, Virgo galaxies in the central cluster region (cluster A) do reach velocities up to 2600 km/s (Binggeli et al. 1987, Figure 23) exceeding the velocity of VUCD10. We therefore consider VUCD10 a new Virgo cluster UCD, and include it in the following analysis.

6.2.2 Photometry

To obtain nucleus and UCD magnitudes, we use SDSS DR5 *r*-band images to which we applied our own sky subtraction procedure (see Lisker et al., 2007). We also correct them for Galactic extinction, following Schlegel et al. (1998), and use the flux calibration provided directly by the SDSS. A Virgo distance modulus of $m - M = 31.09$ mag (Mei et al., 2007; Blakeslee et al.,

Table 6.1: The UCD sample. In the first four columns, we provide UCD number, position in the sky (RA, Dec), and radial velocity. In the last column, we indicate whether UCDs are in common with the studies of E07 or Firth et al. (2009).

UCDs name	RA (h:m:s)	Dec (^{o} :' :")	RV (kms)	Age Gyr	[Z/H] dex	[α/Fe] dex	m_r mag	Remark
VUCD1	12:30:07.61	12:36:31.10	1227 ± 1.7	$11.9^{+1.8}_{-2.0}$	-0.90 ± 0.05	0.38 ± 0.09	18.6	E07
VUCD2	12:30:48.24	12:35:11.10	0911 ± 6	$5.9^{+1.7}_{-0.5}$	-0.77 ± 0.09	-0.14 ± 0.08	18.6	F09
VUCD3	12:30:57.40	12:25:44.8	0710 ± 3.5	$15.0^{+0.1}_{-1.3}$	0.13 ± 0.03	0.38 ± 0.03	18.1	E07
VUCD4	12:31:04.51	11:56:36.8	0919 ± 1.7	$11.9^{+1.1}_{-2.0}$	-1.24 ± 0.05	-0.00 ± 0.12	18.6	E07
VUCD5	12:31:11.90	12:41:01.20	1290 ± 3	$10.7^{+0.9}_{0.1}$	-0.40 ± 0.03	0.31 ± 0.02	18.5	E07
VUCD6	12:31:28.41	12:25:03.30	2101 ± 4	$8.3^{+6.7}_{-1.3}$	-1.03 ± 0.12	0.41 ± 0.09	18.7	E07
VUCD7	12:31:52.93	12:15:59.50	0985 ± 5	$10.7^{+0.9}_{0.1}$	-0.54 ± 0.03	0.13 ± 0.04	18.0	E07
VUCD8	12:32:04.33	12:20:30.62	1531 ± 19	$11.6^{+1.0}_{-0.9}$	-1.24 ± 0.03	-0.09 ± 0.09	19.1	F09
VUCD9	12:32:14.61	12:03:05.40	1325 ± 5	$11.6^{+1.0}_{0.1}$	-1.03 ± 0.06	0.07 ± 0.11	18.8	F09
VUCD10	12:30:30.86	12:18:41.66	2425 ± 103	$9.8^{+2.8}_{-0.8}$	-0.89 ± 0.09	0.50 ± 0.04	19.1	New

2009), corresponding to $d = 16.5$ Mpc and an SDSS pixel scale of 32 pc (80 pc/"), is adopted here and in the further analysis.

Nucleus magnitudes are derived as follows. A Sérsic fit to the radial profile of the galaxy is done, measured with elliptical annuli and using only the radial interval from 2" to 1/3 of the half-light radius, or extending it if the interval subtends less than 2.5" (200 pc). From this fit, a two-dimensional elliptical model image, taking into account the median SDSS PSF of 1.4" FWHM, is created and subtracted from the original image, leaving only the nucleus in the center. The nucleus magnitude is then measured by circular aperture photometry with $r = 2$". We estimate the magnitude error to be 0.2 mag, which is consistent with the RMS scatter of a comparison to the *Hubble Space Telescope (HST)* ACS Virgo cluster survey (Côté et al., 2006) for the 10 objects in common.[1]

The same aperture photometry is done to obtain UCD magnitudes. To be comparable to the nucleus measurements, this aperture is also applied to VUCD7, even though it is known to be extended, as mentioned previously. For the UCD magnitudes we estimate an error of 0.1 mag.

6.2.3 Spectroscopy

The spectroscopic observations were carried out at ESO Very Large Telescope (VLT) with FORS2. The 1" slit and V300 grism provide an instrumental resolution ~11 Å FWHM. Details of the observational layout and data reduction are described in Chapter 3. The new additional sample dEs were observed in 2010A using the same instrumental setup. We provide the basic characteristic of this dE sample in Table 6.2. In total our sample covers the full range of local projected galaxy density that is populated by nucleated dEs in Virgo, from less than 10 to more than 100 galaxies per square degree. The UCDs were observed in 2007A together with the first set of dEs, using the same instrumental configuration. We provide the basic properties such as position and radial velocity in Table 6.1 and the detailed UCD sample selection criteria in Section 6.2.1.

As we described in Chapter 5, we use galactic light subtracted nuclear spectra to measure the stellar population parameters for the dEs nuclei. We actually employ the derived values of age, metallicity and [α/Fe]-abundant directly from the previous chapter for our main dEs sample. In

[1] Nucleus r magnitudes were converted into g by adding the $g-r$ color value of the nucleated dE's center ($r \leq 2$"), and were then compared to ACS g magnitudes, showing no systematic offset.

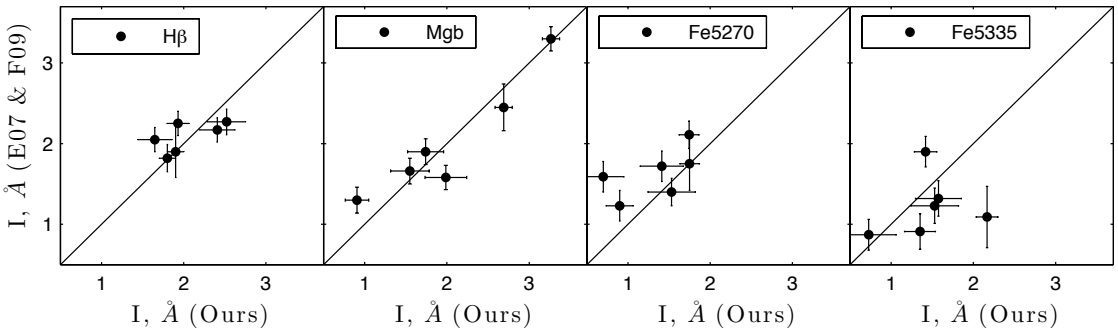

Figure 6.3: Comparison of fully corrected line strength with the previously published data set of E07 and F09.

addition, we derive stellar population parameters for the new sample dEs nuclei using the same methodology. To keep homogeneity of data quality, we use the same 0".75 aperture to extract nuclear spectra. Then, the galaxy spectrum is extracted in a radial interval from 3" to 8", scaled accordingly, and subtracted from the centrally extracted spectrum. However, we re-derive the sensitivity function observing the new set of standard star during the new observing run 2010A. Finally, the observed spectra of dEs nuclei are flux calibrated using the new sensitivity function.

We also use the same procedure to calibrate the extracted one-dimensional spectra, and then to measure the absorption line strengths form it, as described in Chapter 3 for both UCDs and new sample dEs. In Figure 6.3, we show comparison of fully corrected absorption line strengths of UCDs at Lick system with previously values from E07 and F09. We see two indices Hβ and Mg*b* fairly agree in one to one plot. However, Fe indices show slightly large scattering. But interestingly, it seems that Fe5270 is slightly under-estimated and the other Fe5335 is slightly over-estimated in our measurement.

6.3 Results

In order to derive stellar population parameters from the measured line strengths, we translate our Lick index measurements into SSP-equivalent ages, metallicities, and α-element abundance ratios by comparing them to the model of Thomas et al. (2003) by χ^2-minimization, following Proctor & Sansom (2002). We use nine well-measured indices (Hδ_F, Hγ_F, Fe4383, Hβ, Fe5015, Mgb, Fe5270, Fe5335 & Fe5406) in case of the dE nuclei. For the UCDs we use only Hβ, Mgb, Fe5270 and Fe5335, because we only find these four indices available in the literature for those three UCDs that we did not target ourselves. Moreover, due to the slit mask placement, our observations only cover the full range of indices (i.e., ~4000 Å to ~5600Å) for three of the observed UCDs. For completeness, we also checked whether the use of different sets of indices produces any significant discrepancy in the estimated SSP parameters. We find that the estimated SSP parameters agree well within the errors, although the use of a larger set of indices naturally leads to smaller errors in the SSP parameters. Therefore, we keep using all nine indices for the dE nuclei in the further analysis.

The relation between the stellar population parameters and the local projected galaxy density is plotted in Figure 6.5. The local projected density has been calculated from a circular projected area enclosing the 10th neighbor. It seems that there is a weak correlation between the local projected density and the ages of the nuclei. But, more prominent than the correlation, an age break is seen at a projected density ≈40 sq.deg.$^{-1}$. We thus use this value to divide our dE sample in two groups, located in cluster regions of lower/higher density. We find median ages

Table 6.2: New dEs sample

VCC No.	RA h:m:s	Dec °:':"	M_r (total) mag	M_r (nuc) mag	Density sq^{-2}	R_{eff} "	RV Kms^{-1}	Age Gyr	[Z/H] dex	[α/Fe] dex
0592	12:22:50.86	13:35:34.42	−15.66	−10.95	017.97	26.22	1118.0	$12.7^{+2.3}_{-2.0}$	-0.86±0.06	-0.02±0.08
0765	12:25:03.48	13:14:40.84	−15.68	−10.74	070.14	15.39	0968.0	$11.6^{+3.4}_{-5.2}$	-0.54±0.11	+0.16±0.06
0786	12:25:14.47	11:50:58.09	−16.90	−11.43	045.52	52.86	2388.0	$9.8^{+1.8}_{-0.8}$	-0.89±0.06	+0.50±0.05
0940	12:26:47.07	12:27:14.17	−17.19	−11.27	087.32	51.25	1411.0	$11.6^{+1.0}_{-0.3}$	-0.89±0.03	+0.09±0.07
0965	12:27:03.13	12:33:37.96	−16.47	−11.18	104.39	48.52	0851.0	$1.6^{+0.3}_{-0.3}$	-0.11±0.17	+0.41±0.20
1069	12:28:06.54	12:53:53.22	−15.49	−10.55	139.26	36.95	2308.0	$12.7^{+0.3}_{-2.0}$	-1.21±0.03	-0.20±0.05
1122	12:28:41.71	12:54:57.08	−16.98	−11.67	065.99	48.30	0476.0	$1.6^{+0.3}_{-0.3}$	-0.11±0.03	-0.15±0.02
1386	12:31:51.33	12:39:24.44	−17.22	−10.69	052.80	72.44	1297.0	$15.0^{+0.3}_{-11.5}$	-0.86±0.40	+0.20±0.26

Table 6.3: Measured central line-strength indices corrected to the Lick/IDS system, measured for the new sample dEs nuclei.

Galaxy	Hδ_F	Hγ_F	Fe4383	Hβ	Fe5015	Mgb	Fe5270	Fe5335	Fe5406
0592	1.40±0.21	1.98±0.16	2.84±0.38	1.6018±0.17	4.84±0.34	1.97±0.1690	1.81±0.1919	1.36±0.2172	1.46±0.15
0765	-0.11±0.24	-0.27±0.19	4.23±0.40	3.3448±0.17	4.52±0.39	2.75±0.1894	2.10±0.2078	1.87±0.2328	1.12±0.17
0786	1.57±0.14	1.27±0.11	1.11±0.26	2.2019±0.11	3.47±0.23	0.59±0.1207	1.16±0.1344	0.84±0.1501	1.04±0.10
0940	0.97±0.19	0.93±0.15	1.82±0.35	1.7303±0.15	4.07±0.31	1.97±0.1574	1.61±0.1737	1.60±0.1987	1.12±0.14
0965	2.58±0.17	2.26±0.14	2.89±0.32	3.0580±0.13	4.27±0.29	0.81±0.1513	1.94±0.1622	1.49±0.1817	1.07±0.13
1069	2.03±0.22	1.22±0.18	2.94±0.41	2.0674±0.18	3.31±0.41	1.14±0.2015	0.79±0.2243	1.63±0.2459	0.97±0.18
1122	1.81±0.22	1.66±0.17	4.88±0.39	2.8779±0.17	6.00±0.37	2.20±0.1858	2.36±0.2073	2.07±0.2309	1.74±0.17
1386	1.56±0.72	-0.01±0.61	2.10±1.31	2.3836±0.56	1.59±1.26	2.58±0.5835	2.32±0.6641	1.12±0.7664	1.88±0.54

of 2.6 Gyr for the low density group and 11.6 Gyr at high densities.

Almost all UCDs lie in the high density region as defined above. Their ages have a median of 11.7 Gyr, strikingly consistent with the nuclei in the same density regime. As a statistical comparison, we performed a Kolmogorov-Smirov (K-S) test with the null hypothesis that there is no difference in the distribution of SSP parameters between the UCDs and the dE nuclei of the high density group. We find that there is a probability of 88%, 97% and 73% for having the same age, metallicity, and [α/Fe]-abundance distribution, respectively.

The metallicities of dE nuclei also show a difference between the low and high density regions: the median values differ by more than 0.5 dex, although the scatter is fairly large. The UCDs also have a fairly large scatter in metallicity, ranging from +0.1 to −1.4 dex. However, it is remarkable that only two UCDs (VUCD3 and 4) have a metallicity above −0.5 dex. The [α/Fe]-abundances are more or less consistent with solar in case of the dE nuclei, but also a slight increase with density can be recognized for the nuclei and (more clearly) for the UCDs. Although the scatter is fairly large, the Spearman's rank correlation coefficients are 0.3 and 0.7 for dE nuclei and UCDs, with the probabilities for the null hypothesis that there is no correlation being 8.5% and 1.5%, respectively. In case of the UCDs, 7 out 10 have super-solar values of [α/Fe].

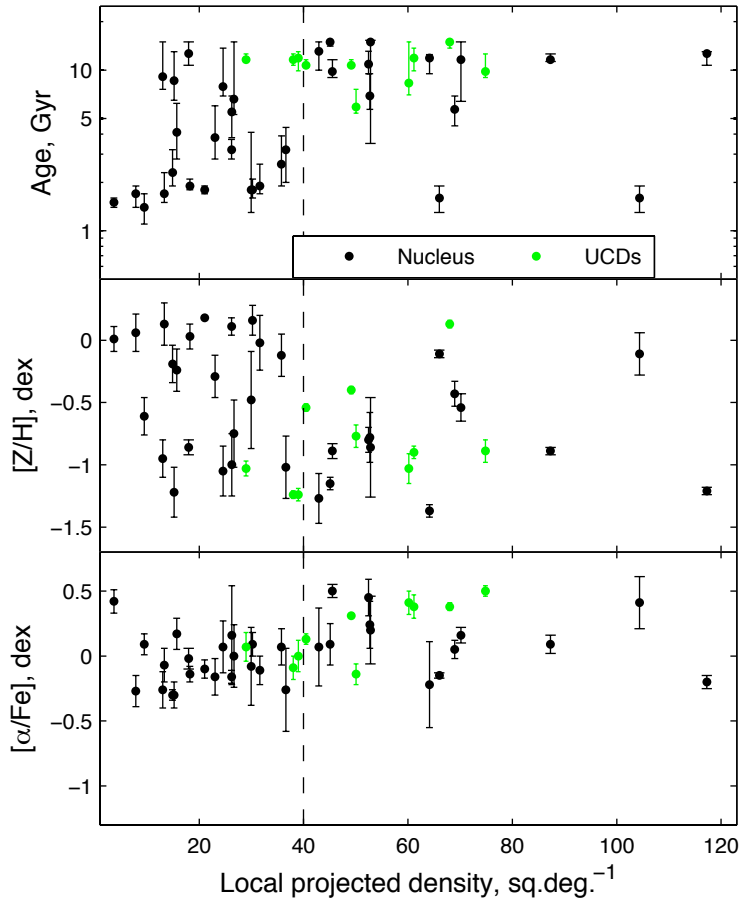

Figure 6.4: Age, metallicity, and [α/Fe]-abundance versus local projected galaxy density are shown for dE nuclei (black) and UCDs (green)

The relation between the stellar population parameters and the *r*-band magnitudes of UCDs and nuclei is presented in Figure 5.9. We do not see a relation of age and [α/Fe]-abundance with luminosity, both for nuclei and UCDs. Unlike that, the metallicity of both UCDs and dE nuclei tends to increase with increasing luminosity, following the well known metallicity-luminosity

relation. However, bimodal peaks of the age and metallicity distributions of dE nuclei can be seen as a striking feature in Figure 5.9 (right panel). This indicates the inhomogeneous nature of dE nuclei, which can be divided into two different groups of stellar population characteristics: a young metal-rich group and an old metal-poor group. Brighter nuclei predominantly have metal-rich stellar populations consistent with solar values. The metal-poor nuclei (metallicity <-0.5 dex) have an average of −1.0 dex, and most of them are less luminous than m_r = 19.2 mag (M_r = −11.9 mag).

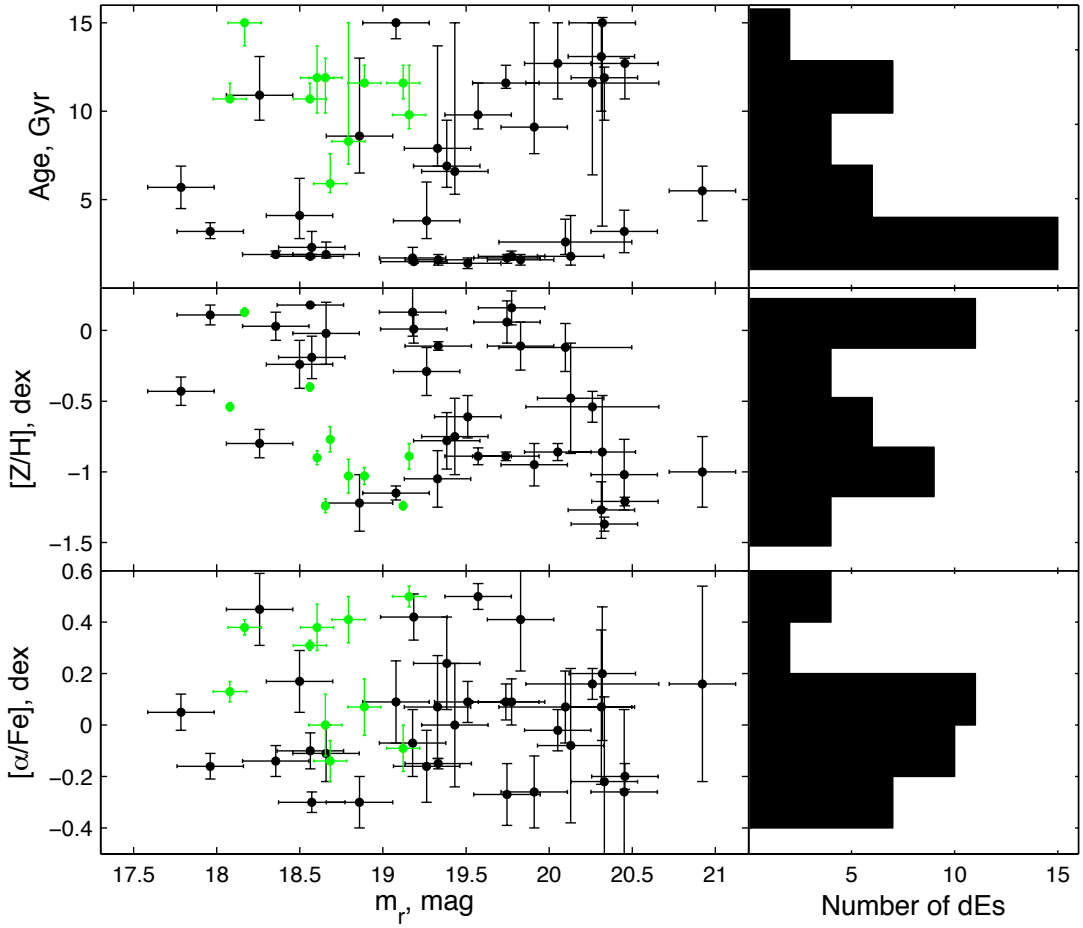

Figure 6.5: Age, metallicity and [α/Fe]-abundance versus nucleus/UCD magnitude, for dE nuclei (black) and UCDs (green).

6.4 Summary and discussion

We have derived stellar population parameters of Virgo cluster UCDs and nuclei of early-type dwarf galaxies, through fitting measured Lick absorption line strengths to models of Thomas et al. (2003). Since we use simple stellar population models, it must be noted that our estimated parameters are interpreted as *SSP-equivalent.*

Indications that the UCDs in the Virgo cluster more likely have formed via dE destruction in dense cluster regions than in the Fornax cluster have already been presented in the literature (Mieske et al., 2006; Côté et al., 2004, 2006). An explanation could be the higher mass of the Virgo cluster, which provides a deeper potential well with stronger tidal forces than in the Fornax

cluster. Virgo UCDs were also found to be significantly different from GCs in colors and sizes, as they are bluer and larger than GCs (Haşegan et al., 2005). E07 showed that Virgo UCDs have structural properties similar to the Fornax UCDs. Furthermore, De Propris et al. (2005) showed with the HST that Fornax UCDs are more extended and have higher surface brightnesses than typical dwarf nuclei. That is not necessarily inconsistent with the stripping scenarios, because the stripping process can alter structural parameters of the embedded nuclei. Therefore, a direct comparison of structural parameters may not be able to constrain the formation scenarios of UCDs properly.

In the light of our new age and metallicity estimates in the previous section, we want to address the possibility of formation of Virgo UCDs via tidal destruction of nucleated dEs. We observe that UCDs exhibit significantly older and more metal deficient stellar populations as compared to dE nuclei *on average*. However, if we compare the ages of UCDs and nuclei only in high density regions, where most of the UCDs are located, we do not find any significant difference in their age and metallicity distribution. Only two dE nuclei (VCC0965 and VCC1122) out of 13 from the high density group have ages less than 5 Gyr and metallicities above -0.2 dex. Note, however, that due to projection effects, a number of objects that are actually located in the outskirts of the cluster must fall into regions of high *projected* density, lying in front or behind the center along the line of sight. If we consider the low density group of our sample to be representative for nuclei of dEs outside of the (three-dimensional) cluster center, then we actually *expect* to have a few objects with young ages and high metallicities in the high density group, consistent with what we observe. Moreover, even without taking this effect into account, our statistical tests already show that the age distributions of UCDs and dE nuclei are similar when considering only the group of nuclei in the high density. This supports the idea of the threshing of dEs in high density environments to form the UCDs.

At low densities, a certain fraction of dEs probably still retained some central gas and transformed it into stars (some dEs are still doing this, see Lisker et al. 2006). Consequently, their nuclei today would indeed show a younger stellar population than a UCD, the latter being an "old nucleus". For such dEs, not only the orbital average should be located in the outskirts, but they should also not have passed right through the center (e.g. on an eccentric orbit), otherwise the gas would have been stripped by ram pressure and tidal forces. This would explain the fact that we do not see young UCDs: a dE destruction is only possible if the galaxy really goes through the center and experiences the strongest tidal forces. If we assume that the *full* destruction, i.e. the complete removal of the dE's main body, takes significantly more orbital time than the gas stripping, then nucleated dEs with an orbit leading through the center first lost their gas, halting any star formation, and then became destroyed. Therefore, we have no young UCDs.

In any case, young and bright dE nuclei have either late or prolonged star formation activity. We assess this by modeling spectra of composite stellar populations through superposition of a young and an old component, using the model spectra of Vazdekis et al. (2010). We fix the old population at an age of 11 Gyr and a metallicity of -1.2 dex, and add a component with solar metallicity and exponentially declining star formation rate, starting from an age of 11 Gyr. We find that spectra like those of the young nuclei (with an SSP-equivalent age of $\sim$3 Gyr) can be achieved when the exponentially declining component formed stars until 2 Gyr ago, at which point it is truncated. This means, if we assume our model to represent the observed young nuclei, their star formation activity would have stopped 9 Gyr later than that of the old nuclei.

On the one hand, the estimated ages and metallicities of UCDs nicely agree with the ages and metallicities of nuclei of dEs from the dense cluster regions. On the other hand, most of the old nuclei are fainter than the UCDs. However, the UCD discoveries might suffer a selection effect: if a *faint* nucleus was stripped, it would now be automatically counted into the globular

cluster system of M87. We can hardly estimate how many nucleated dEs have already been destroyed and transformed into UCDs during the lifetime of the cluster. Thus we cannot rule out or confirm any scenario *just by counting* the number of bright nuclei or that of UCDs. Only detailed future simulations can resolve this issue.

7

On the nature of stellar population properties of dEs: are dEs special?

Abstract

In this chapter, we re-examine the stellar population properties of dEs. First, we build a metallicity -luminosity relation for a large sample of dEs and compare it with the metallicity-luminosity relation of other class of early-type galaxies. We confirmed that metallicity of galaxies correlate with galaxies luminosity in all class of early-type galaxies i.e. Es, dEs and dSphs. However, the slopes of these relations are not similar for all classes of galaxies. We see the dEs have steepest slope among all classes and Es have almost flat. After dividing the all galaxies into two groups (i.e. metal poor Z < 0.5 dex and other metal rich Z > -0.5 dex), the metallicity-luminosity relation revealed that these different groups have fairly different slopes, and the metal poor galaxies group has a steeper slope than the metal rich. We discovered a clear break in this relation in the dEs region. Therefore dEs show a special stellar population property, not only they exhibit heterogeneous stellar population properties but also they rather show a dichotomy. The bright metal rich dEs seems a faint end extension of Es and metal poor, and old dEs are either a genuine class of early-type galaxies or bright end extension of dSph.

Contents

Figures

7.1 Introduction

After having established a diverse nature of stellar population properties of Virgo cluster early-type dwarfs, we can now proceed to make a comparative study between the stellar population properties of different classes of early-type galaxies. This chapter will provide a comprehensive analysis of the derived stellar population parameters of dEs with comparing their bright and faint counterparts Es and dSphs respectively. It has been already noticed that the difference in stellar population properties between Es and dEs such that Es have an average older and more metal enhanced stellar populations than dEs. But, the fainter dEs and dSphs show relatively inhomogeneous stellar population properties than Es. Here, we particularly focus on the luminosity-metallicity (L-Z) relation. We will derive the L-Z relations for different classes of early-type galaxies. We will then discuss these relations in a way to get a better understanding of overall dE properties.

7.1.1 Luminosity-metallicity relation

It is well known that the early-type galaxies follow a trend of increasing metallicity with galaxy luminosity (Caldwell et al., 1992), which was first noticed by McClure & van den Bergh (1968), and later Lequeux et al. (1979) were the first to show correlation metallicity with the total mass of the galaxies for a sample of irregular and blue compact dwarf galaxies. A usual explanation of this global phenomenon is the tug of war between the galactic out flow (i.e. Supernovae and stellar wind Larson 1974; Tinsley & Larson 1979; Dekel & Silk 1986) and the depth of the potential well of the galaxies, i.e. as the depth of potential well increases the mass ejection through these out flow become less efficient. Therefore, more luminous/massive galaxies are able to retain their gases more effectively than low luminous galaxies, thus the metallicity can build up to higher values because following generations of stars will be formed in an enriched gas environment, while the low luminosity galaxies lose their metals through galactic winds (see Köppen et al., 2007).

However, it is not clear yet whether the all early-type galaxies (i.e. Es, dEs and dSph) follow the same relation or the slopes varied between these different subclasses. For example: Caldwell et al. (1992) noticed that normal ellipticals have relatively steeper slope than dEs. In contrast, Tremonti et al. (2004) and Panter et al. (2008) found the relation is relatively steep in less massive galaxies and flat at the high mass end. However, a considerable scatter in the relation has been noticed in the dwarf regime. Barazza et al. (2002) argued that the scattering in the relation can be explained with taking account of ellipticity effect i.e., flat galaxies are metal poorer than equal luminosity round galaxies. In any case, various theoretical explanations of the L-Z relation have been proposed so far, which may work at different level in different class of early-type galaxies. 1) Starburst-induced galactic outflows are more efficient in dwarf galaxies than in giant galaxies. 2) It is expected that dominant fraction of stars in the luminous galaxies are formed by means of a burst of star formation at high redshift, enriching quickly their ISM to solar or super-solar metallicities, contrarily dwarf galaxies with lower star formation efficiency dilute their ISM in the longer infall time, and have sub-solar Interstellar metallicities (Martin, 1999). 3) And the variation of Initial Mass Function (IMF), i.e. more massive galaxies may have different IMF slope than dwarf (Köppen et al., 2007).

On the other hand, the previous conviction of the dichotomy in the early-type galaxies, normal early-type galaxies (Es) are formed differently then the dwarf early-type galaxies (Kormendy, 1985; Kormendy et al., 2009), is continuously challenged by the recent observations arguing

that they might have formed through the similar mechanism of galaxy evolution (Graham & Guzmán, 2003; Chilingarian, 2009). A well proposed idea is the all early-type galaxies might also have got their present days shapes through the galaxy merging and gas dissipation during the merger. However, the environmental influences on these less luminous galaxies are also a well accepted idea, particularly in the cluster environment: see discussion in Chapter 4.

In this chapter, we will derive a L-Z relation for early-type galaxies of entire luminosity range $-23 < M_b < -9$. We will try to examine the homogeneity of this relation. As an important explanation of this relation comes from the gas infall/loss in the galaxies, this relation can provide a valuable constraint to the model of galaxy formation that attempt to account for the chemical evolution of the system (e.g. Prantzos, 2000), and particularly helps to differentiate the physical mechanism which involved in the galaxy evolution. Therefore, we will see whether the L-Z relation can be better described in single slope or multiple. Then finally, we will discuss the possible consequences of these relations.

7.2 The sample

For this investigation, we compile a large sample of early-type galaxies from the different previous stellar population studies. This contains early-type galaxies of the luminosity range -23 < M_b < -9. It covers the all classes of early-type galaxies i.e., Es, dEs and dSph located in various environments i.e., field, group and cluster.

1. We collect a sample of normal ellipticals from the literature i.e., Sánchez-Blázquez et al. (2006). This sample contains 86 early-type galaxies. This sample covers Es form all environments such as field, cluster and group including 12 Es from the Virgo cluster. They have performed an extensive analysis of stellar population in Es to find the environmental dependency on the stellar population properties of Es. Thanks to P. Sanchez, she provides us the final and fully corrected values of absorption line strengths in the Lick system of 86 Es in machine-readable form.

2. We use our all dEs sample from previous study (See chapter 3 and 6), which consist 50 dEs in Virgo cluster. For this dEs sample, we use the derived values of stellar population parameters from the Chapter 4.

3. We collect the derived values of metallicity for Centaurus A and Local Group dSph from the literature. We would like to give special thank to our colleague Denija Crnojevic for helping the compilation of these parameters (Sharina et al., 2008; Crnojević et al., 2010). Note, metallicities were derived for these galaxies using the different approach i.e. isochrones fitting with high-resolution photometric data of the galaxies and individual stellar spectroscopy. Isochrone fits to RGBs may yield rather different metallicities depending on which isochrone models are used. Metallicities based on individual stellar spectroscopic measurements may differ considerably from photometric integrated ones. In any case, it is generally expected that the inconsistencies between these methods is $\sim \pm 0.3$ dex, which is usually within the measurement errors using these methods.

7.2.1 Near-infrared magnitude

The near infrared bands are a much better proxy for stellar masses than optical bands, since they are sensitive to the light of old, low-mass stars and less sensitive to the effects of dust.

In general the optical colors are biased tracer of young and hot stellar populations, and thus is more sensitive to star formation than stellar mass. We calculate K_{total} 2.2 μm near-infrared magnitude from Two Micron All Sky Survey (2MASS) (Jarrett et al., 2003) to compare the derived stellar population parameters with luminosity of galaxies. We do not use correction for galactic extinction in K-band magnitude.

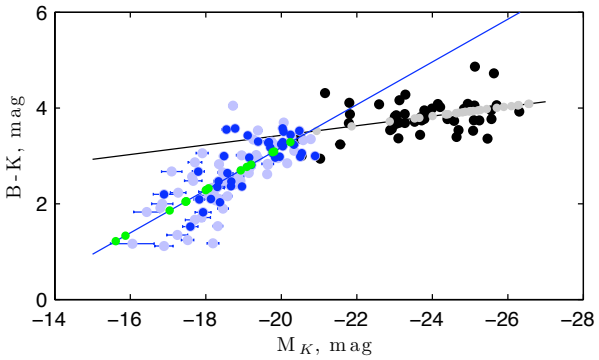

Figure 7.1: Color magnitude relation B-V Vs K. The black symbols represent the Es, which have 2MAAS K-band magnitude and the gray dots, align in the black straight line, are derived. The faint blue dots represent the dEs and those, which are common to this study, are represented by dark blue. The green dots, aligned in the blue straight line, are derived.

We derived the K-band magnitude for the 92 dEs of Lisker et al. (2006) sample from the 2MASS catalogue and among them 35 dEs are common to this study. We found K-band magnitude for the 79 Es of our sample in 2MASS catalogue. In Figure 7.1, we show the B−K color-magnitude relation for elliptical galaxy, which contain 92 dEs and 80 Es. It is also not sure yet that the color-magnitude relation of early-type families can be described by single linear fit or multiple i.e. each for different class. We derived the different linear fits for the dwarfs and giants early-type galaxies, as we can see in the Figure 7.1. We find that, dEs have relatively steeper slope than Es in the B-K Vs K color magnitude relation. The best-fitted equations are:

$$B - K = -0.45M_K - 5.8 : \text{for dEs} \tag{7.1}$$

$$B - K = -0.10M_K + 1.4 : \text{for Es} \tag{7.2}$$

Those dEs and Es, which do not have K-band magnitude, we derive the K-band magnitude using the equations 7.1 and 7.2 respectively.

7.3 Results

In this section, we present the results and analysis from the study of stellar-population of early type galaxies. First, we provide the relation between total galactic luminosity and the measured line strengths. The derived stellar population parameters would have influence of the model dependency, which may bias the results toward the model ingredient. Therefore, the single stellar population (SSP) parameters never consider as perfect unbiased indicator. The incompleteness of stellar library and lack of knowledge of stellar evolution such as calibration of mass loss in the Asymptotic Giant Branch (AGB) phase, color evolution of the Blue Horizontal Branch (BHB) stars make them vary with the model to model as they are calibrated and synthesized from different physics and different stellar library (Renzini, 2006). On the other hand, the age metallicity degeneracy always comes at the front line of the discussion, though there are several strategies have been already proposed to disentangle this degeneracy (Worthey et al., 1994b; Thomas et al., 2003; Proctor et al., 2004). Therefore, we first show the relation between the measured absorption line strengths and luminosity, and then we present the relation between

derived stellar population parameters and luminosity. For this purpose, we use the infra-red magnitude as galactic parameter (see the Section 7.2.1).

7.3.1 Analysis of Indices

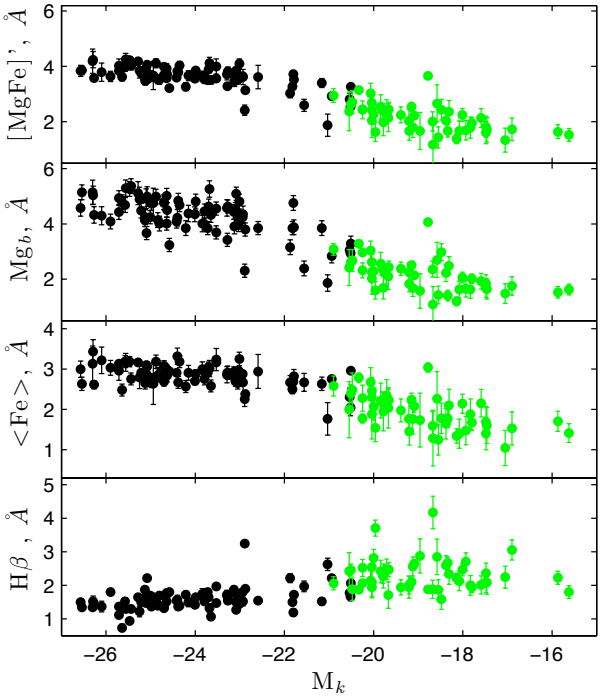

Figure 7.2: Relation between the measured indices and galactic K-band luminosity. Es are represented by black dots and green dots are for dEs.

In Figure 7.2, we provide the relations between the total galactic luminosity and the measured absorption line strengths at lick system. Top panel shows a relation between the combined index [MgFe]′ (i.e., $\sqrt{Mgb \times (0.78 \times Fe5270 + 0.28 \times Fe5335)}$ (Thomas et al., 2003, here after TMB03)) with the K-band galactic magnitude. The other indices Mg*b*, <Fe> and $H\beta$ Vs K-band galactic magnitude are subsequently below.

We see almost no correlation between the age indicator index Hβ with K-band magnitude in both cases dEs and Es. Both show almost flat relation with M_K, however the median difference of Hβ of Es and dEs is 0.5 Å. The metallicity indicator index <Fe> seems to correlate with galactic K-band luminosity. We see that dEs follows a slightly steeper relation than Es. On the other hand, Mg*b* shows a continuous correlation of strength versus magnitude. Or perhaps, a slight steep in middle around −22.5 mag might occur, where data points are sparsely populated and then again flattens at the very faint end. The combined index [MgFe]', which is also considered to be a good mean metallicity indicator, shows a week correlation with the luminosity all together i.e., Es and dEs. The prominent outlier in the top three panels above the other dEs points is VCC916.

7.3.2 Age, metallicity and alpha-abundance ratio

In this section, we present the relations between the derived SSP-equivalent ages, metallicities and α-abundant ratios and the K-band absolute magnitude of early-type galaxies (Es and dEs). Here we have used the derived values of SSP parameters of dEs from Chapter 4. However, we derive the SSP parameters for Es sample. We use the same nine indices Hδ_F, Hγ_F, Fe4383, Hβ, Fe5015, Mgb, Fe5270, Fe5335 & Fe5406. As we described in Chapter 4, the χ^2- minimization

technique has been employed to compare the SSP model prediction and the observables i.e absorption line strength. The derived values of age, metallicity and α-element abundant ratio for Es are tabulated in the Table 7.1.

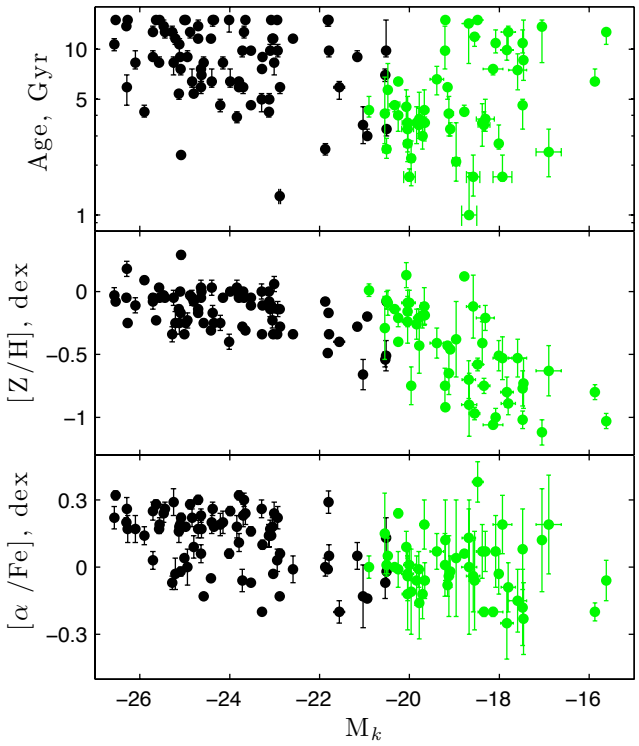

Figure 7.3: Relation between the derived stellar population parameters with K-band absolute magnitude. The colors are similar to the Figure 7.2

In Figure 7.3, we show the relations of the derived stellar population parameters with K-band magnitude of galaxies. We see no correlation between age and M_K. However, It is clear that majority of Es are relatively older than dEs. Note that, these ages represent the light weighted ages. Which means, they are preferentially biased towards younger ages (Trager et al., 2000a, 2005), since in the optical, most of the light comes from the youngest component of the stellar populations, and the age correlates more strongly with last star formation activity. Therefore, the measured ages are influenced to a large extent by the last star formation activity in the galaxy. In any case, the old Es seem to host a genuinely old stellar population, in contrast they could show the younger ages if they have hosted only a minor fraction of stars that are born recently. Therefore, these measurement of ages can only be regarded as a mean tracer rather than absolute (Trager et al., 2008). However, recent observations of Es in Ultra Violet (UV)-band have shown a prominent detection of UV fluxes in Es, and it is generally interpreted as a presence of young stellar population or sign of residual star formation activity (Deharveng et al., 2002; Kaviraj et al., 2007). In contrary, several authors have argued that the UV-excess can also be caused by an old stellar population Welch (1982); Faber & Lin (1983) due to hot horizontal branch (HB) stars and the evolutionary phases which follow the HB. Yi et al. (1997) noticed that the extreme excess of UV flux in some early-type cannot be explained without adding some residual star formation activity. Interestingly, some of the Es in our sample also show significant young stellar population properties, i.e. nearly 10% have ages of less than 5 Gyr.

It is quite prominent that the dEs follow a well-known correlation of metallicity luminosity. But in case of Es this correlation is almost flat. The error-bars of measured metallicity in the dEs are larger than in the Es. In addition, dEs also show a larger scattering in luminosity-metallicity relation than that of Es. Moreover, the range of dEs metallicity is almost twice larger

NGC no.	M_b mag	M_k mag	Age Gyr	[Z/H] dex	[α/Fe] dex
2329	-21.51	-25.25 ± 0.03	$8.3^{+0.8}_{-1.4}$	-0.05 ± 0.06	0.29 ± 0.06
2778	-19.22	-22.94 ± 0.03	$15.0^{+0.1}_{-0.1}$	-0.34 ± 0.03	0.03 ± 0.05
3605	-17.14	-20.51 ± 0.02	$3.3^{+0.1}_{-0.4}$	-0.08 ± 0.03	-0.01 ± 0.04
3608	-19.74	-23.1 ± 0.02	$9.8^{+1.0}_{-0.1}$	-0.14 ± 0.06	0.17 ± 0.04
3665	-20.86	-24.84 ± 0.01	$6.4^{+1.3}_{-0.6}$	-0.05 ± 0.06	0.22 ± 0.04
3818	-19.37	-23.03 ± 0.03	$11.6^{+0.1}_{-1.0}$	-0.34 ± 0.03	-0.02 ± 0.01
4278	-19.35	-23.08 ± 0.01	$15.0^{+0.1}_{-0.1}$	-0.11 ± 0.03	0.14 ± 0.01
4415	-17.54	-20.54 ± 0.07	$7.0^{+0.7}_{-0.7}$	-0.54 ± 0.06	-0.06 ± 0.07
4431	-17.16	-20.52 ± 0.05	$9.8^{+5.3}_{-0.9}$	-0.51 ± 0.12	0.13 ± 0.09
4464	-17.95	-21.82 ± 0.03	$15.0^{+0.1}_{-1.3}$	-0.49 ± 0.03	0.0 ± 0.01
4467	-16.85	-21.16 ± 0.09	$9.0^{+0.9}_{-0.1}$	-0.28 ± 0.03	0.05 ± 0.06
4478	-19.59	-23.28 ± 0.01	$7.6^{+0.1}_{-0.1}$	-0.34 ± 0.01	-0.19 ± 0.01
4564	-19.4	-23.27 ± 0.02	$9.0^{+0.1}_{-0.1}$	-0.11 ± 0.03	0.1 ± 0.02
4673	-20.27	-25.13 ± 0.02	$5.4^{+0.1}_{-0.5}$	-0.14 ± 0.03	0.16 ± 0.05
4742	-19.35	-22.89 ± 0.02	$1.3^{+0.1}_{-0.1}$	-0.14 ± 0.01	-0.12 ± 0.01
5638	-19.98	-23.72 ± 0.02	$9.8^{+0.1}_{-0.9}$	-0.28 ± 0.03	-0.05 ± 0.05
5796	-20.86	-24.94 ± 0.00	$9.0^{+0.9}_{-0.1}$	-0.23 ± 0.06	0.0 ± 0.08
5831	-19.82	-23.53 ± 0.03	$4.6^{+0.1}_{-0.1}$	-0.05 ± 0.01	-0.06 ± 0.01
5845	-18.51	-22.59 ± 0.02	$11.6^{+0.1}_{-0.1}$	-0.34 ± 0.03	0.0 ± 0.06
636	-20.02	-23.79 ± 0.03	$5.9^{+0.6}_{-0.1}$	-0.05 ± 0.03	0.11 ± 0.04
6482	-22.11	-25.47 ± 0.01	$13.8^{+1.3}_{-1.2}$	-0.03 ± 0.03	0.24 ± 0.04
6577	-21.16	-24.7 ± 0.03	$11.6^{+0.1}_{-0.1}$	-0.17 ± 0.03	0.17 ± 0.04
6702	-21.56	-25.08 ± 0.03	$2.3^{+0.1}_{-0.1}$	0.3 ± 0.03	0.22 ± 0.02
6703	-20.85	-24.58 ± 0.02	$8.3^{+0.8}_{-0.1}$	-0.25 ± 0.03	-0.12 ± 0.01
7052	-20.91	-25.64 ± 0.02	$15.0^{+0.1}_{-0.1}$	-0.23 ± 0.01	0.28 ± 0.02
4486	-17.69	-21.8 ± 0.02	$15.0^{+0.1}_{-1.3}$	-0.17 ± 0.03	0.29 ± 0.05
4843	-20.07	-24.15 ± 0.03	$8.3^{+0.8}_{-0.8}$	-0.05 ± 0.03	0.2 ± 0.05
4842	-19.19	-23.01 ± 0.06	$8.3^{+0.1}_{-1.4}$	0.1 ± 0.06	0.24 ± 0.05
4864	-20.63	-24.4 ± 0.00	$6.4^{+1.3}_{-0.6}$	0.0 ± 0.06	0.2 ± 0.05
4867	-19.01	-23.29 ± 0.06	$5.0^{+0.5}_{-0.9}$	0.0 ± 0.06	0.26 ± 0.04
2693	-21.65	-25.71 ± 0.02	$12.7^{+1.2}_{-0.1}$	-0.08 ± 0.06	0.25 ± 0.04
2694	-19.37	-22.93 ± 0.00	$9.8^{+1.0}_{-0.9}$	-0.14 ± 0.06	0.22 ± 0.05
2832	-22.38	-26.3 ± 0.02	$13.8^{+0.1}_{-0.1}$	-0.05 ± 0.03	0.2 ± 0.02
3641	-18.11	-21.79 ± 0.04	$9.8^{+0.1}_{-0.9}$	-0.34 ± 0.03	0.05 ± 0.05
4692	-21.8	-25.57 ± 0.03	$8.3^{+0.8}_{-0.1}$	0.0 ± 0.03	0.17 ± 0.02
4865	-19.89	-23.7 ± 0.00	$5.9^{+0.1}_{-0.6}$	0.0 ± 0.03	0.23 ± 0.05
4875	-19.84	-23.79 ± 0.05	$6.4^{+0.1}_{-0.6}$	-0.03 ± 0.03	0.32 ± 0.02
4908	-21.07	-25.12 ± 0.03	$10.7^{+1.0}_{-1.8}$	-0.25 ± 0.09	0.18 ± 0.04
6127	-21.36	-25.1 ± 0.02	$9.0^{+0.1}_{-0.1}$	0.0 ± 0.03	0.19 ± 0.03
6411	-21.25	-24.64 ± 0.02	$5.9^{+0.1}_{-0.6}$	-0.05 ± 0.03	0.06 ± 0.04
1453	-21.61	-25.56 ± 0.02	$15.0^{+0.1}_{-0.1}$	-0.05 ± 0.03	0.19 ± 0.03

Table 7.1: Stellar population parameters derived for Es sample of Sánchez-Blázquez et al. (2006).

NGC no.	M_b mag	M_k mag	Age Gyr	[Z/H] dex	[α/Fe] dex
221	-17.42	-20.94 ± 0.00	$3.0^{+0.4}_{-0.1}$	-0.20 ± 0.03	-0.13 ± 0.01
315	-22.46	-26.54 ± 0.00	$15.0^{+0.1}_{-0.1}$	-0.08 ± 0.03	0.32 ± 0.02
507	-22.06	-26.1 ± 0.00	$8.3^{+1.6}_{-0.8}$	-0.11 ± 0.06	0.17 ± 0.06
584	-20.89	-24.8 ± 0.00	$5.4^{+0.6}_{-0.1}$	-0.08 ± 0.03	0.09 ± 0.05
821	-20.74	-24.63 ± 0.00	$7.0^{+0.7}_{-0.7}$	0.0 ± 0.03	0.17 ± 0.04
1700	-21.88	-25.9 ± 0.00	$4.2^{+0.5}_{-0.4}$	0.1 ± 0.03	0.14 ± 0.04
2300	-20.75	-24.64 ± 0.00	$7.6^{+0.1}_{-1.3}$	0.0 ± 0.06	0.23 ± 0.03
3115	-19.75	-23.53 ± 0.00	$9.8^{+0.1}_{-0.1}$	-0.11 ± 0.03	0.16 ± 0.02
3377	-19.16	-22.88 ± 0.00	$5.9^{+0.1}_{-0.6}$	-0.28 ± 0.03	0.06 ± 0.02
3379	-20.55	-24.42 ± 0.00	$11.6^{+0.1}_{-0.1}$	-0.31 ± 0.01	-0.04 ± 0.01
4261	-21.32	-25.28 ± 0.00	$12.7^{+1.2}_{-1.1}$	-0.34 ± 0.06	-0.06 ± 0.03
4365	-20.96	-24.88 ± 0.00	$12.7^{+0.1}_{-1.1}$	-0.03 ± 0.03	0.28 ± 0.02
4374	-21.05	-24.98 ± 0.00	$15.0^{+0.1}_{-0.1}$	-0.25 ± 0.01	0.18 ± 0.01
4472	-21.71	-25.71 ± 0.00	$9.0^{+0.9}_{-0.1}$	-0.05 ± 0.03	0.03 ± 0.04
4489	-18.25	-21.87 ± 0.00	$2.5^{+0.3}_{-0.3}$	-0.08 ± 0.03	0.0 ± 0.04
4552	-20.8	-24.7 ± 0.00	$13.8^{+1.3}_{-0.1}$	-0.14 ± 0.03	0.3 ± 0.02
4594	-22.21	-26.27 ± 0.00	$15.0^{+0.1}_{-0.1}$	-0.25 ± 0.03	0.17 ± 0.06
4621	-20.49	-24.35 ± 0.00	$15.0^{+0.1}_{-0.1}$	-0.25 ± 0.01	0.18 ± 0.01
4636	-20.51	-24.38 ± 0.00	$15.0^{+0.1}_{-1.3}$	-0.17 ± 0.06	0.26 ± 0.03
4649	-21.47	-25.44 ± 0.00	$12.7^{+1.2}_{-1.1}$	-0.05 ± 0.03	0.26 ± 0.03
4697	-21.15	-25.09 ± 0.00	$7.6^{+0.1}_{-0.7}$	-0.17 ± 0.03	-0.01 ± 0.02
4839	-22.23	-26.29 ± 0.00	$5.9^{+1.2}_{-1.4}$	0.2 ± 0.06	0.26 ± 0.05
4874	-22.48	-26.57 ± 0.00	$10.7^{+1.0}_{-1.0}$	-0.03 ± 0.06	0.22 ± 0.05
5813	-21.08	-25.01 ± 0.00	$15.0^{+0.1}_{-0.1}$	-0.34 ± 0.01	0.04 ± 0.01
5847	-20.18	-24.01 ± 0.00	$15.0^{+0.1}_{-2.4}$	-0.40 ± 0.06	0.06 ± 0.02
5846	-21.26	-25.21 ± 0.00	$11.6^{+1.1}_{-1.0}$	-0.25 ± 0.09	-0.02 ± 0.07
IC no.					
767	-18.09	-21.03 ± 0.07	$3.5^{+1.1}_{-0.9}$	-0.66 ± 0.12	-0.12 ± 0.14
794	-18.32	-21.56 ± 0.12	$5.9^{+0.6}_{-1.0}$	-0.40 ± 0.03	-0.19 ± 0.05
832	-20.19	-24.21 ± 0.04	$4.6^{+0.5}_{-0.5}$	-0.25 ± 0.06	0.19 ± 0.05
3957	-19.2	-23.05 ± 0.07	$11.6^{+0.1}_{-1.0}$	-0.23 ± 0.06	0.18 ± 0.04
3959	-20	-23.99 ± 0.04	$6.4^{+1.3}_{-0.6}$	0.0 ± 0.03	0.25 ± 0.02
3963	-19.43	-23.12 ± 0.06	$5.0^{+0.5}_{-0.1}$	-0.08 ± 0.06	0.14 ± 0.05
3973	-18.97	-23.13 ± 0.04	$4.2^{+0.1}_{-0.4}$	0.0 ± 0.03	0.14 ± 0.05
4026	-19.98	-23.84 ± 0.06	$3.9^{+0.4}_{-0.4}$	0.0 ± 0.06	0.18 ± 0.05
4051	-20.24	-23.68 ± 0.00	$12.7^{+1.2}_{-1.1}$	-0.05 ± 0.03	0.3 ± 0.03
4042	-19.86	-23.65 ± 0.00	$15.0^{+0.1}_{-0.1}$	-0.31 ± 0.03	0.24 ± 0.05

Table 7.2: Continuation of Table 7.1

than Es metallicity range within the equal magnitude range of 5 mag. Here we have used K-band luminosity, which is also a good tracer of stellar mass. In that sense, we can interpret it as a mass-metallicity relation, and which is particularly important to test the galaxy formation models (Finlator & Davé, 2008). This relation shows that, dEs and Es do not follow that the same mass-metallicity relation described by single linear regression line.

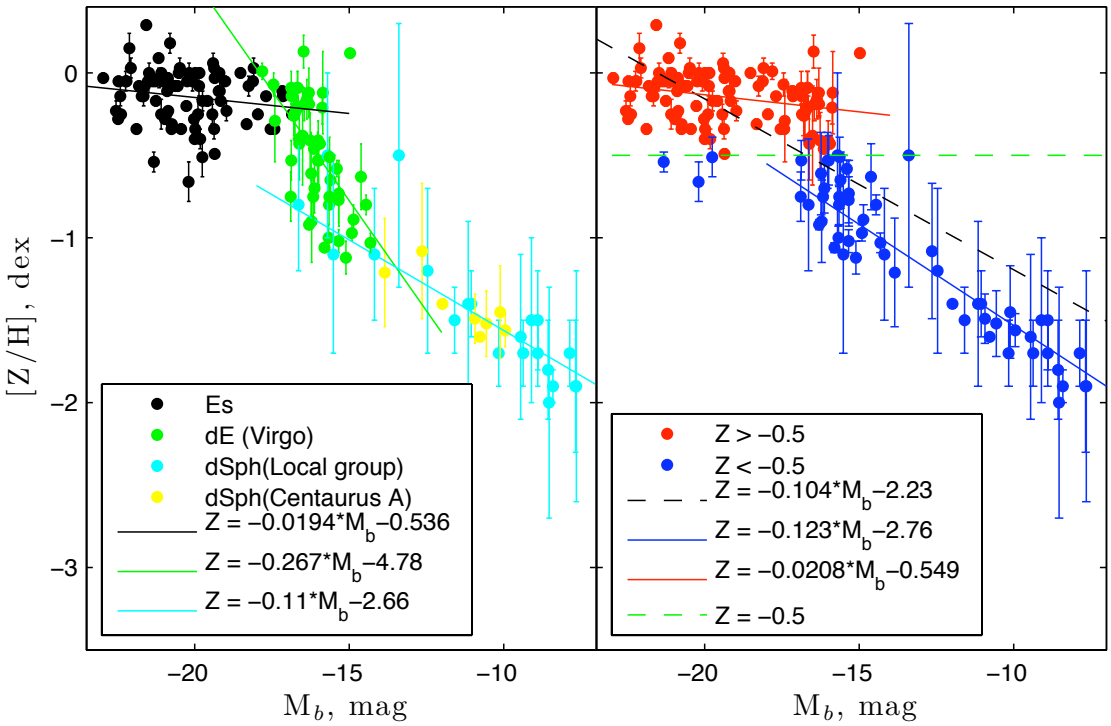

Figure 7.4: Luminosity-metallcity relation for all class of early-type galaxies in B-band magnitude.

In Figure 7.4, we compile mass metallicity relation of early-type galaxies for a large range of magnitude varying from M_b = -23 to -9 mag. Which covers the different classes of early-type galaxies i.e. Es, dEs and dSphs. A clear luminosity-metallicity relation can be seen in these samples of early-type galaxies. However, the slopes of these relations are not similar for all classes. We see the dEs have steepest slope among all classes and Es have almost flat. Three clear outliers above the dEs and dSph points in this metallicity-luminosity relation are VCC0916, VCC1947 and M32. Each of them have a special characteristic such as VCC0916 is M32 type, VCC1947 is only a possible member of Virgo cluster and M32 is itself regarded as a special type of dEs.

It is also interesting to see that the overall metallicity-luminosity relation seems to have a break at the dEs region. In right side of the Figure 7.4, we divide our total galaxy sample into two groups: one is metal poor (i.e. Z < 0.5 dex) and the other is metal rich (Z > -0.5 dex). The metallicity-luminosity relations clearly show that these different groups have fairly different slopes and metal poor galaxies group has steeper slope than metal rich. It is prominent that the merging point of these two different groups exactly lies on the dEs region $M_b \approx$ -16.5 mag, where the dichotomy in age was prominent, see Chapter 4. The metal rich dEs seem to follow the L-Z relation along with normal Es and metal poor dEs seem to join at the brighter end of L-Z along with dSph.

In Figure 7.5, we show the relations between the derived stellar population parameters. We do not see any strong relation between each others. It seems that metallicity correlate with [α/Fe]

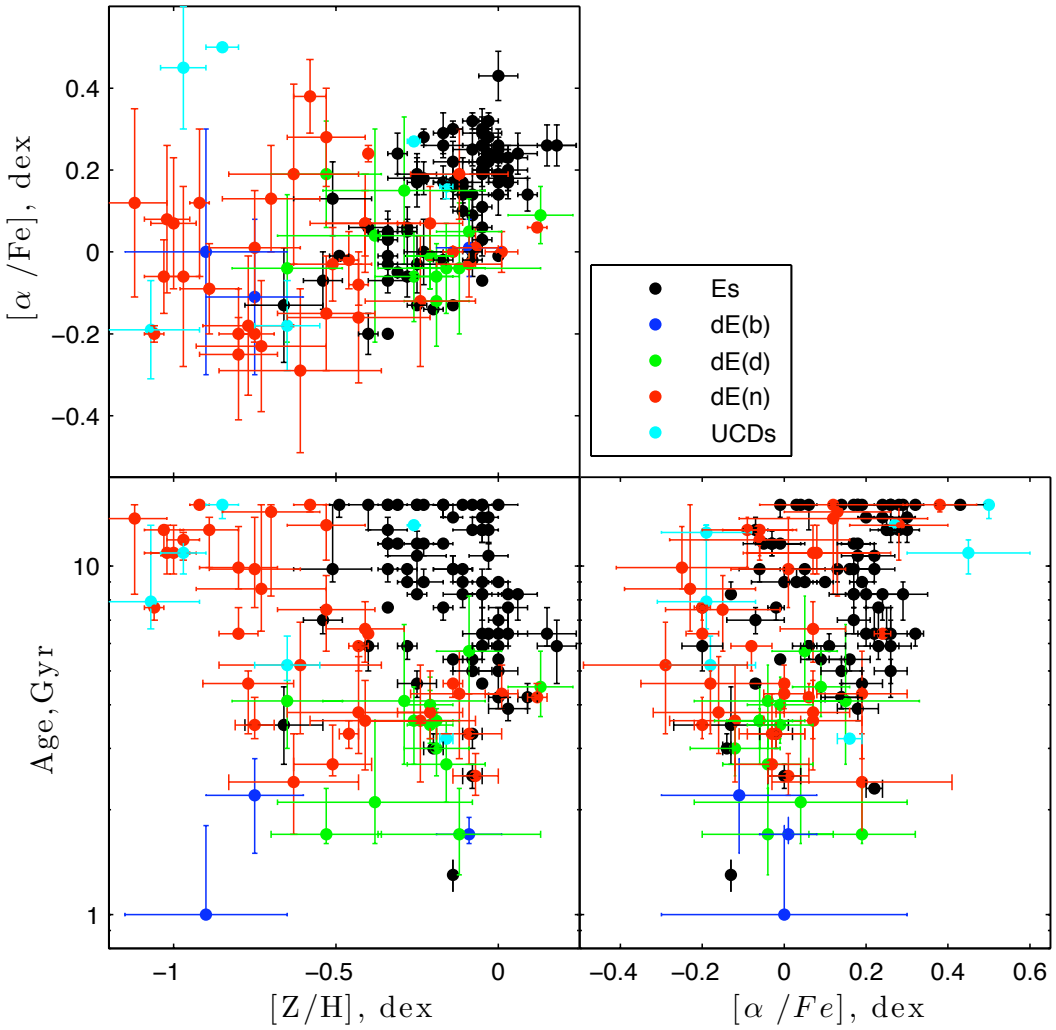

Figure 7.5: Relation between SSP parameters.

in case of Es, however the scattering is fairly large. But interestingly, the dEs with metallicity larger than Z = -0.5 dex seem to continue the [α/Fe] - [Z/H] relation defined by Es, and the rest of metal poor dEs are scattered in a large range of [α/Fe] at the left portion of diagram. In the bottom left diagram of the Figure 7.5, we see the spreading of points all over the place that hints no relation between the age and metallicity in the Es and dEs. It is worth to notice that there is almost no overlap between the dE(d)s and Es. We also do not see any relation between [α/Fe] and SSP equivalent ages of galaxies, the points are scattered all over the diagram.

7.4 Discussion and conclusions

It is well known fact that dEs and Es exhibit different stellar populations i.e Es are generally considered that older and metal enhanced than dEs. We also confirm these results here as the average properties of Es and dEs. But we see that the ages of both Es and dEs spread over fairly large range. Almost all Es in our sample have metallicity larger than [Z/H] = -0.5 dex and all dSphs have metallicity less than [Z/H] = -1 dex. The metallicities of dEs show the intermediate properties between Es and dSphs. We also see that the Es and dEs have shared almost equal

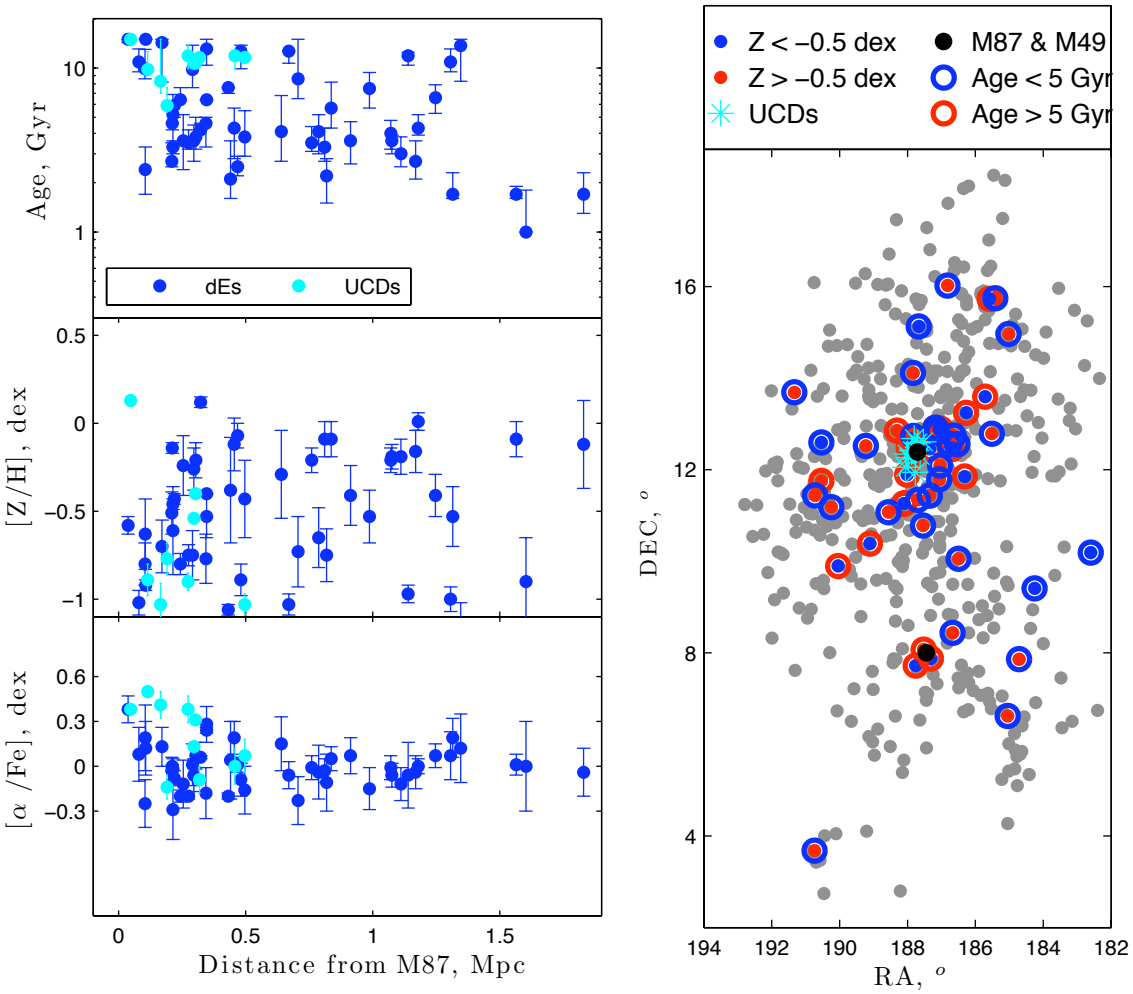

Figure 7.6: Left: Derived ages, metallicity and [α/Fe] versus the projected Virgocentric distance (R, in degrees). Right: The distribution of Virgo dEs in the sky, here we have divided our dEs sample in several groups: dEs with Z > -0.5 dex are represented by red solid circle and Z < -0.5 are represented by blue solid circle, similarly dEs with age > 5 Gyr are shown in red circle and age < 5 Gyr are shown in blue circle.

range of α-element abundant ratios i.e from [α/Fe] $\approx$ - 0.3 to [α/Fe] $\approx$ 0.4 dex. We will now discuss these findings in the context of metallicity-luminosity relation and try to see whether dEs have the special characteristic or not.

Clemens et al. (2006) found that the metallicity grows monotonically with velocity dispersion. We confirm this trend as a form of L-Z relation. However, the slopes of these relations in different classes of early-type galaxies are different. An interpretation of this relation generally focuses around the efficiency of stellar outflow at the low luminosity galaxies. In any case, interpreting these differences in slopes are not easy, since the role of other factors such as IMF variation, the environment and also the method used to estimate the metallicity cannot be ruled out. We have sampled the galaxies from the different environment: dSph are from group, dEs are from cluster and Es are fairly mixed from field, group and cluster. But a detail study of Mendel et al. (2009) have shown that the environment is likely to play a small role in establishing mass/luminosity-metallicity relation. Nevertheless, a clear break in this relation at the dEs region may suggest that not all the dEs have homogeneous stellar population properties. Some dEs seem to follow the L-Z relation along with Es, at least those that have metallicity larger than -0.5 dex. On the other hand, the metal poor dEs show a special behavior not only in

metallicity-luminosity relation but also in [α/Fe] - [Z/H] relation. They have fairly large range of [α/Fe] but relatively poor metallicity. It may be the selection effect that we have not included any dE(nN) in this study, therefore the majority of metal poor dEs are dE(n) class and they have fairly old stellar population, which are also located in the cluster core. Unfortunately, there are no reliable measurements of [α/Fe] for many dSph so we cannot compare this parameter of dEs to the dSph.

An another explanation of the luminosity-metallicity relation is related to the decreasing efficiency of star formation activity with decreasing luminosity (Tremonti et al., 2004; Gallazzi et al., 2006). In this interpretation of the luminosity-metallicity relation one expect to see low luminosity galaxies trend towards lower α-element abundances, as the relationship of α-element abundance to supernovae timescale, namely SNII versus SNI. Examining the observed relation of [α/Fe] with luminosity in Figure 7.3 we find considerable scatter in the dEs. But the majority of bright dEs (M_K < -19.5) seem to have lower values of [α/Fe].

In general, there is no sharp difference between dEs and dSphs. However, dSphs are supposed to have on average lower surface brightnesses (μ > 22 mag arcsec^{-2}) and surface brightness gradients than dEs. The prototypes of dSphs are Sculptor and Fornax dSphs in the Local group (LG). dSphs are not supported by rotation and appear to contain large amounts of dark matter. The existence of large amount of dark matter is inferred from the high velocity dispersion and the resulting high mass-to-light ratios derived under the assumption of Virial equilibrium (Strigari et al., 2008). Grebel et al. (2003) show that their luminosity-metallicity relation differs from the their irregular counterpart, and have a offset in the sense that they are more metal-rich for a given luminosity. Since dSphs have fairly low mass, it is believed that they are more vulnerable to environmental effects than any other.

The environment in which a dE evolves can influence its stellar population properties, since it can regulate the strengths of violent activity in which dEs evolved in cluster environment and set the number of interactions with other galaxies. Such as harassments are more frequent in the cluster core than outskirts of the cluster. One therefore expects to see differences between dEs in the outskirts of the cluster and near to the centre of the cluster. In Figure 7.6, we plot the SSP parameters as a function of cluster-centric distances. It is fact that, the nucleated dEs are preferentially found in the dense region of the cluster, we see almost all dEs from cluster core are fairly old (see Figure 7.6).

8

Summary and outlook

In this thesis, we have studied stellar population properties of a sample of early-type dwarf galaxies (dEs) in the Virgo cluster. We have exploited low-resolution spectroscopic data sets that obtained from the ESO-Very Large Telescope during the month of April 2007 and April 2010. An ideal method to perform this study is the analysis of absorption line strengths in the Lick/IDS system. Using this method we have derived stellar population parameters such as age, metallicity and α-element abundant ratio from the central and spatially resolved spectra of dEs. We started with characterizing the central stellar population properties of dEs (Chapter 4). In this study, we have used an additional sample of dEs from the study of Michielsen et al. (2008), which makes this the largest sample of dEs for a similar kind of studies to date. Then next, to probe the nature of dEs nuclei, we have investigated a spatially resolved stellar population characteristics of our original sample dEs in Chapter 5. The stellar population properties of a sample of Ultra-Compact Dwarf (UCD) galaxies in the Virgo cluster are studied in Chapter 6. Finally, we discussed the overall stellar population properties of dEs by comparing a large set of different class of early-type galaxies in Chapter 7. We have expanded this study to the luminosity range $M_b = -9$ to $M_b = -23$, which includes the bright normal ellipticals (Es) to faint dwarf Spheroidal (dSph), and try to answer the question whether a classical early-type dwarf galaxies constitute a genuine class of galaxies or are merely a low luminosity extension of Es.

According to these studies, our main findings can be summarized as follows:

- The central stellar population properties showed that not all dEs exhibit same stellar population properties. We found that, dEs with disc feature are relatively younger and metal enhanced than dEs without disc. The α-element abundance ratio appears to be consistent with the solar value for both morphological types.

- Besides a well-defined relation of metallicity and luminosity, we also found a clear anti-correlation between age and luminosity. More specifically, there appeared to be bimodality: brighter galaxies ($M_r \leq -16.5$ mag), including the discy ones, exhibit significantly younger ages than fainter dEs ($M_r \geq -17.0$ mag).

- We thus argue that that these galaxies cannot originate from same evolutionary history for different morphology. Old and metal poor dEs could have early termination of star formation activity with infall of primordial galaxy in the cluster potential are normal nucleated. By contrast, the discy galaxy, which are metal rich and relatively young, must have undergone through structural transformation of a late-type spiral into a spheroidal system.

- The analysis of spatially resolved stellar populations showed that ages of the nuclei are lower than those of the respective galactic main bodies for the most dEs with an average of

3.5 Gyr age difference. We also observed the dE nuclei to be more metal rich compared to their host galaxies. The metallicity of both nucleus and galactic main body of dEs correlates with the total luminosity of dEs.

- We noticed that different behaviour of SSP gradient in dEs i.e, both flat and steeper profile are frequent, however the observed overall trend of increasing age and decreasing metallicity with the radius is consistent with earlier studies. Estimates of the α-abundance ratio as function of radius are consistent with no gradient along the major axis.

- Our analysis of stellar population parameters of the nuclei of 34 Virgo dEs, as well as ten Virgo UCDs showed that nuclei of Virgo dEs have younger stellar population ages than UCDs, with averages of 5 Gyr and >10 Gyr, respectively.

- Comparing the stellar population parameters at the same local galaxy density, with UCDs being located in the high density cluster regions, we do not find any difference in the stellar populations of dE nuclei and UCDs. In those regions, the dE nuclei are as old and metal poor as UCDs. This evidence suggests that the Virgo UCDs may have formed through the stripping of dE nuclei.

- We confirmed that the metallicity of galaxies correlate with the galaxies luminosity in all classes of early-type galaxies i.e. Es, dEs and dSphs. However, the slopes of these relations are not similar for all classes of galaxies. We see the dEs have steepest slope among all classes and Es have almost flat in metallicity-luminosity relation.

- We discovered a clear break in luminosity-metallicity relation in the dEs region. The bright and metal rich dEs seem to follow a faint end extension of Es and metal poor, old and old dEs are either holds a genuine class of early-type dwarf galaxies or just a bright end extension of dSph.

8.1 Future prospect

There are a number of logical extensions of this thesis need to be done in the future to get more comprehensive understanding of the early-type galaxies properties. The immediate extension would be the inclusion of kinematical data sets, which provides a more reliable estimate of total galactic energetics than luminosity. Using the kinematic we can derive total mass (light + dark component) of the galaxy. Galaxy mass is one of the main drivers of galaxy evolution and appearance. We have seen that the early-type galaxies are not homogeneous in appearance nor in kinematic. There are frequent evidences of kinematically-decoupled core, miss-alignment of rotation axis and anisotropic velocity distribution in early-type galaxies (Krajnović et al., 2008). Which also adds the importance of kinematic study to get a better picture of formation and evolution of early-type galaxies.

In this thesis, we have derived SSP-equivalent age and metallicity with the assumption that all star are formed in a single event. However, in practice, this is not true, the recent studies have shown that the galaxies build up their stellar masses by several episodic or wider star formation history (Mayer et al., 2001; Haines et al., 2007). Therefore, the information extracted from star formation history would be more practical then using the SSP-equivalent age and metallicity to get the evolutionary time scale of these systems. But it is not easy to derive a star formation history from the integrated light of a galaxy. A slightly different approach has been suggested that the integrated spectra of early-type galaxies can be decomposed into several different SSPs

and then one can estimate the relative strength of star formation activity at a given SSP age Koleva et al. (2009).

The formation of early-type dwarfs is expected to be strongly linked to the environment in which these objects reside. However, we found dEs in isolation, which must have formed in the absence of any environmental transformation process. Therefore, to put constraints over the various formation channels that followed by the dEs, I will analyze the ESO VLT/FORS2 spectra (program 087.B-0841, PI S. Paudel, continuing collaboration with T. Lisker). I plan to perform a stellar population analysis from these spectra, which possibly helps to link the formations paths to stellar population characteristics, shedding light on the assembly history of groups and clusters, above all a test of hierarchical theory of galaxy formation. Moreover, a similar study with a much larger sample size could be performed when complementing the optical photometry from SDSS with NIR data, which we have planed to obtain within the framework of much larger collaboration as a SMAKCED project.

Abbreviations

ACS	Advanced camera for surveys
AGB	Asymptotic giant branch
CCD	Charge-coupled device
CDM	Cold dark matter
CMB	Cosmic microwave background
CMD	Color magnitude diagram
CMR	Color magnitude relation
dE	Dwarf elliptical galaxy or Early-type dwarf galaxy
DEC	Declination
dIrr	Dwarf irregular galaxy
dSph	Dwarf spheroidal galaxy
E	Elliptical galaxy
ESO	European southern observatory
FORS	Focal reducer and low dispersion spectrograph
FWHM	Full width at half maximum
GC	Globular cluster
Gyr	Giga year
H	Hydrogen
HB	Horizontal branch
He	Helium
HST	Hubble space telescope
IDS	Image dissector scanner
IMF	Initial mass function
IRAF	Image reduction & analysis facility
IRF	Instrument responce function
ISM	Interstellar Medium
kpc	Kiloparsec
LTT	Luyten two-tenths catalogue
KS-test	Kolmogorov-Smirnov-test to compare 2 distributions
$M_\odot$	Solar mass
MILES	Medium-resolution Isaac Newton Telescope library of empirical spectra
MOS	Multi object spectroscopy
MXU	Multi-object spectroscopy with exchangable masks
PSF	Point spread function
RGB	Red giant branch
RPS	Ram pressure stripping
RA	Right ascension
RMS	Root mean square

SDSS	Sloan digital sky survey
SED	spectral energy distribution
SF	Star formation
SSP	Simple stellar population
SN	Supernova
SNR	Signal to noise ratio
UCD	Ultracompact dwarf galaxies
ULYSS	University of Lyon spectroscopic analysis software
UT	Unit telescope
UV	Ultra violet
2MASS	Two micron all sky survey
VCC	Virgo cluster catalogue
VLT	Very large telescope
WF	Wide field planetary camera

Bibliography

Aguerri J. A. L., González-García A. C., 2009, A&A, 494, 891

Appenzeller I., Fricke K., Fürtig W., Gässler W., Häfner R., Harke R., Hess H.-J., Hummel W., 1998, The Messenger, 94, 1

Arimoto N., Yoshii Y., 1987, A&A, 173, 23

Babul A., Rees M. J., 1992, MNRAS, 255, 346

Balogh M. L., Navarro J. F., Morris S. L., 2000, ApJ, 540, 113

Barazza F. D., Binggeli B., Jerjen H., 2002, A&A, 391, 823

Bassino L. P., Muzzio J. C., Rabolli M., 1994, ApJ, 431, 634

Beasley M. A., Cenarro A. J., Strader J., Brodie J. P., 2009, AJ, 137, 5146

Bekki K., Couch W. J., Drinkwater M. J., Shioya Y., 2003, MNRAS, 344, 399

Bender R., Burstein D., Faber S. M., 1992, ApJ, 399, 462

Bender R., Paquet A., Nieto J., 1991, A&A, 246, 349

Binggeli B., Cameron L. M., 1991, A&A, 252, 27

Binggeli B., Cameron L. M., 1993, A&AS, 98, 297

Binggeli B., Popescu C. C., 1995, A&A, 298, 63

Binggeli B., Sandage A., Tammann G. A., 1985, AJ, 90, 1681

Binggeli B., Sandage A., Tarenghi M., 1984, AJ, 89, 64

Binggeli B., Tammann G. A., Sandage A., 1987, AJ, 94, 251

Blakeslee J. P., Jordán A., Mei S., Côté P., Ferrarese L., Infante L., Peng E. W., Tonry J. L., West M. J., 2009, ApJ, 694, 556

Blumenthal G. R., Faber S. M., Primack J. R., Rees M. J., 1984, Nature, 311, 517

Böhringer H., Briel U. G., Schwarz R. A., Voges W., Hartner G., Trümper J., 1994, Nature, 368, 828

Böker T., Laine S., van der Marel R. P., Sarzi M., Rix H., Ho L. C., Shields J. C., 2002, AJ, 123, 1389

Böker T., Sarzi M., McLaughlin D. E., van der Marel R. P., Rix H., Ho L. C., Shields J. C., 2004, AJ, 127, 105

Boselli A., Boissier S., Cortese L., Gavazzi G., 2008, ApJ, 674, 742

Boselli A., Cortese L., Deharveng J. M., Gavazzi G., Yi K. S., Gil de Paz A., Seibert M., Boissier S., Donas J., Lee Y., Madore B. F., Martin D. C., Rich R. M., Sohn Y., 2005, ApJ, 629, L29

Boselli A., Gavazzi G., 2006, PASP, 118, 517

Bressan A., Chiosi C., Tantalo R., 1996, A&A, 311, 425

Bruzual G., Charlot S., 2003, MNRAS, 344, 1000

Burstein D., Faber S. M., Gaskell C. M., Krumm N., 1984, ApJ, 287, 586

Buzzoni A., 1995, ApJS, 98, 69

Caldwell N., Armandroff T. E., Seitzer P., Da Costa G. S., 1992, AJ, 103, 840

Caldwell N., Rose J. A., Concannon K. D., 2003, AJ, 125, 2891

Cardiel N., Gorgas J., Cenarro J., Gonzalez J. J., 1998, A&AS, 127, 597

Cardiel N., Gorgas J., Sánchez-Blázquez P., Cenarro A. J., Pedraz S., Bruzual G., Klement J., 2003, A&A, 409, 511

Cayatte V., van Gorkom J. H., Balkowski C., Kotanyi C., 1990, AJ, 100, 604

Cecil G., Rose J. A., 2007, Reports on Progress in Physics, 70, 1177

Cenarro A. J., Peletier R. F., Sánchez-Blázquez P., Selam S. O., Toloba E., Cardiel N., Falcón-Barroso J., Gorgas J., Jiménez-Vicente J., Vazdekis A., 2007, MNRAS, 374, 664

Chilingarian I. V., 2009, MNRAS, 394, 1229

Chilingarian I. V., Cayatte V., Durret F., Adami C., Balkowski C., Chemin L., Laganá T. F., Prugniel P., 2008, A&A, 486, 85

Clemens M. S., Bressan A., Nikolic B., Alexander P., Annibali F., Rampazzo R., 2006, MNRAS, 370, 702

Côté P., Blakeslee J. P., Ferrarese L., Jordán A., Mei S., Merritt D., Milosavljević M., Peng E. W., Tonry J. L., West M. J., 2004, ApJS, 153, 223

Côté P., Piatek S., Ferrarese L., Jordán A., Merritt D., Peng E. W., Haşegan M., Blakeslee J. P., Mei S., West M. J., Milosavljević M., Tonry J. L., 2006, ApJS, 165, 57

Cowie L. L., Songaila A., Hu E. M., Cohen J. G., 1996, AJ, 112, 839

Crnojević D., Grebel E. K., Koch A., 2010, A&A, 516, A85

De Propris R., Phillipps S., Drinkwater M. J., Gregg M. D., Jones J. B., Evstigneeva E., Bekki K., 2005, ApJ, 623, L105

De Rijcke S., Dejonghe H., Zeilinger W. W., Hau G. K. T., 2001, ApJ, 559, L21

De Rijcke S., Dejonghe H., Zeilinger W. W., Hau G. K. T., 2003, A&A, 400, 119

de Vaucouleurs G., 1961, ApJS, 6, 213

Deharveng J., Boselli A., Donas J., 2002, A&A, 393, 843

Dekel A., Silk J., 1986, ApJ, 303, 39

Dressler A., 1980, ApJ, 236, 351

Drinkwater M. J., Gregg M. D., Couch W. J., Ferguson H. C., Hilker M., Jones J. B., Karick A., Phillipps S., 2004, PASA, 21, 375

Drinkwater M. J., Gregg M. D., Hilker M., Bekki K., Couch W. J., Ferguson H. C., Jones J. B., Phillipps S., 2003, Nature, 423, 519

Durrell P. R., 1997, AJ, 113, 531

Eggen O. J., Lynden-Bell D., Sandage A. R., 1962, ApJ, 136, 748

Evstigneeva E. A., Drinkwater M. J., Peng C. Y., Hilker M., De Propris R., Jones J. B., Phillipps S., Gregg M. D., Karick A. M., 2008, AJ, 136, 461

Evstigneeva E. A., Gregg M. D., Drinkwater M. J., 2005, in H. Jerjen & B. Binggeli ed., IAU Colloq. 198: Near-fields cosmology with dwarf elliptical galaxies The origin of ultra-compact dwarf galaxies in the Virgo cluster. pp 413–415

Evstigneeva E. A., Gregg M. D., Drinkwater M. J., Hilker M., 2007, AJ, 133, 1722

Faber S. M., 1973, ApJ, 179, 731

Faber S. M., Lin D. N. C., 1983, ApJ, 266, L17

Ferguson H. C., Binggeli B., 1994, A&AR, 6, 67

Ferguson H. C., Sandage A., 1989, ApJ, 346, L53

Finlator K., Davé R., 2008, MNRAS, 385, 2181

Firth P., Evstigneeva E. A., Drinkwater M. J., 2009, MNRAS, 394, 1801

Freedman W. L., 1995, in P. C. van der Kruit & G. Gilmore ed., Stellar Populations Vol. 164 of IAU Symposium, M31 and Companions A Key to Baade's Stellar Populations Then and Now. pp 165

Gallazzi A., Charlot S., Brinchmann J., White S. D. M., 2006, MNRAS, 370, 1106

Gavazzi G., Bonfanti C., Sanvito G., Boselli A., Scodeggio M., 2002, ApJ, 576, 135

Gavazzi G., Scodeggio M., 1996, A&A, 312, L29

Geha M., Guhathakurta P., van der Marel R. P., 2003, AJ, 126, 1794

Girardi L., Bressan A., Bertelli G., Chiosi C., 2000, A&AS, 141, 371

Girardi M., Borgani S., Giuricin G., Mardirossian F., Mezzetti M., 1998, ApJ, 506, 45

Goerdt T., Moore B., Kazantzidis S., Kaufmann T., Macciò A. V., Stadel J., 2008, MNRAS, 385, 2136

González J. J., 1993, PhD thesis, Thesis (PH.D.)–UNIVERSITY OF CALIFORNIA, SANTA CRUZ, 1993.Source: Dissertation Abstracts International, Volume: 54-05, Section: B, page: 2551.

Gorgas J., Pedraz S., Guzman R., Cardiel N., Gonzalez J. J., 1997, ApJ, 481, L19+

Graham A. W., Guzmán R., 2003, AJ, 125, 2936

Grant N. I., Kuipers J. A., Phillipps S., 2005, MNRAS, 363, 1019

Grebel E. K., 1999, in P. Whitelock & R. Cannon ed., The Stellar Content of Local Group Galaxies Vol. 192 of IAU Symposium, Evolutionary Histories of Dwarf Galaxies in the Local Group. pp 17

Grebel E. K., 2001, Astrophysics and Space Science Supplement, 277, 231

Grebel E. K., Gallagher III J. S., 2004, ApJ, 610, L89

Grebel E. K., Gallagher III J. S., Harbeck D., 2003, AJ, 125, 1926

Gunn J. E., Gott J. R. I., 1972, ApJ, 176, 1

Haşegan M., Jordán A., Côté P., Djorgovski S. G., McLaughlin D. E., Blakeslee J. P., Mei S., West M. J., Peng E. W., Ferrarese L., Milosavljević M., Tonry J. L., Merritt D., 2005, ApJ, 627, 203

Haines C. P., Gargiulo A., La Barbera F., Mercurio A., Merluzzi P., Busarello G., 2007, MNRAS, 381, 7

Hamuy M., Suntzeff N. B., Heathcote S. R., Walker A. R., Gigoux P., Phillips M. M., 1994, PASP, 106, 566

Hilker M., 2009, UCDs - A Mixed Bag of Objects. pp 51

Hilker M., Baumgardt H., Infante L., Drinkwater M., Evstigneeva E., Gregg M., 2007, A&A, 463, 119

Hilker M., Infante L., Vieira G., Kissler-Patig M., Richtler T., 1999, A&AS, 134, 75

Hilker M., Mieske S., Infante L., 2003, A&A, 397, L9

Holmberg E., 1958, Meddelanden fran Lunds Astronomiska Observatorium Serie II, 136, 1

Janz J., Lisker T., 2008, ApJ, 689, L25

Janz J., Lisker T., 2009, ApJ, 696, L102

Jarrett T. H., Chester T., Cutri R., Schneider S. E., Huchra J. P., 2003, AJ, 125, 525

Jerjen H., 2010, AiA, 2010

Jerjen H., Binggeli B., 1997, in M. Arnaboldi, G. S. Da Costa, & P. Saha ed., The Nature of Elliptical Galaxies; 2nd Stromlo Symposium Vol. 116 of Astronomical Society of the Pacific Conference Series, Are ”Dwarf” Ellipticals Genuine Ellipticals?. pp 239

Jerjen H., Kalnajs A., Binggeli B., 2000, A&A, 358, 845

Jones J. B., Drinkwater M. J., Jurek R., Phillipps S., Gregg M. D., Bekki K., Couch W. J., Karick A., Parker Q. A., Smith R. M., 2006, AJ, 131, 312

Jones L. A., 1997, PhD thesis, Univ. North Carolina, Chapel Hill.

Kaviraj S., Schawinski K., Devriendt J. E. G., Ferreras I., Khochfar S., Yoon S., Yi S. K., Deharveng J., Boselli A., Barlow T., 2007, ApJS, 173, 619

Kodama T., Arimoto N., 1997, A&A, 320, 41

Koleva M., de Rijcke S., Prugniel P., Zeilinger W. W., Michielsen D., 2009, MNRAS, 396, 2133

Koleva M., Prugniel P., Ocvirk P., Le Borgne D., Soubiran C., 2008, MNRAS, 385, 1998

Köppen J., Weidner C., Kroupa P., 2007, MNRAS, 375, 673

Kormendy J., 1985, ApJ, 295, 73

Kormendy J., Fisher D. B., Cornell M. E., Bender R., 2009, ApJS, 182, 216

Korn A. J., Maraston C., Thomas D., 2005, A&A, 438, 685

Krajnović D., Bacon R., Cappellari M., Davies R. L., de Zeeuw P. T., Emsellem E., Falcón-Barroso J., Kuntschner H., McDermid R. M., Peletier R. F., Sarzi M., van den Bosch R. C. E., van de Ven G., 2008, MNRAS, 390, 93

Kuntschner H., 2000, MNRAS, 315, 184

Kuntschner H., Lucey J. R., Smith R. J., Hudson M. J., Davies R. L., 2001, MNRAS, 323, 615

Larson R. B., 1974, MNRAS, 169, 229

Larson R. B., Tinsley B. M., Caldwell C. N., 1980, ApJ, 237, 692

Le Borgne J.-F., Bruzual G., Pelló R., Lançon A., Rocca-Volmerange B., Sanahuja B., Schaerer D., Soubiran C., Vílchez-Gómez R., 2003, A&A, 402, 433

Lequeux J., Peimbert M., Rayo J. F., Serrano A., Torres-Peimbert S., 1979, A&A, 80, 155

Lisker T., 2009, Astronomische Nachrichten, 330, 1043

Lisker T., Fuchs B., 2009, A&A, 501, 429

Lisker T., Glatt K., Westera P., Grebel E. K., 2006, AJ, 132, 2432

Lisker T., Grebel E. K., Binggeli B., 2006, AJ, 132, 497

Lisker T., Grebel E. K., Binggeli B., 2008, AJ, 135, 380

Lisker T., Grebel E. K., Binggeli B., Glatt K., 2007, ApJ, 660, 1186

Lisker T., Han Z., 2008, ApJ, 680, 1042

Lotz J. M., Miller B. W., Ferguson H. C., 2004, ApJ, 613, 262

Mac Low M.-M., Ferrara A., 1999, ApJ, 513, 142

Maraston C., 1998, MNRAS, 300, 872

Maraston C., Greggio L., Renzini A., Ortolani S., Saglia R. P., Puzia T. H., Kissler-Patig M., 2003, A&A, 400, 823

Martin C. L., 1999, ApJ, 513, 156

Mastropietro C., Moore B., Mayer L., Debattista V. P., Piffaretti R., Stadel J., 2005, MNRAS, 364, 607

Mateo M. L., 1998, ARA&A, 36, 435

Mayer L., Governato F., Colpi M., Moore B., Quinn T., Wadsley J., Stadel J., Lake G., 2001, ApJ, 547, L123

McClure R. D., van den Bergh S., 1968, AJ, 73, 313

Mei S., Blakeslee J. P., Côté P., Tonry J. L., West M. J., Ferrarese L., Jordán A., Peng E. W., Anthony A., Merritt D., 2007, ApJ, 655, 144

Mendel J. T., Proctor R. N., Rasmussen J., Brough S., Forbes D. A., 2009, MNRAS, 396, 2103

Michielsen D., Boselli A., Conselice C. J., Toloba E., Whiley I. M., Aragón-Salamanca A., Balcells M., Cardiel N., Cenarro A. J., Gorgas J., Peletier R. F., Vazdekis A., 2008, MNRAS, 385, 1374

Mieske S., Hilker M., Infante L., 2002, A&A, 383, 823

Mieske S., Hilker M., Infante L., Jordán A., 2006, AJ, 131, 2442

Mieske S., Hilker M., Jordán A., Infante L., Kissler-Patig M., Rejkuba M., Richtler T., Côté P., Baumgardt H., West M. J., Ferrarese L., Peng E. W., 2008, A&A, 487, 921

Moore B., Ghigna S., Governato F., Lake G., Quinn T., Stadel J., Tozzi P., 1999, ApJ, 524, L19

Moore B., Katz N., Lake G., Dressler A., Oemler A., 1996, Nature, 379, 613

Moore B., Lake G., Katz N., 1998, ApJ, 495, 139

Moss C., Whittle M., 2000, MNRAS, 317, 667

Nieto J., Davoust E., Bender R., Prugniel P., 1990, A&A, 230, L17

Nomoto K., Thielemann F.-K., Yokoi K., 1984, ApJ, 286, 644

Norris M. A., Sharples R. M., Kuntschner H., 2006, MNRAS, 367, 815

Oh K. S., Lin D. N. C., 2000, ApJ, 543, 620

Oke J. B., 1990, AJ, 99, 1621

Panter B., Jimenez R., Heavens A. F., Charlot S., 2008, MNRAS, 391, 1117

Paudel S., Lisker T., 2009, Astronomische Nachrichten, 330, 969

Paudel S., Lisker T., Janz J., 2010, ApJ, 724, L64

Paudel S., Lisker T., Kuntschner H., Grebel E. K., Glatt K., 2010, MNRAS, 405, 800

Pedraz S., Gorgas J., Cardiel N., Sánchez-Blázquez P., Guzmán R., 2002, MNRAS, 332, L59

Phillipps S., Drinkwater M. J., Gregg M. D., Jones J. B., 2001, ApJ, 560, 201

Poggianti B. M., Bridges T. J., Mobasher B., Carter D., Doi M., Iye M., Kashikawa N., Komiyama Y., Okamura S., Sekiguchi M., Shimasaku K., Yagi M., Yasuda N., 2001, ApJ, 562, 689

Prantzos N., 2000, NewAR, 44, 303

Press W. H., Teukolsky S. A., Vetterling W. T., Flannery B. P., 1992, Numerical recipes in C. The art of scientific computing

Proctor R. N., Forbes D. A., Beasley M. A., 2004, MNRAS, 355, 1327

Proctor R. N., Sansom A. E., 2002, MNRAS, 333, 517

Rakos K., Schombert J., 2004, AJ, 127, 1502

Rakos K., Schombert J., Maitzen H. M., Prugovecki S., Odell A., 2001, AJ, 121, 1974

Renzini A., 2006, ARA&A, 44, 141

Ryden B. S., Terndrup D. M., 1994, ApJ, 425, 43

Sanchez-Blazquez P., Jablonka P., Noll S., Poggianti B. M., Moustakas J., Milvang-Jensen B., Halliday C., Aragon-Salamanca A., Saglia R. P., Desai V., De Lucia G., Clowe D. I., Pello R., 2009, ArXiv e-prints

Sánchez-Blázquez P., Peletier R. F., Jiménez-Vicente J., Cardiel N., Cenarro A. J., Falcón-Barroso J., Gorgas J., Selam S., Vazdekis A., 2006, MNRAS, 371, 703

Sandage A., Binggeli B., Tammann G. A., 1985, AJ, 90, 1759

Schaller G., Schaerer D., Meynet G., Maeder A., 1992, A&AS, 96, 269

Schlegel D. J., Finkbeiner D. P., Davis M., 1998, ApJ, 500, 525

Searle L., Zinn R., 1978, ApJ, 225, 357

Serra P., Trager S. C., 2007, MNRAS, 374, 769

Seth A. C., Dalcanton J. J., Hodge P. W., Debattista V. P., 2006, AJ, 132, 2539

Sharina M. E., Karachentsev I. D., Dolphin A. E., Karachentseva V. E., Tully R. B., Karataeva G. M., Makarov D. I., Makarova L. N., Sakai S., Shaya E. J., Nikolaev E. Y., Kuznetsov A. N., 2008, MNRAS, 384, 1544

Silk J., Wyse R. F. G., Shields G. A., 1987, ApJ, 322, L59

Smith R., Davies J. I., Nelson A. H., 2010, MNRAS, 405, 1723

Smith R. J., Lucey J. R., Hudson M. J., Allanson S. P., Bridges T. J., Hornschemeier A. E., Marzke R. O., Miller N. A., 2009, MNRAS, 392, 1265

Spolaor M., Hau G. K. T., Forbes D. A., Couch W. J., 2010, ArXiv e-prints

Strigari L. E., Bullock J. S., Kaplinghat M., Simon J. D., Geha M., Willman B., Walker M. G., 2008, Nature, 454, 1096

Tantalo R., Chiosi C., Bressan A., 1998, A&A, 333, 419

Thomas D., Maraston C., Bender R., 2003, MNRAS, 339, 897

Thomas D., Maraston C., Bender R., Mendes de Oliveira C., 2005, ApJ, 621, 673

Thuan T. X., 1985, ApJ, 299, 881

Tinsley B. M., 1972, A&A, 20, 383

Tinsley B. M., Larson R. B., 1979, MNRAS, 186, 503

Toloba E., Boselli A., Gorgas J., Peletier R. F., Cenarro A. J., Gadotti D. A., Gil de Paz A., Pedraz S., Yildiz U., 2009, ApJ, 707, L17

Tonnesen S., Bryan G. L., van Gorkom J. H., 2007, ApJ, 671, 1434

Trager S. C., Faber S. M., Dressler A., 2008, MNRAS, 386, 715

Trager S. C., Faber S. M., Worthey G., González J. J., 2000a, AJ, 119, 1645

Trager S. C., Faber S. M., Worthey G., González J. J., 2000b, AJ, 119, 1645

Trager S. C., Somerville R. S., 2009, MNRAS, pp 401

Trager S. C., Worthey G., Faber S. M., Burstein D., Gonzalez J. J., 1998, ApJS, 116, 1

Trager S. C., Worthey G., Faber S. M., Dressler A., 2005, MNRAS, 362, 2

Tremonti C. A., Heckman T. M., Kauffmann G., Brinchmann J., Charlot S., White S. D. M., Seibert M., Peng E. W., Schlegel D. J., Uomoto A., Fukugita M., Brinkmann J., 2004, ApJ, 613, 898

Tripicco M. J., Bell R. A., 1995, AJ, 110, 3035

Tully R. B., Somerville R. S., Trentham N., Verheijen M. A. W., 2002, ApJ, 569, 573

van den Bergh S., 1986, AJ, 91, 271

van Zee L., Skillman E. D., Haynes M. P., 2004, AJ, 128, 121

Vazdekis A., Arimoto N., 1999, ApJ, 525, 144

Vazdekis A., Casuso E., Peletier R. F., Beckman J. E., 1996, ApJS, 106, 307

Vazdekis A., Cenarro A. J., Gorgas J., Cardiel N., Peletier R. F., 2003, MNRAS, 340, 1317

Vazdekis A., Sánchez-Blázquez P., Falcón-Barroso J., Cenarro A. J., Beasley M. A., Cardiel N., Gorgas J., Peletier R. F., 2010, MNRAS, 404, 1639

Walcher C. J., Böker T., Charlot S., Ho L. C., Rix H., Rossa J., Shields J. C., van der Marel R. P., 2006, ApJ, 649, 692

Weiss A., Peletier R. F., Matteucci F., 1995, A&A, 296, 73

Welch G. A., 1982, ApJ, 259, 77

White S. D. M., 1980, MNRAS, 191, 1P

White S. D. M., Frenk C. S., 1991, ApJ, 379, 52

White S. D. M., Rees M. J., 1978, MNRAS, 183, 341

Wirth A., Gallagher III J. S., 1984, ApJ, 282, 85

Woosley S. E., Weaver T. A., 1995, ApJS, 101, 181

Worthey G., Faber S. M., Gonzalez J. J., Burstein D., 1994a, ApJS, 94, 687

Worthey G., Faber S. M., Gonzalez J. J., Burstein D., 1994b, ApJS, 94, 687

Worthey G., Ottaviani D. L., 1997, ApJS, 111, 377

Yi S., Demarque P., Oemler Jr. A., 1997, ApJ, 486, 201

Zinn R., West M. J., 1984, ApJS, 55, 45

Zwicky F., 1957, PASP, 69, 518

Acknowledgment

There are several people and organizations I would like to thank for their assistance during the course of my thesis. First, I would like to thank Heidelberg Graduate School of Fundamental Physics (HGSFP) for giving me an opportunity to study in Germany and supporting my stay in Heidelberg. Second, the Graduate Academy of University of Heidelberg and IMPRS Heidelberg for funding my travel to attend the several conferences. I would like to give a special thank to the Astronomisches Rechen-Institut (ARI) and their members for providing scientific working environment.

It is a great pleasure to thank my supervisor, Thorsten Lisker for having offered me the opportunity of coming to Heidlberg and working on an exciting research project. I truly appreciated the amount of time and energy that he has invested in helping me to make life easier in Heidelberg. Thank for his patience, for pushing me to see beyond the results and for teaching me to be independent and critical in my research. Thank you for your help in the writing of publications and this thesis.

My deep thanks to Harald Kuntschner whose discussions and consultation, during my visits to ESO or via email, significantly assisted me to accomplish this thesis.

Thanks to the all the students, staff and astronomers at ARI. Special thanks to Eva Grebel and Stefan Jordan, for being my thesis committee. Thanks to Jonathan for reading through text and helping to improve the thesis text. I would like to thank my colleagues at Heidelberg, Alex, Hagan, Stefan, Isabell, Olivar, Sophia, Denija, Joachim for shearing the ideas and technical work experiences.

Thank you all very very much!
Vielen Dank aller sehr!

Sanjaya Paudel